

**An Agent-based Model for Evaluating Cellular Mechanisms of
Bone Remodeling**

Submitted in partial fulfillment of the requirements for

the degree of

Doctor of Philosophy

in

Biomedical Engineering

Lyndsey J. Schutte

B.A., Biochemistry, Mount Holyoke College

Carnegie Mellon University
Pittsburgh, PA

December, 2012

Acknowledgements

I would like to thank Dr. Hollinger for his financial support, academic knowledge, and enthusiasm for this project. Without his help, none of this thesis would exist. I would also like to thank my committee—Dr. Robert Murphy, Dr. Kathleen Carley, and Dr. Lance Davidson—for all their expert advice and tireless patience. It requires a sincere devotion to education to teach a biochemist like myself to setup and analyze a model of this complexity. Every instance of the correct technique or method of analysis is a sign of their help.

I also wish to thank my family for all their support and kindness. This project is a reflection of all the Sutton's, Peatman's, and Schutte's love for learning and knowledge. I would not still be in school, nor would I have wandered so far into the medically unknown without your influence and support. Life might have been easier sticking to what I already knew or doing what we knew could be done, but what kind of an adventure would that be?

A giant thanks goes out to all my friends and labmates. This would not have been nearly as fun without you. Amy Donovan in particular—I think you've edited everything I've had to write (which is fantastic since you are the best scientific editor I've ever met); thank you. Ivan Jager—thank you for being marvelous, for putting up with the thesis sucking away all our free time, for setting up the linux cluster (seriously, that would have taken me days), and for lovingly teasing me into writing scripts for all the data manipulations. I would have been here till 2013 with those eight thousand spreadsheets. Lastly, I'd like to thank my God for challenging me to think deeper, for being such a solid center, and for making me into a better person than I am.

Abstract

In this thesis I present a mechanistic computational model of the cells and processes involved in bone remodeling. Despite decades of progress uncovering the mysteries of bone biology and developing a wide base of information on the cells and processes involved in bone maintenance, the most popular hypotheses for how bone cells interact and orchestrate controlled remodeling remain controversial and unverified. In order to leverage the primary literature towards testing the feasibility of two particular hypotheses, I created an agent-based model (ABM) structured on the known locations, properties, and behaviors of osteoclasts, osteocytes, and osteoblasts.

Bone's ability to minimize mass without jeopardizing mechanical integrity can be explained by a disuse signaling threshold, but the mechanics and source of this signaling pathway are still largely a mystery. The preliminary model presented here simulates the hypothesis that a simple osteocyte-released and osteoclast-received signal could maintain trabecular width at the minimum required to support the applied load. Using a series of different initialization parameters, the initial simulation suggests that a mechanically stimulated osteocyte signal can dynamically maintain an optimized trabecular width.

The second iteration of the ABM incorporated known information on osteoblasts and simulated the hypothesis that osteoclasts could be temporally and spatially coupled to osteoclasts via a diffusible signaling molecule released from the bone matrix during osteoclastic resorption. This simulation shows that there exists a set of input parameters, within the range supported by literature, which will generate controlled remodeling. These results support the hypothesis that osteoblasts could be spatially coupled to osteoclasts by a released signal. However, the simulation raises some questions about this popular hypothesis's ability to correctly account for the timing of

osteoblast activation and migration towards the remodeling compartment.

Table of Contents:

1.	Introduction.....	1
1.1.	Motivation.....	1
1.2.	Background Bone Biology.....	5
1.2.1.	Bone Tissue Structure.....	7
1.2.2.	Cells.....	10
1.2.3.	Controlled Remodeling.....	15
1.3.	Previous Models of Bone Remodeling.....	17
1.4.	Overview of the two Remodeling Simulations.....	19
1.4.1.	First Model – Osteocytic Signal for Controlling Resorption.....	19
1.4.2.	Second Model – Osteoclast/Osteoblast Coupling.....	20
2.	First Model - Osteocytic Signal for Controlling Resorption.....	21
2.1.	Introduction.....	21
2.2.	Methods.....	24
2.2.1.	Software.....	24
2.2.2.	Agent-based model.....	24
2.2.3.	Simulation setups and initial conditions.....	35
2.2.4.	Methods of Analysis.....	37
2.3.	Results.....	38
2.3.1.	Osteoclast regulation through surface changes.....	38
2.3.2.	Ability of osteocytes to shield bone from resorption.....	39
2.4.	Discussion.....	46
2.4.1.	The effectiveness of osteocyte signaling.....	46
2.4.2.	The kinetics of resorbing bone.....	47

2.4.3.	The relationship between osteocyte density and trabecular perforations.....	48
2.4.4.	The effect of bone-lining cells as signaling intermediaries.....	48
2.4.5.	Empirical comparison of the model with human parameters.....	50
3.	Second Model - Osteoclast/Osteoblast Coupling.....	52
3.1.	Introduction.....	52
3.2.	Methods.....	56
3.2.1.	Software.....	56
3.2.2.	Agent-based model.....	56
3.2.3.	Simulation setup and initial conditions.....	69
3.2.4.	Methods of Analysis.....	70
3.2.5.	Validation of model and results.....	72
3.3.	Results.....	73
3.4.	Analysis of Results.....	85
3.5.	Discussion.....	89
4.	Conclusions and Future Directions.....	92
4.1.	Motivation.....	92
4.2.	Contributions to the Field.....	95
4.2.1.	Techniques.....	95
4.2.2.	Validation of Hypotheses.....	96
4.3.	Future Directions.....	97
4.4.	Concluding Remarks.....	98
5.	References.....	100

List of Tables:

Table 2.1. Experimental Setup for Osteocyte Shielding virtual experiment..... 37

Table 2.2. Average end point measurements in each condition with normal osteocyte density and more sensitive osteocytes..... 41

Table 2.3. Average end point measurements in each condition with low osteocyte density and more sensitive osteocytes..... 41

Table 2.4. Average end point measurements in each condition with very low osteocyte density and more sensitive osteocytes..... 41

Table 2.5. Average end point measurements in each condition with high osteocyte density and more sensitive osteocytes..... 41

Table 2.6. Average end point measurements in each condition with very high osteocyte density and more sensitive osteocytes..... 42

Table 2.7. Average end point measurements in each condition with normal osteocyte density and less sensitive osteocytes..... 42

Table 2.8. Average end point measurements in each condition with high osteocyte density and less sensitive osteocytes..... 42

Table 2.9. Average end point measurements in each condition with normal osteocyte density, more sensitive osteocytes, but without active BLCs..... 42

Table 3.1. Experimental Setup for the Osteoclast/Osteoblast virtual experiment..... 70

Table 3.2. The Z-scores for all 81 cases..... 86

Table 3.3. The Z-scores for the 22 cases with an average below one σ 89

Table 3.4. The initial conditions of the four independent variables for the thirteen cases that fell within one standard deviation of expected values..... 89

Table 3.5. Linear regression of the main effects on the rate..... 90

Table 3.6. Linear regression of the interactions effects on the rate..... 91

Table 3.7. The comparison of simulated results and biological trends..... 95

List of Figures:

Figure 1.1. An example of cortical bone..... 8

Figure 1.2. A micro-CT reconstruction of trabecular bone..... 9

Figure 1.3. An osteocyte under light microscopy..... 11

Figure 1.4. An osteoclast under light microscopy..... 12

Figure 1.5. An osteoblast under light microscopy..... 13

Figure 1.6. Two bone lining cells under transmission electron microscopy..... 14

Figure 2.1. The Utah Paradigm can explain many of the non-linear bone mass/strength changes that are dependent on applied strains..... 22

Figure 2.2. A set of six different CT-scans of trabecular bone biopsies showing differences in trabecular architecture..... 27

Figure 2.3a and 2.3b. The ABM is initialized with a trabecular region composed of ECM agents that are in a ‘mineralized’ state (labeled white), surrounded by ‘marrow’ ECM agents..... 31

Figure 2.4. A flow diagram of the main body of the ABM code..... 32

Figure 2.5. A flow diagram of the code run by all osteocyte agents..... 27

Figure 2.6. A flow diagram of the code run by all active BLC agents..... 33

Figure 2.7. A flow diagram of the code run by all osteoclast agents..... 34

Figure 2.8. A flow diagram of the code run by all ECM patches..... 35

Figure 2.9. A magnified view of the trabecular surface with the osteoclasts shown in red, the osteocytes in yellow, and demineralized matrix show in shades of grey and blue according to the degree of demineralization. 39

Figure 2.10. The change in width over time given regular osteocytes and various initial widths. 40

Figure 2.11. The change in percent width over time given regular osteocyte density and various initial widths. 41

Figure 2.12. The change in average percent width occurs in the same pattern with less sensitive osteocytes as it does with osteocytes that more quickly signal. 42

Figure 2.13. The number of full-thickness resorptions for different osteocyte population densities and starting widths..... 43

Figure 2.14. The ending width as a percentage of initial width various starting widths, with or without BLCs, and given a normal osteocyte density. 44

Figure 2.15. The percent of simulations with a full-thickness resorption across a range of initial widths, osteocyte sensitivities, and with or without BLCs. 45

Figure 2.16. The average number of full-thickness resorptions across osteocytes densities and initial widths, with and without BLCs.....	45
Figure 3.1. A diagram of the RANKL/OPG pathway.....	54
Figure 3.2. A flow diagram of the code for the whole ABM.....	58
Figure 3.3. A flow diagram of the code run by all ECM patches.....	60
Figure 3.4. The initial condition of the simulation.....	62
Figure 3.5. A flow diagram of the code run by all BLC agents.....	65
Figure 3.6. A flow diagram of the code run by all osteoblast agents.....	68
Figure 3.7. Four representative plots of the average width changing over time.....	75
Figure 3.8. The plots of all 81 cases as the width changes with time.....	77
Figure 3.9. The plots of all 81 cases in the 100-200 micron region.....	78
Figure 3.10. The effect of osteoclast lifespan on all 81 plots.....	79
Figure 3.11. The effect of osteoclast rate on all 81 plots.....	80
Figure 3.12. The effect of osteoblast rate on all 81 plots.....	81
Figure 3.13. The effect of osteoblast lifespan on all 81 plots.....	82
Figure 3.14. The effect of the independent variables on the time of minimum width..	83
Figure 3.15. The effect of the independent variables on the rate of width change.....	83
Figure 3.16. The effect of the independent variables on smoothness and width.....	84
Figure 3.17. The combined effects of the osteoblast rate and (osteoblast rate * osteoblast lifespan) on the rate.....	92
Figure 3.18. The effects of the osteoblasts' lifespan and rate with the osteoblasts' lifespan and rate on the rate of change in width.....	92

List of Appendix Tables and Figures:

Table A2.1. Output measurements given normal osteocyte density and more sensitive osteocytes.....	A1
Table A2.2. Output measurements given low osteocyte density and more sensitive osteocytes.....	A1
Table A2.3. Output measurements given very low osteocyte density and more sensitive osteocytes.....	A1
Table A2.4. Output measurements given high osteocyte density and more sensitive osteocytes.....	A1
Table A2.5. Output measurements given very high osteocyte density and more sensitive osteocytes.....	A2
Table A2.6. Output measurements given normal osteocyte density and less sensitive osteocytes.....	A2
Table A2.7. Output measurements given high osteocyte density and less sensitive osteocytes.....	A2
Table A2.8. Output measurements given normal osteocyte density, more sensitive osteocytes, and no active BLCs.....	A2
Table A3.1. The values for the independent variables and resultant output variables for all 81 cases of the osteoclast/osteoblast coupling model.....	A3
Table A3.2. MANOVA table showing with the four independent variables.....	A38
Table A3.3. The p values for each of the independent variables and their effect on the dependent variables.....	A38
Table A3.4. ANOVA for the ‘Smoothness’ dependent variable.....	A38
Table A3.5. ANOVA for the ‘Average Width’ dependent variable.....	A39
Table A3.6. ANOVA for the ‘Time of Minimum’ dependent variable.....	A39
Table A3.7. ANOVA for the ‘Minimum Width’ dependent variable.....	A39
Table A3.8. ANOVA for the ‘Rate Change’ dependent variable.....	A40
Table A3.9. Confidence intervals for the regression analysis of the main effects.....	A47
Table A3.10. The covariance matrix for the regression of the main effects.....	A47
Figure A3.1. The above plots show the change in the average width, measured in microns, over time for all 81 cases. They also show the change of width alongside the change in the number of osteoclasts (red) and osteoblasts (green) over time.....	A32

Figure A3.2. The Rate of the change in width plotted as a function of the Time of the minimum width.....	A33
Figure A3.4. Box-and-whisker plots for the average width.....	A34
Figure A3.5. Box-and-whisker plots for the smoothness.....	A35
Figure A3.6. Box-and-whisker plots for the time of minimum width.....	A36
Figure A3.7. Box-and-whisker plots for the osteoblast lifespan.....	A37
Figure A3.8. The screenshots of the trabeculae at the end of the last simulation for all 12 replicates of simulation A1.....	A43
Figure A3.9. The screenshots of the trabeculae at the end of the last simulation for two of the replicates of simulation A56.....	A44
Figure A3.10. The screenshots of the trabeculae at the end of the last simulation for two of the replicates of simulation SA72.....	A45
Figure A3.11. The screenshots of the trabeculae at the end of the last simulation for two of the replicates of simulation SA73.....	A46
Figure A3.12. The four diagnostic charts for the first linear regression.....	A49
Figure A3.13. The four diagnostic charts for the linear regression that included interaction effects.....	A51

Abbreviations List:

ABM – agent-based model

BLC – bone lining cell

ECM – Extra-cellular matrix

M-CSF – macrophage-colony stimulating factor

MRI – magnetic resonance imaging

OPG – Osteoprotegerin

RANK – Receptor Activator of Nuclear Factor kappa-B

RANKL – receptor activator of nuclear factor kappa-B ligand

TGF- β - transforming growth factor

1. Introduction

The thesis presented here describes a computational method for studying the cellular actions and interactions that are required for controlled bone remodeling. Remodeling is the process by which bone tissue maintains itself--encompassing both the destruction and removal of old bone matrix as well as the replacement of new bone matrix. A skeleton's mass, shape, and health are all regulated through this remodeling, a process that occurs continuously throughout life.

Our understanding of bone remodeling has made great progress in the past century as a consequence of the successive waves of seminal contributions by brilliant researchers: Frost^{35,38}, Urist¹¹⁰, Parfitt^{84,85}, Delaisse²², Martin⁶⁹, Huiskes⁸³, Villanueva¹¹⁴, and many others. As a result of these contributions to basic fundamental bone biology and clinical disciplines, there is a large pool of data available that detail the different aspects of bone remodeling. These include bone homeostasis, clinical effects of knockouts and imbalances, cellular characterizations, and biomechanics.

However, this large pool of information is spread across multiple disciplines, is of disparate types, lacks a clear application, remains incomplete, and, regrettably, is sometimes unused, forgotten, and must be rediscovered. In other words, that which has been discovered about the biology of bone is not being incorporated into a useful form. The current hypotheses for how cells interact are either assumed true or discounted out of hand without first being evaluated by additional means.

1.1. Motivation

In order for the clinical, pharmaceutical, or tissue engineering communities to be

able to effectively design treatments for patients with bone diseases or injuries, it is critical that those scientists understand how bones form and function. Current therapeutics are often designed around gross estimates of what cells, growth factors, and material properties are required both spatially and temporally. As the medical community has seen with long-term bisphosphonate side effects, misunderstandings about how each type of cell type impacts all the other cell types in bone can lead to therapeutics that are detrimental to skeletal health. Osteoclast cells—the cells that resorb bone—were assumed to be detrimental to bone health when the bisphosphonates were being designed and selected for osteoporosis treatments. In reality, osteoclasts promote bone health by stimulating osteoblastogenesis and osteoblast differentiation as well as creating tunnels for blood vessels. Osteoblast cells, which make bone, require the osteoclasts' simulation and removal of old bone in order to maintain new, strong bone. Instead of strengthening bones, bisphosphonates, by stopping osteoclasts, lead to a decrease in the entire cycle of bone renewal, leading to more fragile bones that cannot effectively fight infections.

Effective design requires a thorough knowledge of the system for which it is being designed. In the case of bone therapeutics, good design requires the utilization and integration of the data from primary literature. This information needs to exist in a form that allows cross-checking of measured data, mechanistic descriptions of cellular activity, and ways to verify that the current hypotheses of the bone community are possible given the known spatiotemporal and physiological limits of bone cells.

Computational modeling offers a unique opportunity to build models that can simulate complex, dynamic systems³⁹. Agent-base modeling (ABM), while more complex

and time-consuming than traditional systems-dynamics or mathematical modeling, provides a platform to more fully realize the potential of computational modeling to elucidate and critically test our understanding of bone biology^{10,48}.

Bone remodeling is difficult to research, for it cannot be replicated *in vitro* and is too dynamic to capture histologically. There is a wealth of information, but it is all in disparate forms that sometimes conflict. Coupling, defined as the interaction between osteoblasts and osteoclasts that creates the local, balanced removal and replacement of bone, is an area of bone biology that incorporates a large fraction of conflicting information. Hypotheses for how coupling works exist, but none have yet to be rigorously verified. The RANKL-OPG signaling hypothesis, generated by a cellular/molecular biology approach, is a common explanation for coupling, but it conflicts with histological findings. The hypothesis that resting osteoblasts are the source of coupled osteoblasts is a favorite theory of histologists, but is contradicted by data from the cellular and molecular fields. There are half a dozen disciplines all generating valuable pieces of information, but the hypotheses generated within each field tend to disregard information outside their discipline.

Much of modern biology is, by necessity, reductionist; each experiment can only provide one piece of information. Researchers in every field are only gathering one piece of the puzzle at a time. The synthesis of these pieces of data into hypotheses often occurs only in mental models and diagrams—a daunting task for a subject with thousands of experimental papers. These traditional thought-experiments and diagrams do a poor job of highlighting either missing components or checking the feasibility of a hypothesis. A new way of unifying vast amounts of information is needed to understand how all the

cells, signals, and structures come together as a whole in bone remodeling.

Computer simulations and biological experiments each have their own distinct advantages that compensate the other's weaknesses. Laboratory science focuses on one hypothesis at a time and computer models can control dozens of interacting variables within system. Animal and clinical research has the advantage of *in vivo veritas*, and, as cleverly stated by George E.P. Box, 'all models are wrong, but some are useful'. Computer models, in particular, offer the chance to combine vast amounts of quantitative and qualitative data from multiple sources, probe interactions in controlled, repeatable ways, and then clearly define the mechanisms occurring between the input parameters and the output parameters. As an example, computer simulations have been used to demonstrate the feasibility of osteocyte signaling based on combined histological, *in vitro*, molecular, and fluid dynamic data. Quantifying the discrepancies between simulation outputs and real world data can highlight deficiencies in a current theory. A computer model both challenges and enables bone biologists to unify and understand experimental and clinical data. A mechanistic simulation provides a working model that both researchers and clinicians can use to add speed and robustness to their own work.

There are many different ways of simulating a biological system. Graphical models (e.g. Bayesian networks) look at correlations and statistical relationships between events or interacting objects in order to understand the structure of a complex system. Finite Element Models (FEM) divide complex systems or geometries into a mesh, lattice, or sets of voxels; this allows the tractable approximate calculations of properties (e.g. local strain) based on equations from material engineering, fluid

dynamics, and other engineering disciplines. These types of models have proven very useful in the past; however, for studying the mechanistic, multi-scale interactions occurring both spatially and temporally during bone remodeling, I chose to create an agent-based model. ABMs are well suited for embodying mechanistic information on the cellular level because, just like cells, the rule-based behaviors of the agents depend only on the local microenvironment, agent-type, and internal state. The overarching behavior of the ABM system is a strong match for the biological tissue. Both are based on small-scaled, incremental changes, as well as spatiotemporal patterns propagating through time in order to direct the form and function of the tissue. In addition, with every agent, variable and initial parameter corresponding to a real biological object or parameter, the ABM provides strong empirical grounding and a straightforward method to verify that all the rules within the simulation have been documented in literature.

1.2. Background Bone Biology

Bone is one of the most complex organs in the body, for all its simplicity of function. Bone's function can be summed up into two tasks: structurally support soft tissue and maintain a mineral reserve. Despite it being one of the longest studied tissue systems, our understanding of how bones accomplish these two tasks is still riddled with mysteries. There are three main reasons why a better understanding of bone biology exceeds current scientific understanding. First, while one component of bone—the mineral portion of the matrix—is easy to detect and study using x-rays, the other two components of bone—the organic matrix and the cells—are extremely difficult to observe. The dense, mineral nature of bone effectively shields the cells from view. Osteocytes, the most abundant bone cells, are particularly difficult to study since they are completely encapsulated within mineralized matrix. Due to the mineral content, a

histological slide of bone often takes at least one month to prepare, as compared to a few days for soft tissue, and there are often many of artifacts created in the process.

Magnetic resonance imaging (MRI) and nano-indentation technologies now offer new insights into bone microstructure and composition, but MRI only provides vague assessments of the marrow's status and nano-indentation only provides another assessment of mechanical strength. Additionally, not all the cells are visible under light microscopy; bone-lining cells are so flat that they only show up as only a thin, faint line on most slides and frequently go unseen in the visually busy areas of the bone surface.

Secondly, bone remodeling also operates on longer time scales than other tissues. The complexity and toughness of bone means that remodeling and regular turnover takes months, as opposed to days like in most tissues. Basic turnover requires more signals over a longer time and spatial scale than other tissues. There is also a substantial delay between the start of bone pathologies and the moment symptoms appear, which usually results in most of the evidence of a disease's mechanisms of action being gone before a biopsy can be taken.

A third reason why bone proves difficult to understand is the complex cellular interactions required for any change to the bone. Bone remodeling relies heavily on spatio-temporal patterns to guide the function of its cells, possibly due to the long time-spans of the remodeling process. Also, since the function of bone is a balance between the release of calcium to maintain serum ion concentrations and the sequestering of calcium for bone strength, there are multiple physiological balances constantly interacting between a many different of cell types. This complexity makes simple cause-and-effect models imprecise and inaccurate in many cases, and the lack of accurate

models is a major problem plaguing in medical treatment and therapy design.

Because of these reasons, there is a pressing need to find novel ways to understand the actions and mechanisms taking place within bone. Computational modeling offers a unique opportunity to build models that can simulate complex, dynamic systems. Agent-based modeling, while more complex and time-consuming than traditional graphical or mathematical modeling, provides a platform to more fully elucidate and critically test our understanding of the complex world of bone biology.

1.2.1. Bone Tissue Structure

Bones, on the supra-millimeter scale, have two main regions or types of osseous tissue: cortical and trabecular. The cortical, or compact, bone is the dense shell of bone that provides the majority of the support and weight to the skeletal system. It is primarily composed of cylindrical subunits called osteons (fig 1.1). The trabecular or cancellous bone (fig 1.2) is the spongy network of thin rods and plates inside the cortical shell that hosts the marrow and provides much of the calcium that is taken from and stored back into the bone. Both of these tissue regions are constantly being replaced and renewed by remodeling, usually within a span of seven years. Both of these tissue regions will remodel to be stronger in the direction of applied force, and both of these types of bone are considered 'lamellar' since the collagen fibrils of each layer are parallel to each other, with regularly spaced bands formed by the resting lines.

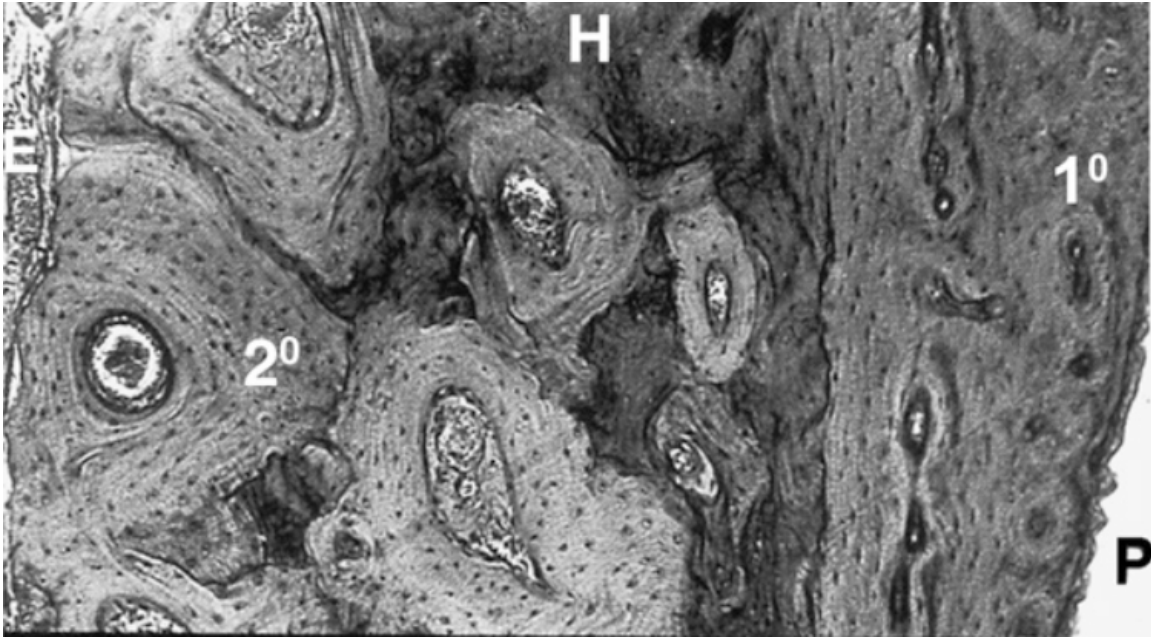


Figure 1.1 A section of cortical bone, the mandible of a monkey, showing the three regions of cortical bone: the inner endosteum (E), the outer shell of periosteum (P), and the Haversian bone (H) in the center. The Haversian bone is made up of both young primary osteons (1°) and the classic bull's-eye shaped secondary osteons (2°). Reproduced from Roberts et al.⁹⁵

Trabecular, or spongy bone, is especially prone to remodeling; it has twice the surface area of dense cortical bone and, therefore, more contact with vascular tissue through which the body extracts and sequesters the flux of calcium ions needed and generated by other tissues⁵¹.

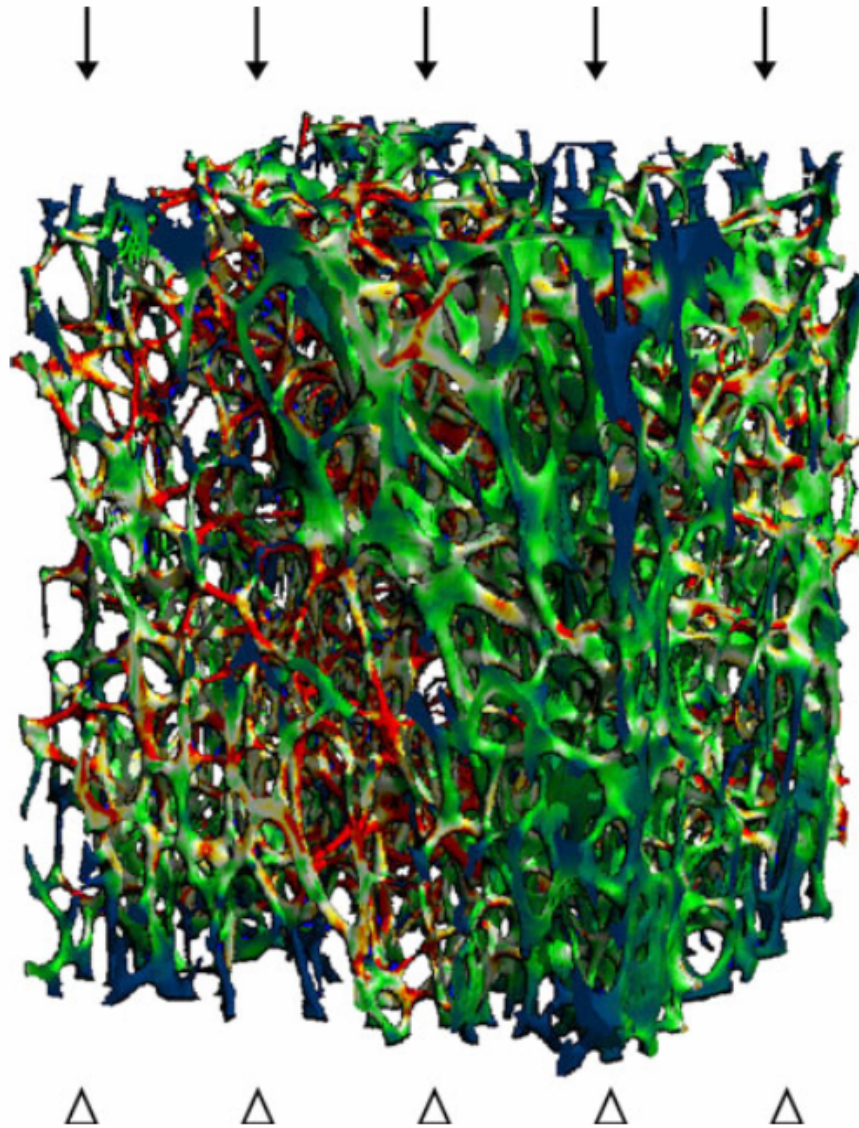


Figure 1.2 A micro-CT reconstruction of a section of trabecular bone. Red areas correspond to regions under the highest calculated local stresses that could be generated by a 1% compressive strain; blue areas experience the lowest stress. Each rod is approximately 100 microns in diameter. From Burghardt et al.¹⁵

1.2.2. Cells

Within bone, there are three classic cell types involved in bone remodeling: the osteoblast, the osteoclast, and the osteocyte²⁴. The osteoblast deposits the organic matrix called osteoid that serves as the nucleation site for the hard calcium phosphate crystals. The osteoclasts are the cells responsible for degrading bone. The osteocyte cells reside within the bone, forming a syncytium of cells communicating through gap junctions.

The most abundant cell in bone is the osteocyte. The osteocytes live trapped within the mineralized matrix; they are descended from osteoblasts and form a spidery network of canaliculi—very small channels—within the bone. Canaliculi average around 250 nm in diameter and each contain the cytoplasmic process of an osteocyte that averages 100 nm in width¹⁰⁰. While these cells are small and relatively quiescent, their canaliculi radiate out into the surrounding bone and connect via gap junctions to neighboring osteocytes and any cells on the bone surface¹⁰⁰.

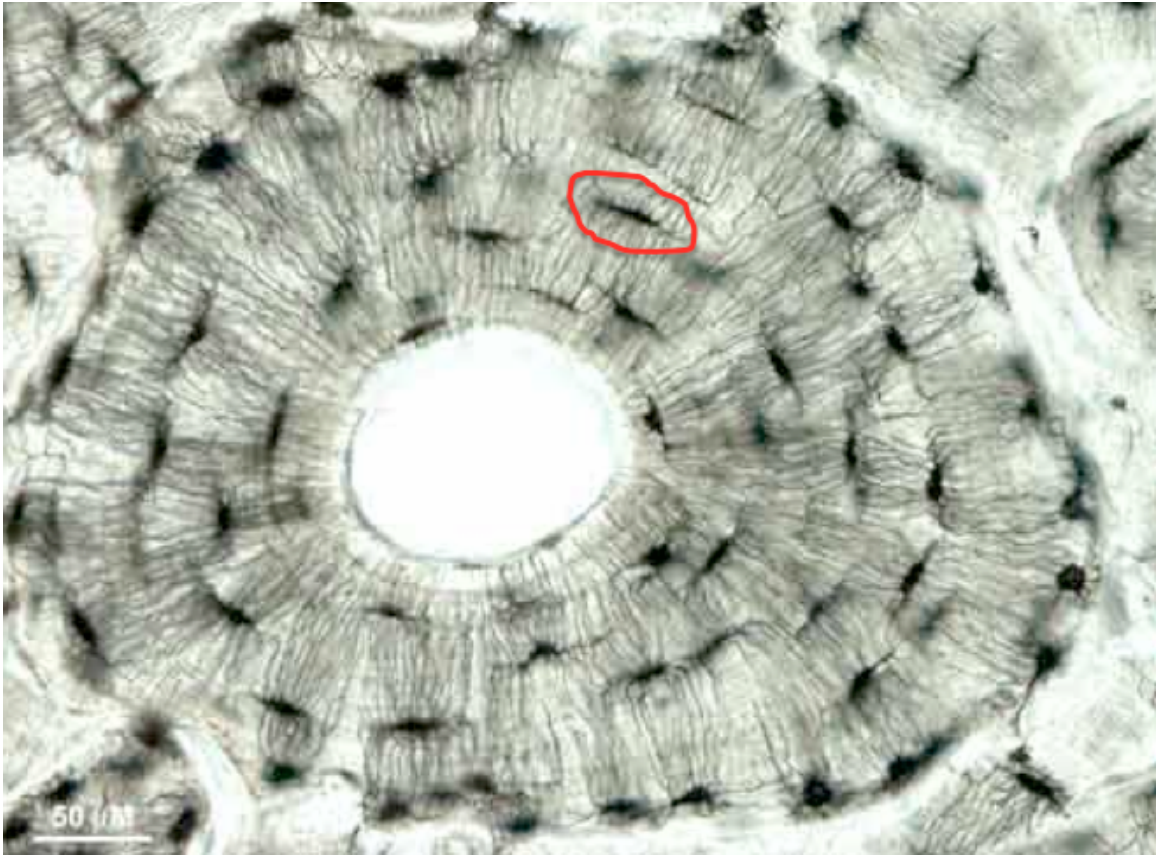


Figure 1.3. An individual osteocyte, circled in red, is part of the larger network of osteocytes, each spreading out many thin dendritic processes through the mineralized matrix in order to communicate with their neighboring osteocytes. Photo courtesy of Tim Arnett.

Due largely to the osteocytes' location, they are considered the most likely candidate for sensing mechanical forces, micro-damage, and other conditions within bone tissue. They could then report that information back to the osteoclasts and osteoblasts. Osteocytes are the only cells within the bone matrix and are uniquely positioned to monitor the local forces and microfractures that occur within the mineralized matrix. However, it is uncertain how they accomplish this or which cells they communicate this information to⁷.

The largest bone cell is the osteoclast, growing over 100 μm and having between 3 to 10 nuclei^{49,88}. It is descended from the monocyte cells of the hematopoietic lineage,

allowing this cell to have the machinery needed to form into giant multinucleated cells that can seal onto bone surfaces and resorb the mineralized matrix.

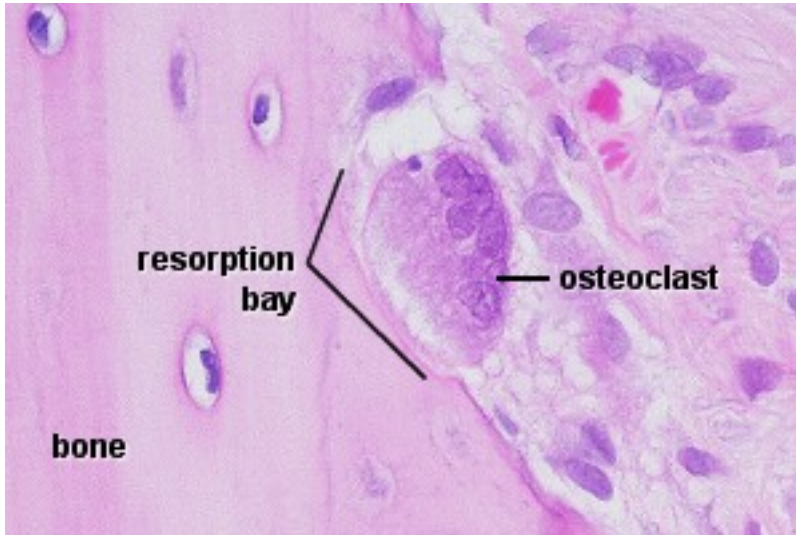


Figure 1.4. The multinucleated osteoclast is actively attached to bone and resorbing a pit in the bone on its basal side. Histology by Lutz Slominanka.¹⁰²

However, while osteoclasts do degrade bone, having an active osteoclast population should not be assumed to be detrimental for bone. Bone naturally accumulates microfractures and becomes weaker with age. Without osteoclasts to remove damaged, infected, or dead bone, new bone cannot take its place. There is also evidence that the osteoclasts play an important role in stimulating osteoblast activity⁵⁵. Therefore, in cases where bone mass is pathologically low, it is due to an incorrect balance between the relative osteoclastic and osteoblastic activities, not necessarily due to a pathological level of osteoclast activity.

The osteoblast cells produce bone—specifically the organic osteoid and the proteins that facilitate its mineralization. They originate from the mesenchymal stem cell line, either on the endosteal and periosteal surfaces of bone or from the marrow's

stromal cells. Once activated and situated on the surface of bone, osteoblasts build up a surface layer of osteoid. Mineralizing enzymes, such as alkaline phosphatase, then cause hydroxyapatite crystals to form along the collagen strands within the new osteoid. Osteoid is normally formed at a rate of roughly 1-2 microns a day^{36,53,86,91,50}, and will slowly mineralize for months afterwards⁶⁸. The osteoblasts usually form as part of a monolayer of other osteoblasts within resorption pits. Over their lifetime, osteoblasts will shift from being plump and round to become smaller and thinner until their osteoid production ceases. It is possible that some of these older osteoblasts then form the extremely thin cells that rest along the inner and outer surfaces of the bone—bone lining cells. These bone-lining cells can also be called ‘resting osteoblasts’, though this term has also been used as a catch-all term for any cell that is too small to be an active osteoblasts but is still associated with a bony surface.

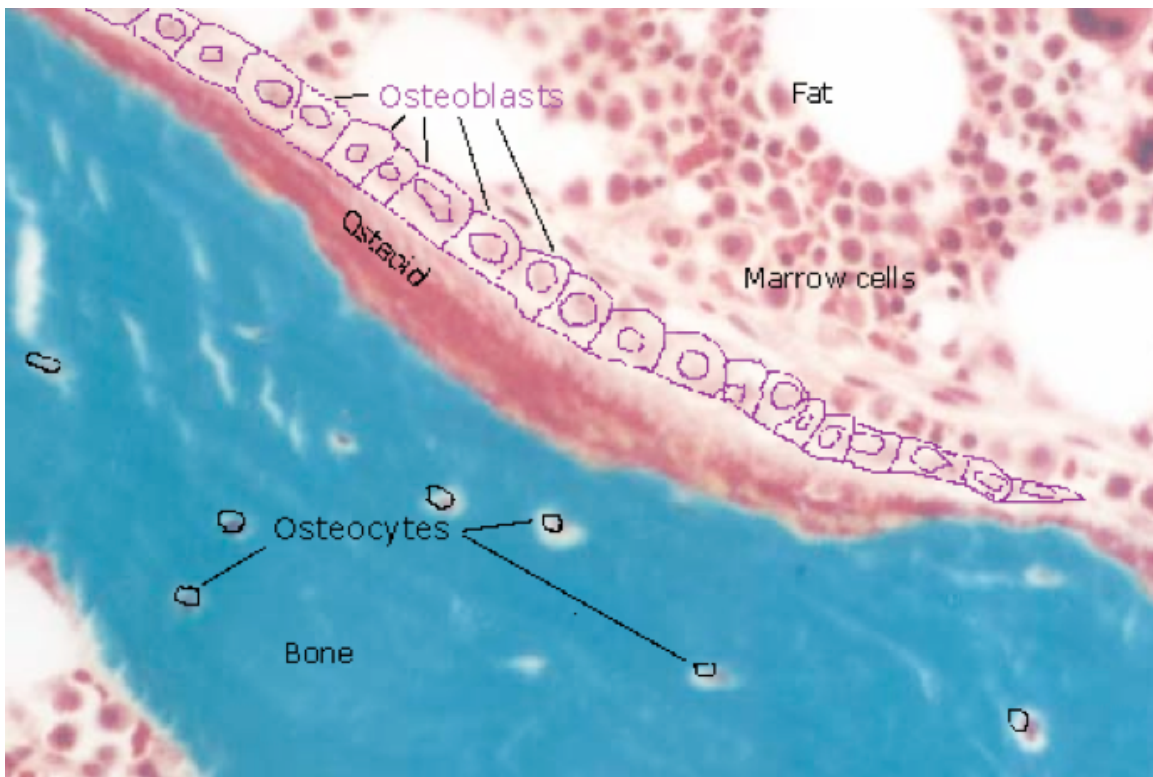


Figure 1.5. The osteoblast agents form a row along the surface of the surface of mineralized bone, producing a layer of osteoid that will slowly mineralize into bone.

Photo courtesy of Russ Turner and Susan Ott.

During the formation of a new layer of bone, a few active osteoblasts are selected to become entrapped within the mineralizing matrix as it is being laid down. As these cells become trapped, they spread out long, thin cellular extensions in all directions and become metabolically quiescent. At this point, these cells are called osteocytes.

There is also a fourth, less well-understood cell type in bone tissue—the bone lining cell. These extremely flat cells line the periosteum and endosteum, including the surfaces of the trabecular bone⁴⁷. BLCs spread out to be roughly 20-30 μm across and, apart from the soma, thin enough to be invisible using light microscopy^{31,66}.

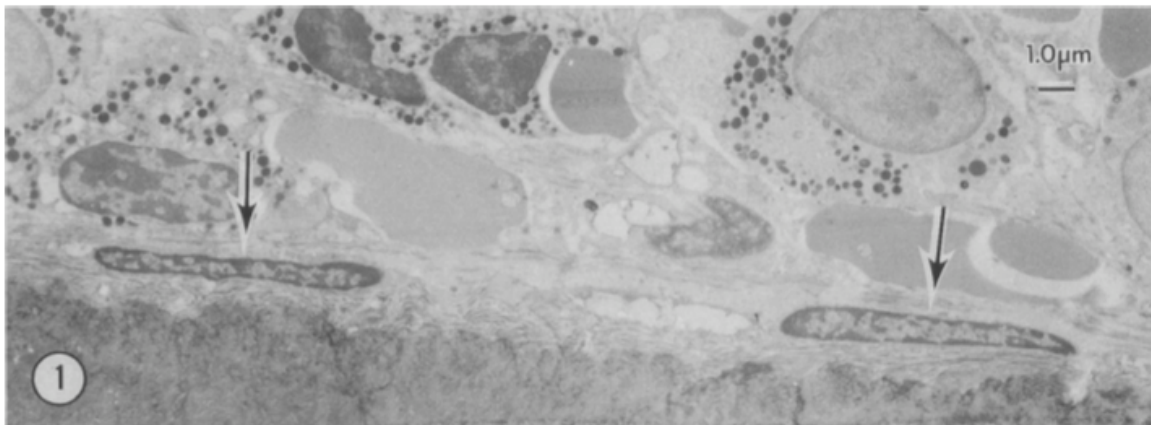


Figure 1.6. Two bone-lining cells resting flat against the surface of the bone. The arrows point to their flat somas. Reproduced from Miller and Jee.⁷⁷

Because this cell has the same mesenchymal lineage as osteoblasts, they share most of the same cell markers as osteoblasts and are identified as osteoblasts under the common informal definition of ‘a mononuclear cell contacting bone’. They have also been called resting osteoblasts, pre-osteoblasts, surface osteoblasts, peri-osteoclasts, and may be the same cell type as the newly coined canopy cells^{3,31,42,66,111}. The BLCs have been observed connecting to the osteocytes through gap junctions at the tips of their

dendritic processes, so it is possible that the BLCs are part of the osteocytes' syncytium³¹. These tight junctions may also allow them to participate in the mechanotransduction of forces within bone⁷⁸. They, or a visually similar cell, have been identified as enwrapping and digesting remaining demineralized matrix that osteoclasts leave behind³⁰ before a new layer of bone is deposited.

Currently in bone biology there is a controversy about whether or not BLCs form a canopy of cells encapsulating a pocket of space around the remodeling site and amplifying the paracrine signaling that activates osteoblasts. There is evidence of tight-junctions between resting osteoblastic cells forming a layer a few microns above the surface of a Howship lacunae^{3,29,42,82}. The tight junctions may prevent diffusion of a signaling molecule from the remodeling site and may concentrate the signal in the location where a pre-osteoblast could contact it. However, despite putative evidence for the existence canopy cells, universal concurrence has not been achieved⁸¹.

1.2.3. Controlled Remodeling

Bone remodeling has three primary goals. The first is to maintain the quality of bone matrix via the general turnover of older bone with newer bone as well as the targeted replacement of damaged bone. The second goal is to optimize the bone mass. Bone is a physiologically expensive organ to maintain and consequently, bone mass must be optimized to prevent both fractures and an undue metabolic burden. The third goal of bone remodeling is the control of the serum levels of calcium, which can be alternately released or sequestered in the bone matrix⁵¹.

All three of these goals represents a balance between two opposing needs that

must be maintained and each requires multiple sources of feedback affecting the cells participating in bone remodeling. Some of these feedback signals systemically affect all bone surfaces, while others are paracrine or juxtacrine in nature. Many of the identified signaling molecules have unknown ranges and cell targets. This makes the cell signaling information from literature difficult to sort out.

What is known about bone is that it has the ability to adapt to changes in mechanical forces by optimizing its mass and shape. Therefore, the remodeling process has to involve mechanosensory cells. Patients who undergo long-term bed rest have less bone and increasing the forces applied to bone, such as through exercise, may increase bone density²⁰. This mechanical optimization is also a major cause of bone-loss in astronauts.

Dr. Wolff first formally proved that bone would strengthen itself in a direction parallel to the normal vector of applied load¹⁶. It has been roughly calculated that human bone can shift any cubic millimeter of bone by up to two square millimeters a year. Later, Dr. Frost, an orthopedic surgeon, played a major role in how bone remodeling is understood, generating the concepts and evidence for bone turnover and developing the mechanostat theory. Based on what he saw in the clinic, Frost's mechanostat theory includes four strain thresholds: one for remodeling, one more modeling, a pathologic threshold, and a fracture threshold⁵². Being above or below one of these thresholds would be enough to change the response of the bone. For example, being above the pathologic threshold would mean there was enough strain on the bone to cause microfractures—leading the bone to direct bone turnover in that area and replacing the injured bone with a larger quantity of new bone. The lowest threshold is

the one that this paper is focusing on since this would have to be a pathway that is always running, unlike the upper pathological threshold, which would only activate if a microfracture or other cell damaging event took place.

There are hundreds of genes and proteins known to increase or decrease bone in humans^{1,8,21,27,40,46,56,61,63,65,70-73,90,99,108,112}. For the purpose of this research I am focusing only on the characteristics of spatiotemporal paracrine signaling required to organize local remodeling on the micron scale. This includes the mechanisms behind the optimization of a trabecula's width and the mechanisms behind the coupling of osteoblasts to osteoclasts within a single bone remodeling site.

1.3. **Previous Models of Bone Remodeling**

There have been many computer simulations made of various aspects of bone remodeling, using a variety of techniques. A large focus of this research has been geared towards understanding the mechanotransduction pathways that connect load bearing with bone growth along the principal axis of the applied stress^{7,34,74,93}. For example, one group looked at the fluid shear along a long bone during tension and compression, providing evidence that small molecules can be transported through the forced convection flow¹⁰³.

On the cellular scale of the bone remodeling process, one group has simulated the theory that osteoclasts could cause trabecular perforations if they resorb bone based on local microdamage. Using an finite element model and this hypothesis, their simulation suggested that a critical pathological resorption pit size, relative to trabecular width, could exist⁷⁵. With the FEM, they calculated the local mechanical behaviors of the tissue

and extrapolated the cellular behaviors based on a threshold response to that strain. This allowed both the mechanical forces and the cellular activity of osteoclasts to interact within the simulation. However, the behavior of the cells is oversimplified and not strongly grounded in documented osteoclast responses, so cellular processes that may not even exist drive the simulation outcomes.

A common theme in the simulation of bone remodeling is an over simplification of the biology or a mismatch in the real abilities of cells and their actions in the simulation. Cells that have no known ability to sense force are simulated to responding to mechanical strain. Biological responses, such as osteoclastic resorption, are normally the result of multiple cells working through multiple signaling pathways, each requiring their own signaling thresholds and complex geometries. Most computer models use only one round cell and one signaling threshold in order to simulate the whole biological response. An example of trend is the work done to test the hypothesis that osteocytes are capable of detecting applied force by the fluid shear in the canaliculi—part of the larger debate over the osteocytes' proposed role as bone's mechanosensor. Early simulations modeled the osteocyte as a smooth oval stated that any applied load would be below the measured detectable range of osteocytes^{23,98}, discrediting the osteocytes as the bones' mechanosensors. However, when a newer simulations took into account either the shaped of the canaliculi on the nanometer scale and incorporated a more detailed account of the anisotropy of the ECM around the osteocytes, the local sheer and local strain respectively increased by an order of magnitude and entered the measured detection range of osteocytes^{5,13}. Only with thorough and precise representation of the osteocytes were the simulations capable of correctly predicting the feasibility of the osteocytes as mechanosensors.

In order to increase the chance that the simulation would accurately represent bone tissue, the models presented here have endeavored to represent the ECM, cell shapes, local forces, and cell locations at a sufficiently high resolution. ‘Sufficiently high resolution’ is defined as a spatial resolution that is functionally equivalent to the amount of detail that cells use to direct their behavior. In addition, to further increase the accuracy of the simulation past those previously created, all the rules for the agents are supported by primary literature documenting those behaviors.

1.4. Overview of the two Remodeling Simulations

Two different models are presented in this thesis in chapter 2 and chapter 3. The first model is a simulation of osteocytes controlling remodeling via a diffusible signal. The second model is built upon the first model—adding osteoblast agents and simulating the full remodeling cycle—in order to examine the coupling between osteoblasts and osteoclasts.

1.4.1. First Model – Osteocytic Signal for Controlling Resorption

The hypothesis tested in the first model proposes that a simple osteocyte-released/osteoclast-received signal can allow the optimization of bone mass according to the applied force placed on trabecula. In other words, the osteoclasts should be able to resorb the bone that is not required based to support a mechanical load, but the bone should not be allowed to thin to the point where the mechanical load would cause a fracture. Using a series of different initialization parameters, the virtual experiment using this simulation shows that a mechanically stimulated osteocyte signal can dynamically maintain a minimum trabecular width dependant on mechanical load.

The feasibility of this hypothesis serves as a reasonable preliminary question to address while creating the preliminary agent-based model. It is a hypothesis that requires more rigorous examination. Simulating this hypothesis also provides a scenario able to provide feedback on the ability of the model to accurately capture the behavior of three key cell types—the osteoclast, the osteocyte, and the bone lining cell.

1.4.2. Second Model – Osteoclast/Osteoblast Coupling

The hypothesis tested in the second ABM model states that within a physiological range of osteoclast resorption, osteoblast apposition, osteoclast life span, and osteoblast life span, there is a region within that parameter space that will generate stable remodeling. Stable remodeling is defined by: 1) having older bone being replaced by newer bone and 2) having an average trabecular width that stays within a standard deviation of the observed average trabecular width of human vertebra.

The rationale for this specific aim is to determine if remodeling can occur in a coupled fashion—as hypothesized by the current experts in the field of bone biology—when the simulation is constrained by known rates of cell activity, cell locations, temporal patterns, each cell’s abilities, and signaling kinetics. While the simulation cannot prove that this hypothesized mechanism for bone remodeling is correct, it will help determine whether or not it is reasonable. In addition, the virtual experiment can show the relative effects of each of the independent variables on overall bone remodeling within the current hypothesized mechanisms of action. Understanding the effect of individual and/or combinations of biological factors on the resultant shape of the trabecula in the simulation can aid in identifying which factors are critical for normal

maintenance of bone.

2. First Model - Osteocytic Signal for Controlling Osteoclastic Resorption

2.1. Introduction

The simulation starts with a biological model of osteoclasts able to dissolve mineralized matrix and osteocytes able to create a signal that stops osteoclasts when the osteocytes detect their microenvironment bearing a mechanical load. The hypothesis is that this will enable the osteocytes to shield useful bone from being resorbed. This simulation tests whether this one cellular interaction would be enough to explain how osteocytes can allow resorption and thinning of trabeculae when there is an excess of bony matrix, but not allow the trabeculae to become so thin that they risk pathologic fracture.

Dr. Frost's mechanostat theory shows how bone matches the bone mass required to the applied forces. It has remained well accepted through the years, likely due to it being based so heavily on the constant stream of clinical data that came through his hospital. More recently, it has matured into the 'Utah Paradigm' (fig 2.1)³⁷.

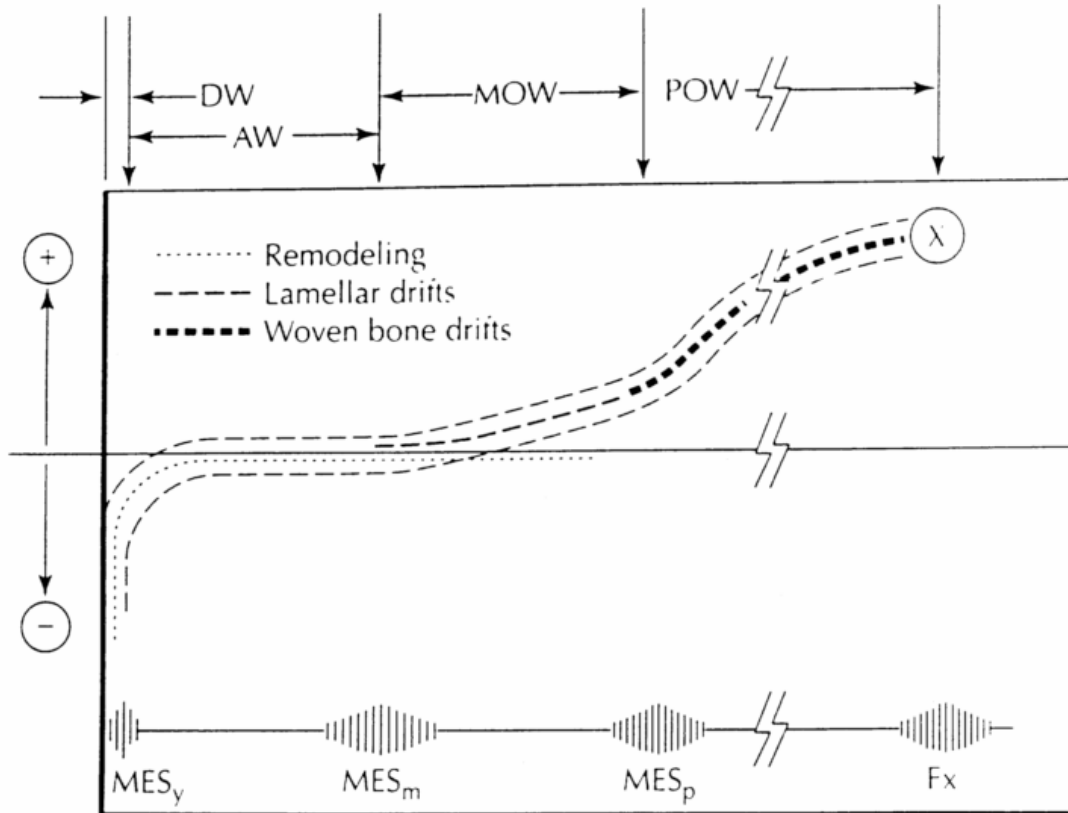


Figure 2.1. The Utah Paradigm, created by Dr. Frost, can explain many of the non-linear bone mass/strength changes that are dependent on applied strains. The bone mass/strength is represented on the vertical axis. The horizontal axis lists a series of strain thresholds, from small to large, with the MES_y threshold being the minimum amount of strain needed to maintain bone remodeling with no net change in bone. MES_m is the minimum strain needed to prompt gains in bone mass (modeling); MES_p is the threshold above which microfractures occur; F_x is the strain needed to cause a fracture. DW is the disuse window; AW is the adapted window where the bone is properly optimized to handle applied loads without damage or extra mass. MOW is the mild overload window while POW is the pathological overload window. In this simulation, the disuse threshold is the same as the Utah Paradigm’s MES_y threshold, under which the strain is low enough that the bone is considered to be in a state of ‘disuse’. Reproduced from Frost³⁷.

Most literature has focused on the mechanisms behind the modeling and pathologic strain thresholds, since there is compelling evidence that osteocytes can sense damage and send signaling molecules—such as NO or apoptotic bodies^{59,107}—which will cause osteoclasts to home in on the damaged areas of bone. However, the MES_y threshold—the threshold below which the bone losses bone mass during remodeling—is

very important for all research involving the maintenance of bone mass in situations where the patient goes through a period of reduced activity. This includes bed rest, space flight, or paralyzing damage. In order to optimize the skeleton's mass, bone that is larger than needed has to be resorbed until it is just large enough to support the range of applied loads used in normal activity.

It is very likely that osteocytes are the mediators of this mechanical threshold—both sensing the mechanical forces and relaying this information to the remodeling cells. No other bone cell has demonstrated the ability to respond to fluid shear or local strain to the degree the osteocyte has. Also, the osteocytes are well positioned to relay information to osteoclasts since they exist everywhere in the bone where the osteoclasts attach; they extend dendritic processes out to the surface that would enable direct communication with cells attaching to the bone. Therefore it is logical to assume that the osteocytes are sensing this threshold and relaying it to remodeling cells. They could be relaying this information to osteoclasts, osteoblasts or both in order to either call for or permit bone remodeling with a net positive or net negative change in bone mass.

This first model proposes that a simple osteocyte-released and osteoclast-received signal could allow the optimization of bone mass according to the applied force placed on the trabecula. The osteocytes should be able to sense when the trabecula is thinning to the point where that width of bone is necessary to support the applied force, at which point the osteocytes will protect that bone with a diffusible signal. Osteoclasts should be able to resorb the bone that is not required based to support a mechanical load, but the bone should not be allowed to thin to the point where the mechanical load would cause microfractures, and so will not resorb when they detect the osteocytes'

signal. If the osteocytes die from microfracture or old age, the aged bone will still be resorbable.

Using a series of different initialization parameters, the simulation shows that a mechanically stimulated osteocyte signal can dynamically maintain a minimal trabecular width dependant on by mechanical load.

2.2 Methods

2.2.1. Software

This ABM was built in NetLogo v4.0.5 freeware (from the Center for Connected Learning and Computer Based Modeling, Northwestern University)¹⁴⁵. NetLogo allows for the creation of multiple agents than can either be free-moving through geographical space or fixed into grid locations.

2.2.2. Agent-based model

The agent-based model presented here is formed in NetLogo, out of a 2D grid composed of ‘extracellular’ (ECM) agents and mobile ‘cell’ agents. The ‘extracellular’ agents represent the non-cellular components, such as mineralized bone or marrow. The ‘cell’ agents fall into three classes: osteoclasts, bone lining cells, and osteocytes. One length of trabecular strut is being simulated in each run, and since they these struts are normally cylindrical and transversely isotropic, a simple 2D plane should be sufficient to capture the basic spatial dynamics.

The goal of the simulation is to better understand how varying different parameters can effect changes in trabecular width and the risk of breaks—as defined by

the trabecula being resorbed all the way through its whole width. Breaking a trabecula in this manner is significant since there is no known way the bone can fix this when it occurs. By matching the initial parameters to physiologic conditions and comparing the simulation's outputs with observed behavior of real bone, the simulation can show the strengths and weaknesses of the osteocyte shielding-signal hypothesis to explain bone remodeling. The simulation can provide evidence for whether the hypothesis can feasibly explain the disuse threshold.

The key variables that can be changed during initialization of the ABM are *trabecular thickness*, *osteocyte density*, *force* placed on the trabecula, and the *threshold level of force* required for the osteocytes to start producing their shielding signal.

The agent-based model presented here is formed in NetLogo, out of a 2D grid composed of 'extracellular' (ECM) agents and mobile 'cell' agents. The 'extracellular' agents represent the non-cellular components, such as mineralized bone or marrow. The 'cell' agents fall into three classes: osteoclasts, bone lining cells, and osteocytes. One length of trabecular strut is being simulated in each run, and since they these struts are normally cylindrical and transversely isotropic, a simple 2D plane should be sufficient to capture the basic spatial dynamics. Once per cycle all the ECM and cell agents go through their particular rule set one time (fig 2.4).

Each ECM grid space has a *mineral* component and an *organic* component that is set on a scale from 0 to 10. The marrow ECM agents are defined as having zero for both of these variables. Fully mineralized bone has 10 for each variable. Each ECM agent has a variable for the amount of *force* in that location and the amount of *signaling*

molecule in that area. The ECM agents, since they represent inanimate material, only have a rule set for evenly diffusing the *signaling molecule* and calculating the estimated *force* passing through that location in the trabecula (fig 2.8). The ECM agents start with an initial pattern of one column of ‘mineralized’ agents with a uniform, user-specified width in the middle of a torus of empty ‘marrow’ agents. The collection of ‘mineralized’ ECM grids is considered the trabecular region. The average trabecular width is calculated as the number of mineralized ECM grids in each row divided by the total number of rows in the simulation. For the virtual experiment, the size of the trabecula was set to be equivalent to the width of human trabeculae, which ranges from around a dozen microns in cases of osteoporosis to 140-300 μm in the iliac crest^{83,87}. Width depends both on the health of the individual’s bones as well as location, so there is no one ‘normal’ average width (fig 2.2). For the virtual experiments simulating just osteocytes and osteoclasts without bone lining cells, the widths correspond to a mildly osteoporotic trabecula, an average trabecula in a long bone, and a trabecula within the upper range of normal width. The virtual experiments looking at the effects of bone lining cells use a trabecular width in the normal range of healthy long bone epiphyseal trabeculae.

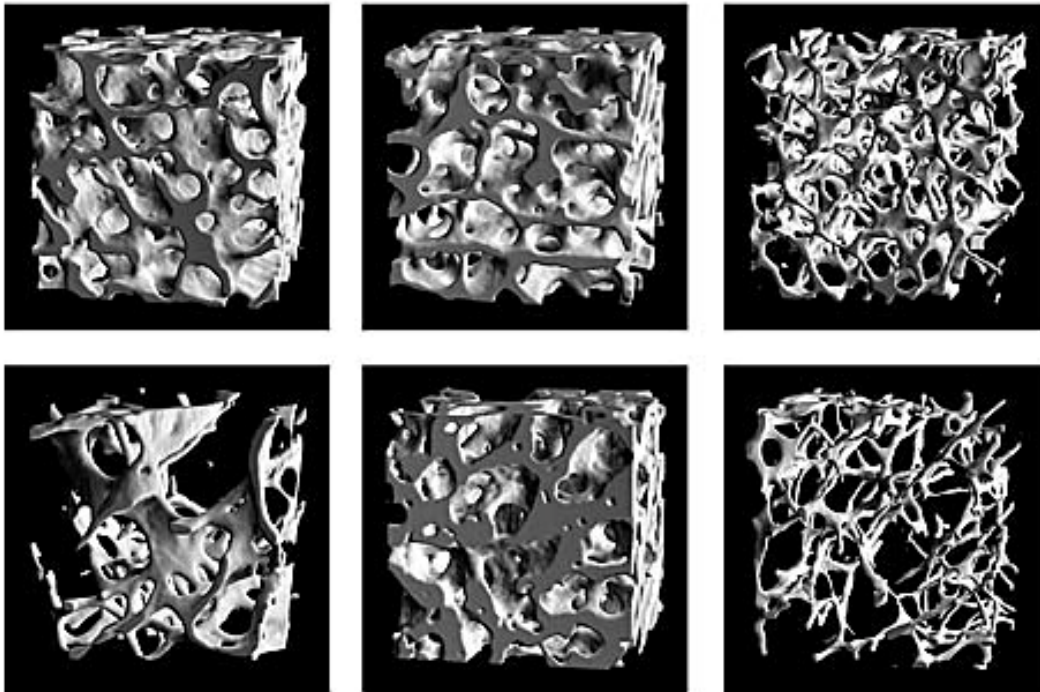


Fig 2.2 A set of six different CT-scans of trabecular bone biopsies showing trabecular architecture differences among three different anatomical locations (iliac crest, femoral head, and lumbar spine), and between two differently aged men (37 vs. 84 yrs). Reproduced from Müller⁸⁰.

The osteocyte agents are created when the model initializes. They are distributed evenly on top of random mineralized ECM agents at a population density roughly in the mammalian range (fig 2.3). As with trabecular width, this figure can vary drastically from location to location and subject to subject. Studies have shown that osteocyte lacunae density is anywhere between 800 per mm^2 and 60,000 per mm^3 ^{44,76}. This puts the densities used in the simulations in a similar range to that found in human bone, though erring on the higher end of the range. It is also worth noting that since the osteocytes are placed using a pseudorandom algorithm, they are spaced out as if they would be in woven bone. In normal lamellar bone, the osteocyte lacunae are spaced more evenly apart.

For the osteocyte rule set, since real osteocytes cannot move through bone—they are literally cemented into place within bone—the osteocytes agents in the model have a geographical location but do not move. During the simulation, they check the force variable of the ECM grids where they are located, and if the force is above a certain user-defined threshold, they will “send out” a shielding signal by increasing the *signaling* variable in the nearest ECM grid by 20 units (fig 2.5). If the osteocyte is located on an ECM grid that changes states from mineralized to marrow, it will die; this mirrors how an osteocyte released from the bone during resorption will apoptose.

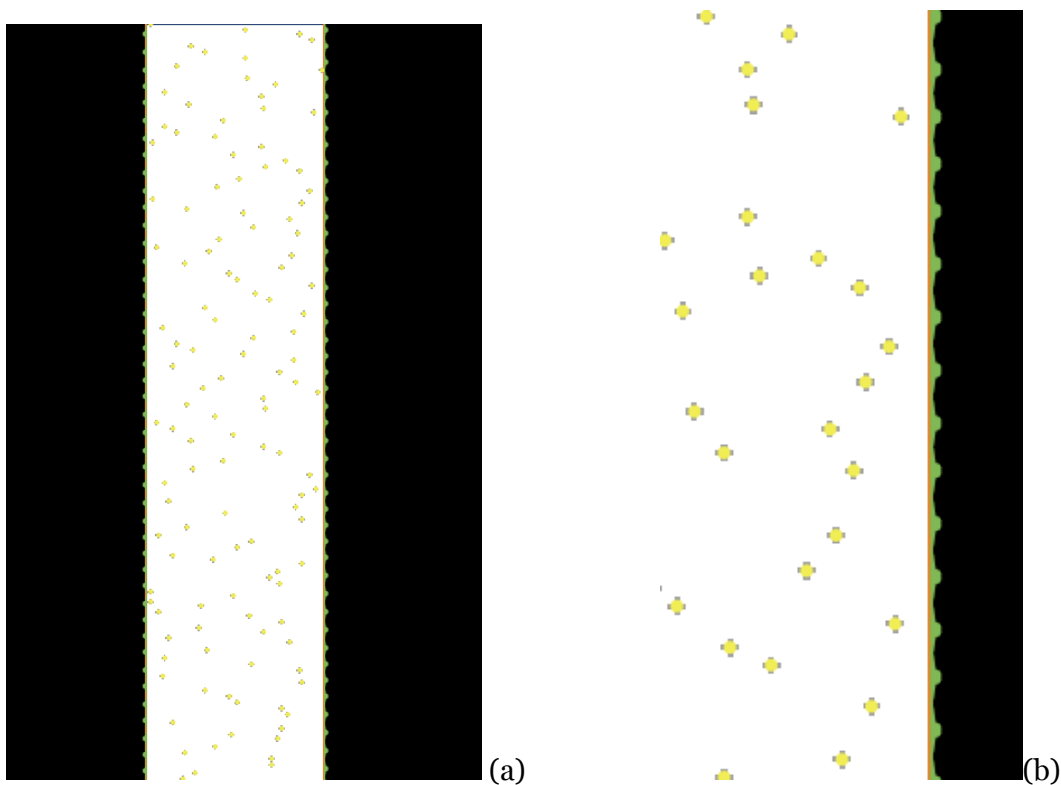


Figure 2.3a and 2.3b. The ABM is initialized with a trabecular region composed of ECM agents that are in a ‘mineralized’ state (labeled white), surrounded by ‘marrow’ ECM agents. Within the trabecular region, osteocyte agents are randomly distributed. The green agents represent the bone lining cells. The figure on the right shows a magnified view of the initialized trabecula.

The osteoclast agents are initially located in the middle of the marrow ECM area and are capable of randomly walking one step each cycle (fig 2.7). They can have one of two states: inactive or active. In the model without bone lining cell activity, the osteoclast agent is initialized as inactive and will only become active if they walk onto an ECM grid that is mineralized. In the simulations where bone lining cells (BLC) are functional, the BLCs are required to lift off the surface of the bone before the osteoclast can pass through the layer of bone lining cells. As strange as it sounds for a giant multinucleated cell to squeeze through a monolayer of cells, there is clear *in vitro* evidence of mature osteoclasts transmigrating through layers of osteoblastic cells⁹⁸. While the simulation is running, if the population of inactive osteoclasts falls below a certain number, a new osteoclast is added to the simulation in order to preserve the pool of osteoclast agents.

If active, the osteoclast agent will first check for *the shielding signal* in the ECM grid at that location. If this *shielding signal* variable is above zero, the osteoclast will die. If not, the osteoclast agents will “release” *cathepsin k* and *acid* into the three ECM agents at the interface between the osteoclast agent and the mineralized ECM surface. The *cathepsin k* and *acid* variables are stored in the ECM agents the same way that the *signaling molecule* variable is stored. When the *cathepsin k* or *acid* variables are non-zero, these variables are allowed to diffuse to neighboring, non-mineralized ECM agents. The *cathepsin k* will decrease the amount of *organic* component in each ECM agent and the *acid* will decrease the amount of *mineral* in each ECM agent. The *cathepsin k* variable reduces the *organic* variable at a different rate than the *acid* variable reduces the *mineral* component. The parameters for this process have been set so the resorption pit is an average of 15 microns wide and 10 microns deep, with the histologically

observed blurred edge^{30,66,104}. The osteoclast was also given a short lifespan once activated, correlating with its average 16-day lifespan³⁶. The osteoclasts are also unable to bind to bone well enough to release the cathepsin k and acid if there is a layer of non-mineralized matrix under their bottom edges, as seen in the literature²².

The bone lining cells (BLCs) here are described by flat agents that rest on the surface of the trabecula. It is uncertain what percentage of the surface they cover in real bone since they are thin enough to be effectively invisible under most microscopes⁶⁶. They are sized at roughly 20 microns across and have the ability to communicate with nearby osteocytes³¹. They do not produce a diffusible signaling molecule to halt osteoclasts, but if they detect a nearby osteocyte or neighboring BLC that is signaling for osteoclasts to halt, the bone lining cell will not lift off the surface of the bone to allow the osteoclasts to resorb (fig 2.6). These cells also cannot sense mechanical forces in this simulation. There is no compelling evidence for a mechanism that would allow BLCs to detect forces and previous simulations have shown that they would not be able to respond to changes in the direction of principal load as well as osteocytes⁷⁸. In this simulation, bone lining cells do have the ability to attach back onto the surface of the trabecula after the osteoclast agents leaves, as well as the ability to break down remaining demineralized organic components, since this is a relatively well-known behavior of bone lining cells³⁰.

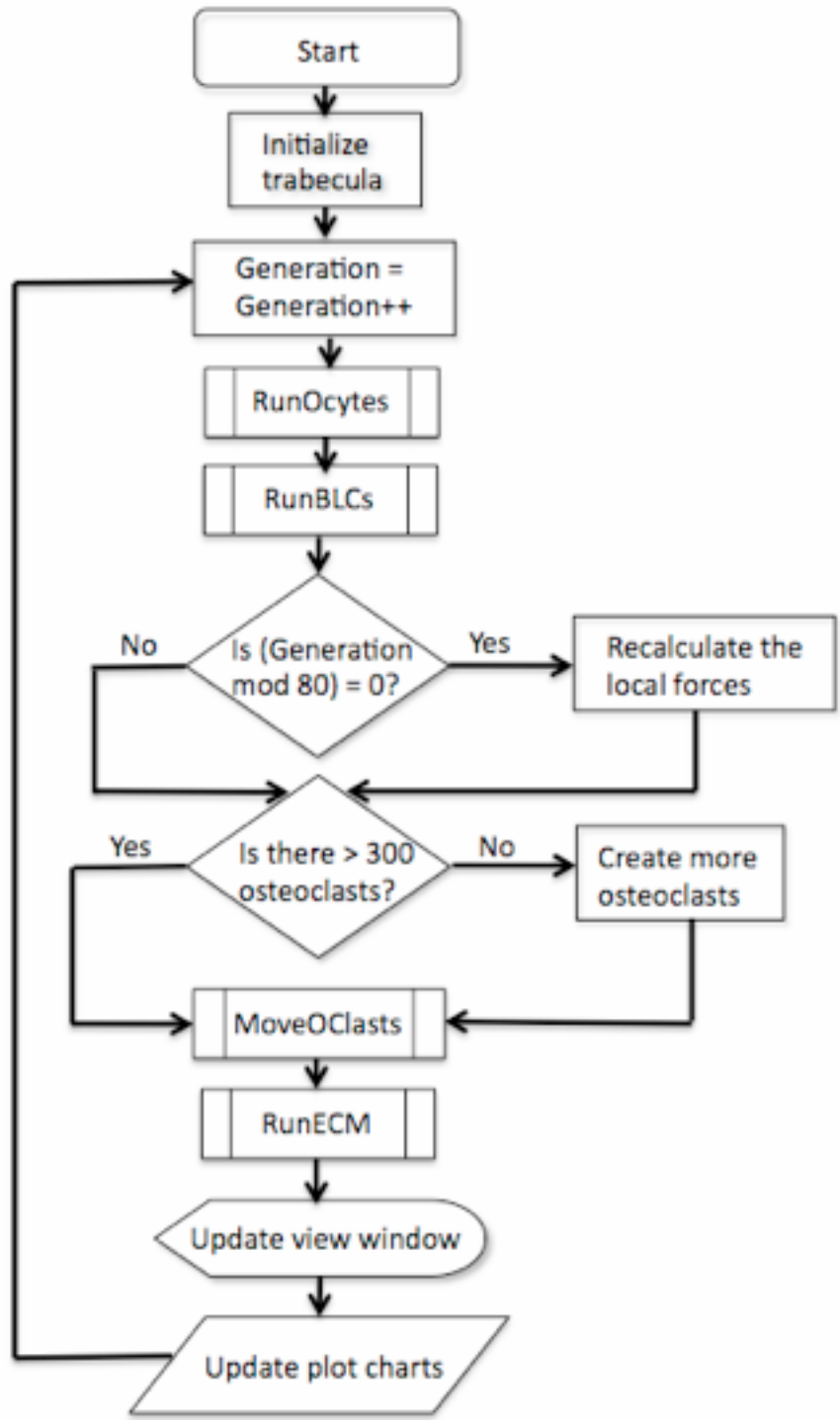


Figure 2.4. A flow diagram of the main body of the ABM code. The double rectangles represent subroutines. Each cycle represents one time through the loop shown above.

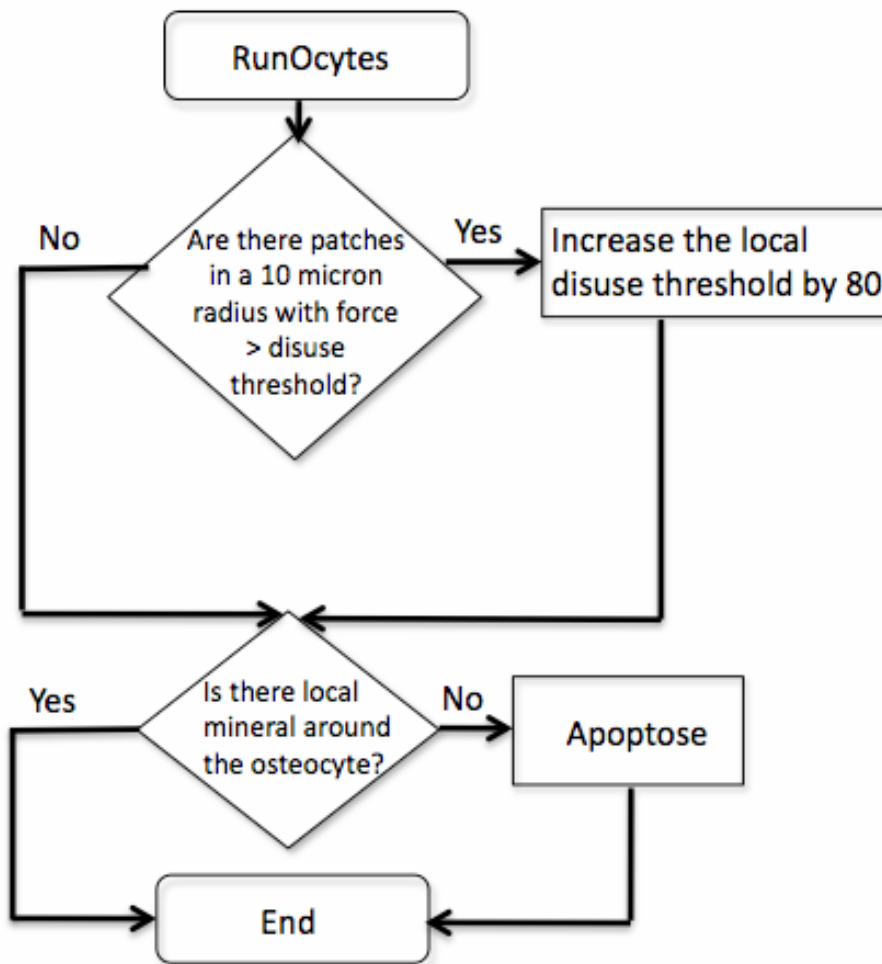


Figure 2.5. A flow diagram of the code run by all osteocyte agents.

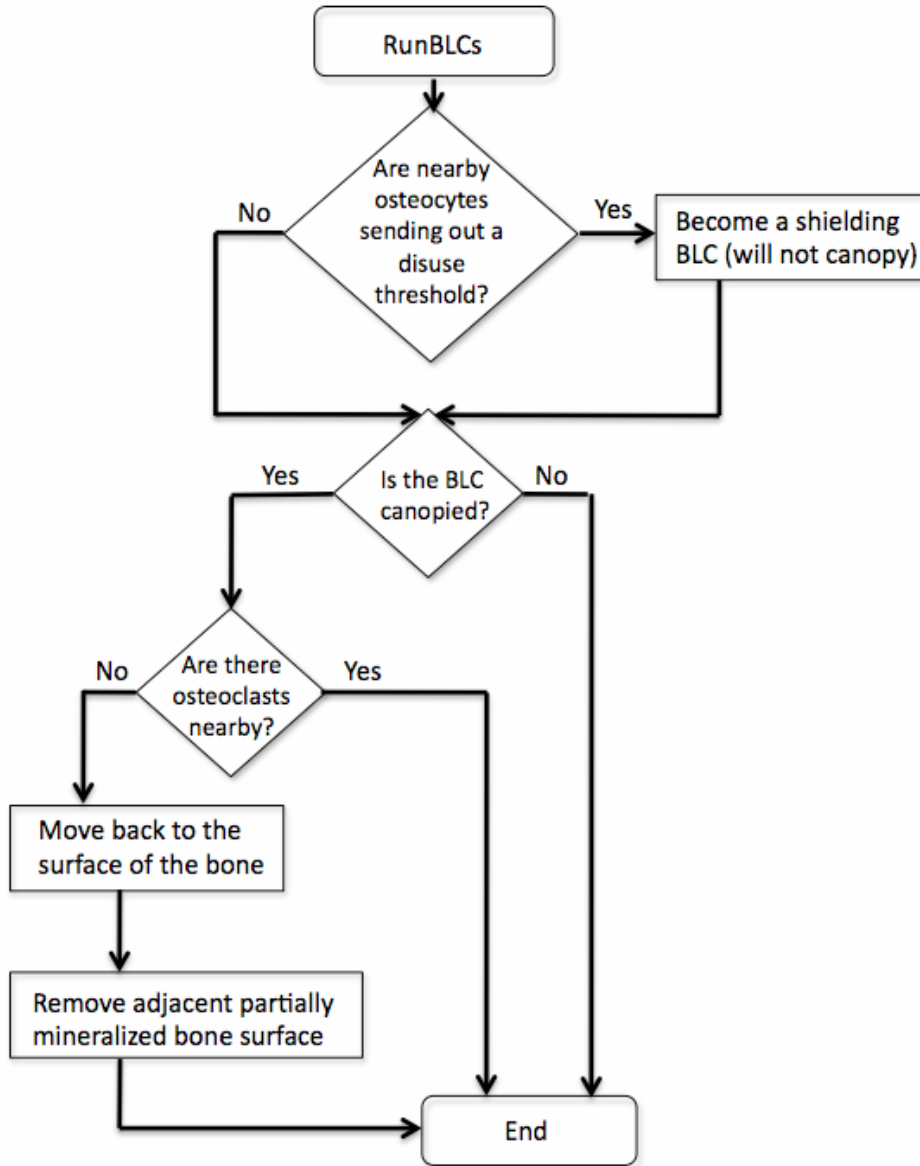


Figure 2.6. A flow diagram of the code run by all active BLC agents. If the BLC agents are not active, they only ask the question ‘Are there osteoclasts nearby?’.

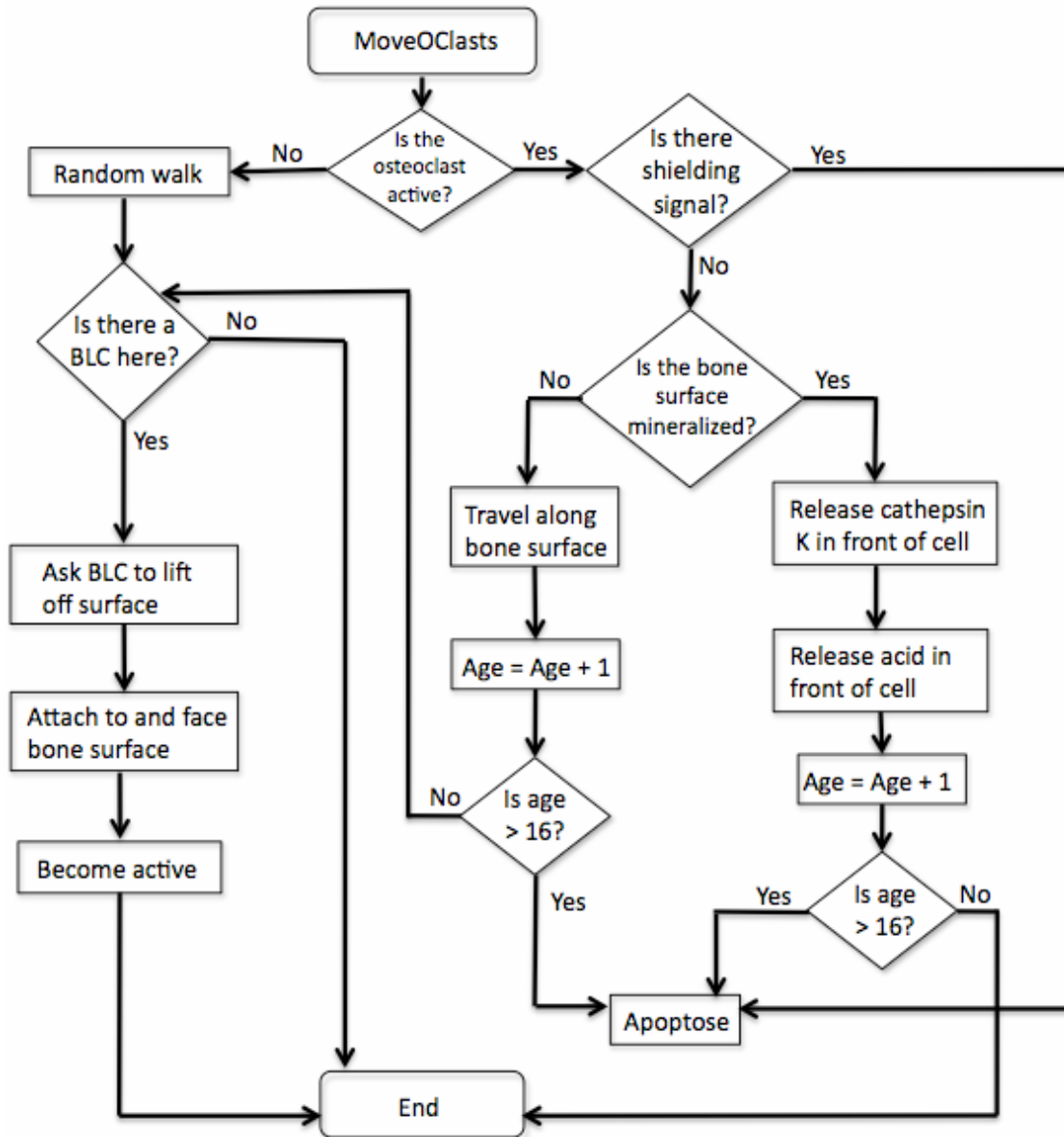


Figure 2.7. A flow diagram of the code run by all osteoclast agents.

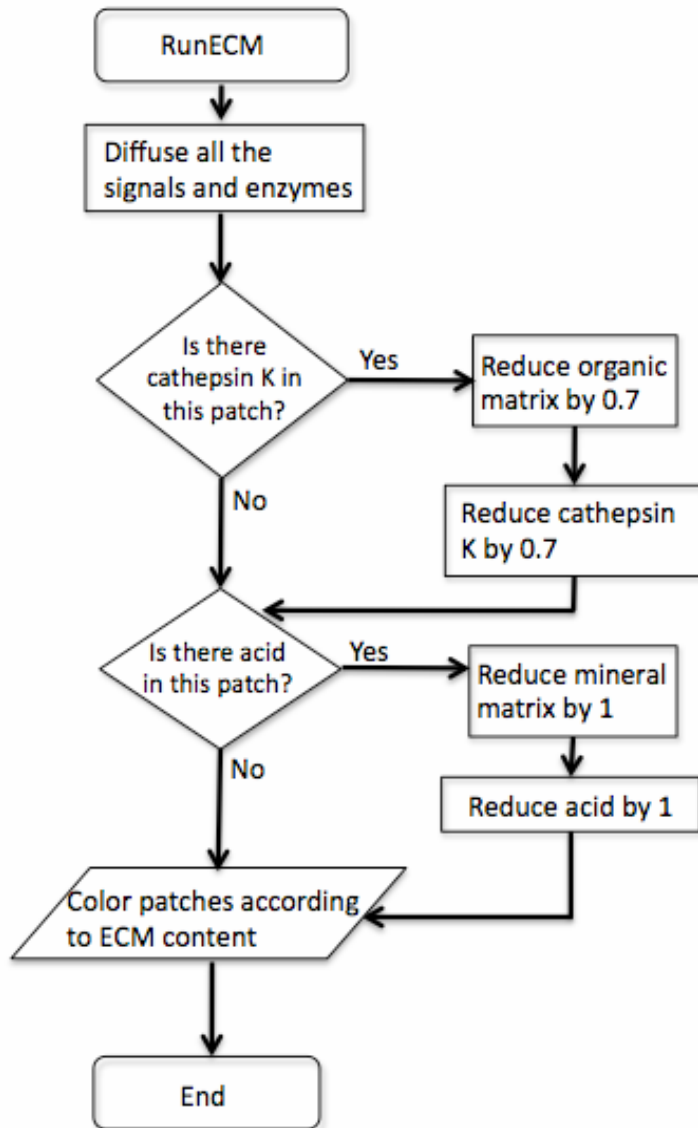


Figure 2.8 A flow diagram of the code run by all ECM patches.

2.2.3. Simulation setup and initial conditions

The simulation was run until the average trabecular width stabilized or the column 'broke' by being resorbed completely through its width by osteoclasts. In bone, when a trabecula develops a perforation, unless a micro-callus is initiated, it corresponds to failure of the trabecula since it would then bear no load. This is a major problem for many osteoporotic patients where the number of trabeculae in their bones reduces and

the bones weaken. The simulation's average run time was 5000 cycles; the run time needed was largely dependent on the difference between initial and ending widths. When there were no bone lining cells, the run times could be as long as 25000 cycles before the average width stopped decreasing. In the model, one grid square corresponds to one micron, which allows the outputs to be in units of microns. The ending width of the trabecula, the percentage change of trabecular width, and the number of trabecular perforations are the three measured outcome variables for each simulation. The standard deviation is calculated with the replicates with the same starting conditions. The minimum number of replicates was twelve, but in cases with higher variability in their outcomes, more replicates were added. This was particularly important in order to calculate the percent chance of a perforation occurring.

The default parameters for the model were based on qualitative estimates from histological slides of healthy human trabecular bone (table 2.1). The default population density of osteocytes in the trabecular region was 0.00379 per square micron. The default threshold amount of force that the osteocytes needed to detect before releasing the shielding signal was 16, which if the trabecula were correctly reduced to the minimal width, would correspond to a 30% reduction in area. The width of the trabeculae ranged from 20 microns to 100 microns. Neither the time-scale nor the osteoclast count in the model were calibrated to any particular condition. The osteocyte density and trabecular width were evenly spaced along a physiological range that incorporates normal values as well as high and low extremes.

Each set of initial conditions were run at least twelve times in order to create enough replicates and gauge the reproducibility of the results. In the case of high

standard deviation, particularly in the percent chance of full-thickness resorption or ending width, the number of replicates was increased. Only one key variable was varied at a time, and so a complete response surface was not mapped out. The goal of this virtual experiment was not to optimize initial conditions, but instead to challenge the osteocyte-shielding hypothesis's ability to maintain trabecular thickness given various initial conditions correlated to physiological conditions. By varying the independent parameters, their influences on the output variables can be identified, similar to how an over-expression or under-expression of a gene illustrates the effect of that gene *in vivo*¹⁴.

Table 2.1. Experimental Setup for Osteocyte Shielding virtual experiment, based on physiological measurements^{9,77,79}.

Independent Variables	Number of Test Cases	Values Used
Initial trabecula width	5	20, 40, 60, 80, 100 microns
Osteocyte sensitivity (local force needed to trigger signaling)	2	16 – (creates a 30% reduction in width) 22 – (creates a 50% reduction in width)
BLC activity	2	Able to shield or not able to shield
Osteocyte population density	5	0.00379/ μm^2 (normal density); 0.00305/ μm^2 (low density); 0.00227/ μm^2 (very low density); 0.00420/ μm^2 (high density); 0.00835/ μm^2 (very high density)
Control Variables	Number of Test Cases	Values Used
Osteoclast location	1	Center of marrow (Bianco, May 2011)
Osteocyte location	1	Evenly distributed in trabecula (Mullender, 1996)
BLC location	1	On trabecular surface (Miller, 1987)
Preosteoclast population	1	50 agents
Length of Trabecula	1	400 microns
Mineral / Organic Component of Trabecula	1	10 / 10
Resorption Pit Size	1	10 microns deep, 15 microns wide
Dependent Variables	Number of Test Cases	Values Seen in Literature
Ending Average Width + Std Dev	-	15 to 300 microns
Trabecular Perforations (breaks)	-	0
This is a 55 case experimental design (Inactive BLCs were only run at normal osteocyte density)		
The simulation will run 12 times for each test case, with a average runtime of 6,000 cycles		

2.2.4. Methods of Analysis

Both the initial trabecular width and the osteocyte density were varied at two different osteocyte mechanosensory thresholds. The effect of BLC activity was also simulated across all five widths. The dependant variables of average final width, the

number of trabecular perforations, and the time it takes the width to stabilize were collected with twelve replications each.

In trabecular bone, perforating the trabecula can lead to its complete resorption since without surface on which to adhere, osteoblast cells are much less likely to activate and deposit bone matrix. Also, when the trabecula is perforated, it is mechanically unloaded, which tends to lead to the resorption of the remaining two halves. For this reason, the simulations that ended with trabecular perforations were considered as having failed to properly control bone resorption. Since the simulation is too preliminary to quantitatively match measured bone pathologies or normal remodeling, the model was analyzed based on trends in the effect of the independent variables on the dependant variables rather than a quantitative matching of the dependent variables to measured values in the literature.

2.3. Results

2.3.1 Osteoclast regulation through surface changes

Before the osteocytes could try to defend bone from osteoclastic resorption, the osteoclast resorption patterns had to be correctly simulated. In particular, it was important to generate the shape of the Howship's lacunae rather than tunnels into the bone (fig 2.9). The regulation of the shape of the resorption pit was caused by the presence of demineralized matrix accumulating during resorption, based on the different activity rates of the cathepsin k and acids. It was previously theorized that broken-down bone products released from the bone would be required to halt the osteoclast's progress down through the bone. However, due to the location and relative surface area where osteoclasts release the enzymes versus where they attach to the surface of the bone, the

osteoclast agents were able to resorb a correctly shaped pit before literally breaking down the mineralized matrix to which they were attached. This allows them to switch to a migratory state and move across the surface until they find a location that had enough mineral exposed to allow for re-binding to the surface.



Figure 2.9. A magnified view of the trabecular surface with the osteoclasts shown in red, the osteocytes in yellow, and demineralized matrix show in shades of grey and blue according to the degree of demineralization. The classic scalloped shape can be seen on the edge where an osteoclast had started eating away at the surface.

2.3.2 Ability of osteocytes to shield bone from resorption

As the simulation runs, the osteoclasts resorb bone until the trabecula reduces in size enough that the applied force is above the threshold that osteocyte agents can sense. When under sufficient force, the osteocytes produce a signal that prevents osteoclasts from activating. When there are no longer any places for osteoclasts to attach, activate, and resorb, the value for the remaining width becomes constant and the simulation is finished (fig 2.10).

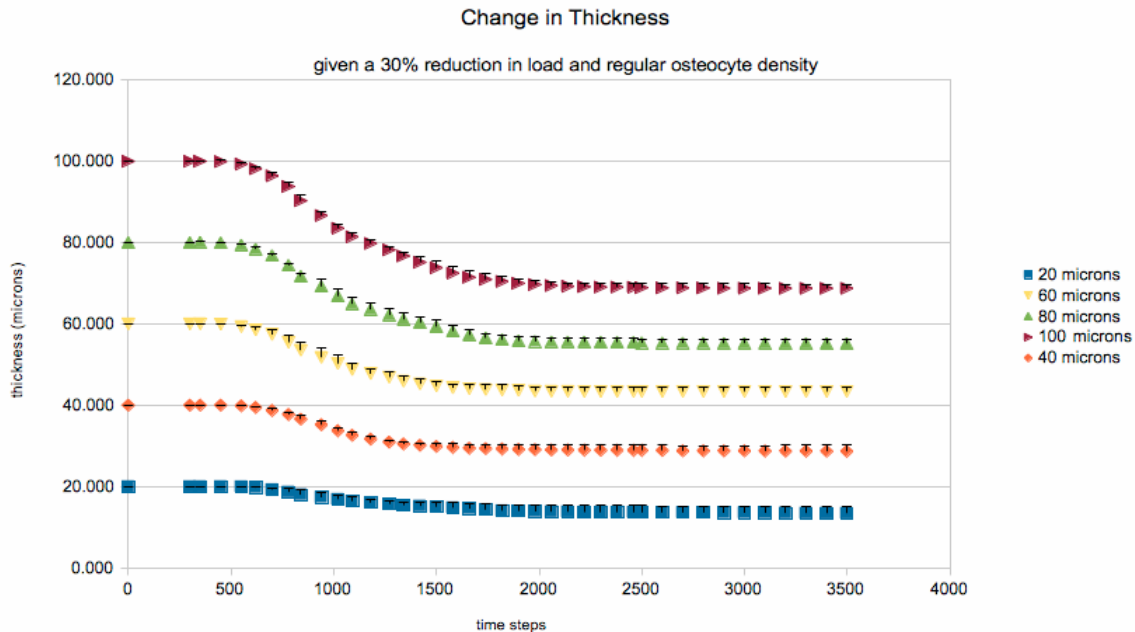


Figure 2.10. The average width will gradually decrease as osteoclasts resorb through the bone and will gradually stabilize at a final width once all the osteocytes are sending a signal that prevents osteoclast activation.

Each width of trabecula had a proportional amount of force placed on it, so the same osteocyte threshold should allow the same proportional amount of resorption. The percent widths over time did overlap (fig. 2.11 and 2.12), and the rate at which the percent change in width reduced was the same across all the initial widths. The most significant differences among the different plots of width over time were the standard deviations, which increased as the initial trabecula became thinner—particularly when the trabecular started out thinner than 40 microns (fig 2.12).

The virtual experiment found that the ending average percent change in width for all the simulations were statistically the same across almost all widths and osteocyte densities given the same osteocytic force threshold (fig 2.11). The change in osteocyte population density did not change the relative time it took to stabilize at either 70% initial width (fig 2.11) or 50% initial width (fig 2.12). The only exception to this was the

combination of very low osteocyte density and low starting widths. The factors that were dependant on both width and osteocyte density were the standard deviation of the ending width and the number of times the trabeculae ‘broke’ by being resorbed all the way through the width—which was the source of the standard deviation (fig 2.15).

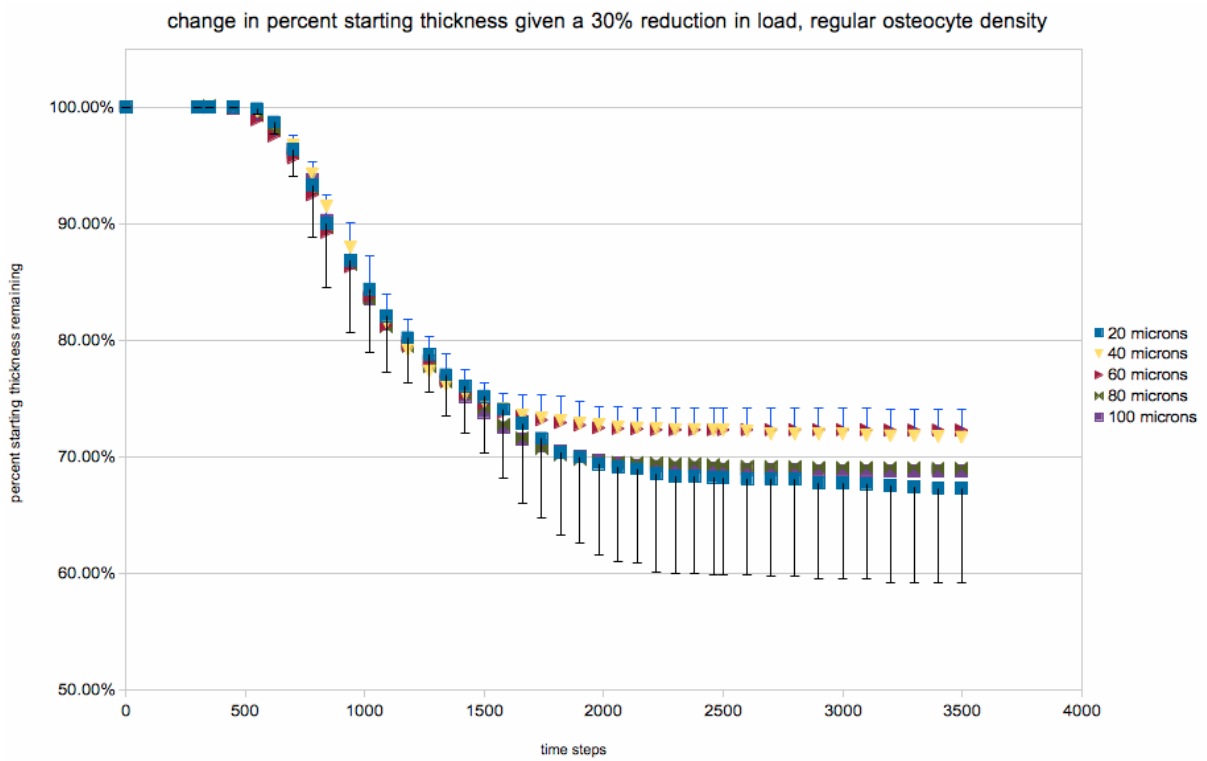


Figure 2.11. The normalized change in width to overlap. The smaller the initial width, the higher the standard deviation.

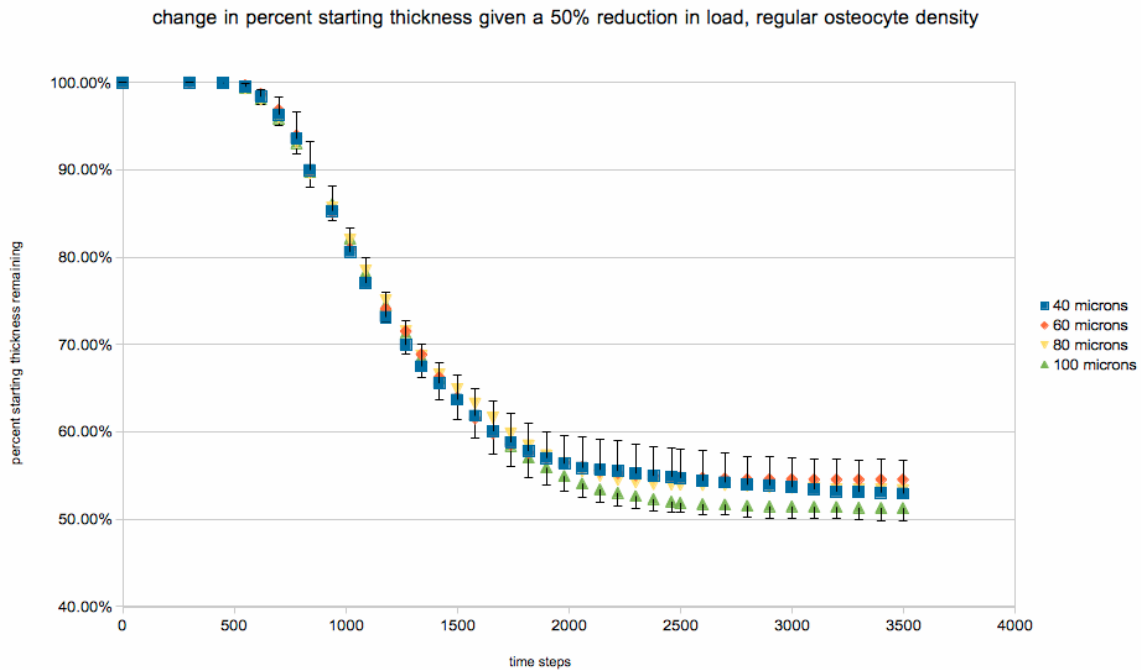


Figure 2.12. The change in average percent width occurs in the same pattern with less sensitive osteocytes as it does with osteocytes that more quickly signal.

The lower the initial width, the less room there was for error. The destruction of one osteocyte before it could start producing the shielding molecule could leave an area of the trabeculae unprotected from resorption even through the local forces were high within the matrix. Having a low osteocyte population density nearly guaranteed this failure, but with high osteocyte densities, there were enough osteocytes that even the thinnest initial widths had only a very slight chance of ‘breaking’ (fig 2.13).

of full-thickness resorptions for different osteocyte population densities and starting widths

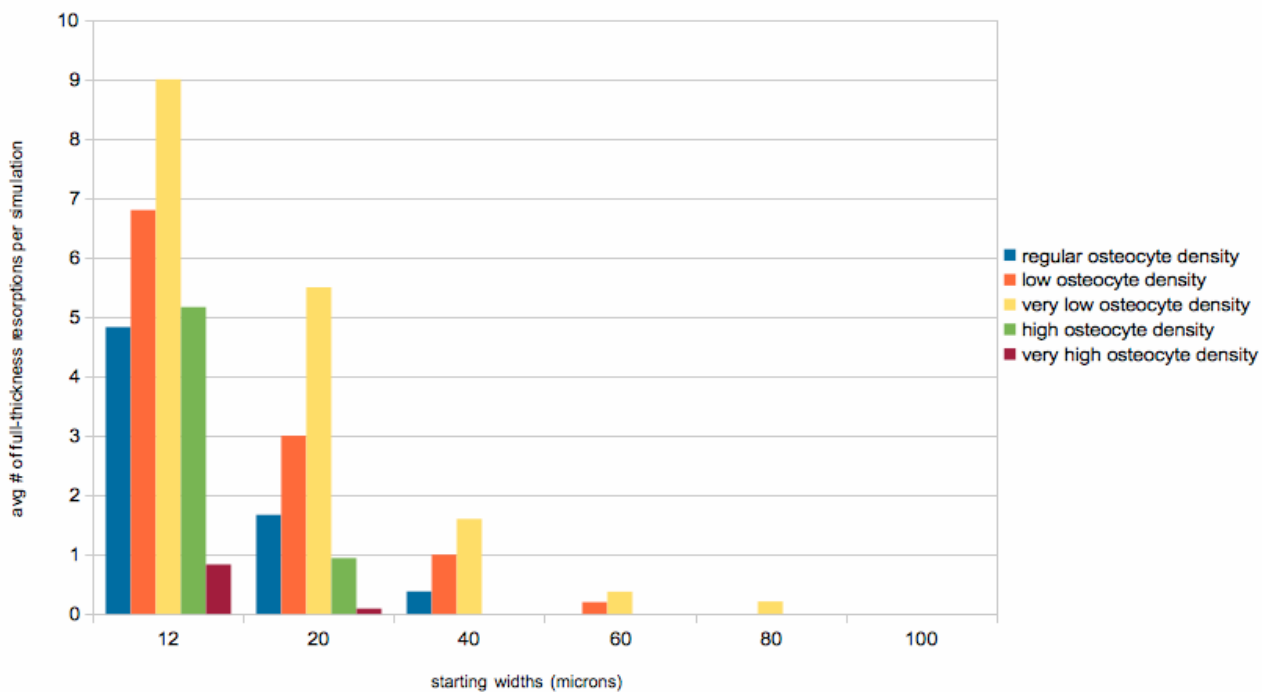


Figure 2.13. The number of times the trabeculae is resorbed all the way through the width is dependent both on osteocyte density and starting width.

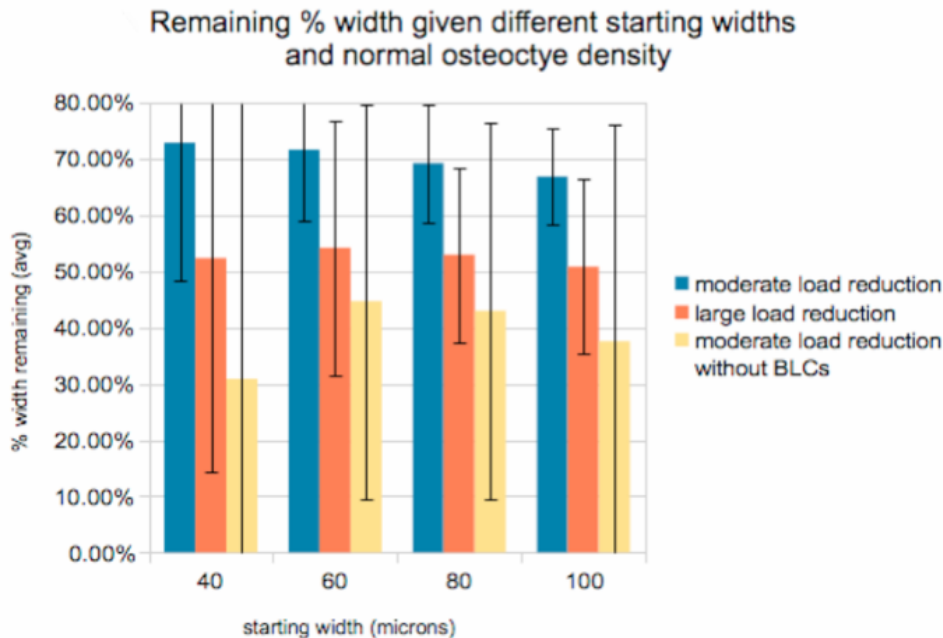


Figure 2.14. The blue and orange groups both have bone lining cells and can approximate both the 70% and 50% reduction in widths within a range of initial thicknesses. The less sensitive osteocyte threshold created a higher standard deviation, but it did not compare to the standard deviation in the group without the bone-lining cells.

The lack of BLCs causes a larger amount of variability and instability in the remaining width than any other factor tested (fig 2.14). Even at one hundred microns, the osteoclasts were able to resorb through the width of some locations along the trabeculae (fig 2.15, 2.16). This causes an enormous increase in the standard deviations at each location and a significant increase in the percent of simulations where the trabeculae broke. Without BLCs, the model stabilized into a final average width, but it was lower than anticipated since the osteocyte signaling threshold used was the one that would otherwise cause only a 70% reduction in size. Instead of a 30% reduction, the size of the trabeculae stabilized at more than a 65% reduction (fig 2.14).

The complete set of tables summarizing the results of the virtual experiment can be found in the appendix. The calculated coefficient of variation for standard deviation of the average width shows a clear correlation with the initial width, reducing with the

increase of the initial width (tables 2.1A - .

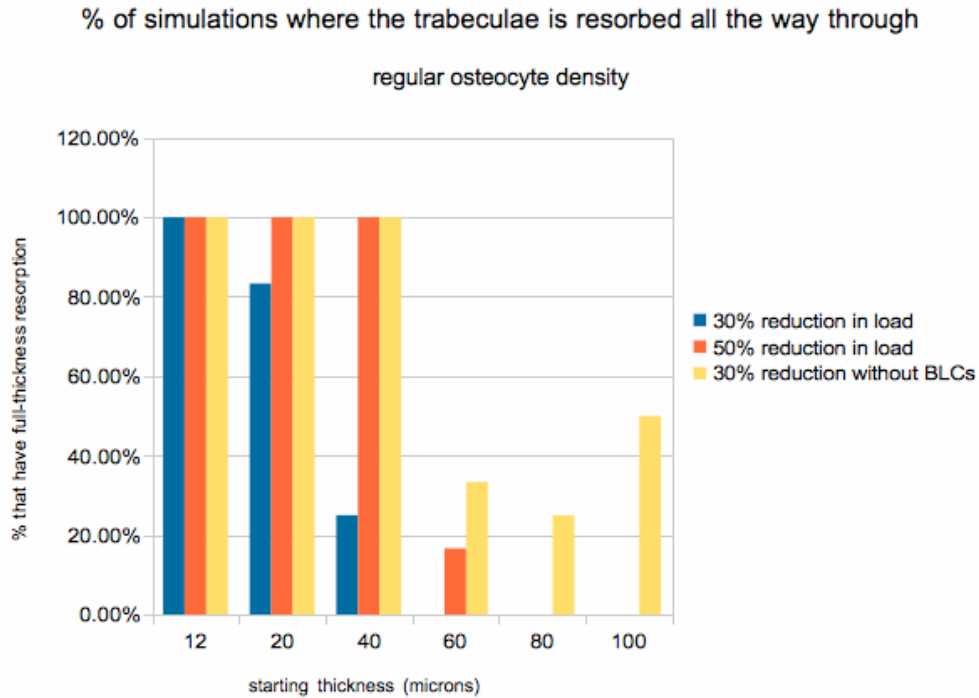


Figure 2.15. In both of the simulations with bone-lining cells, the chance of having a trabeculae break was proportional to the starting width. The lower the starting width, the less room there was for error and the greater the chances of an osteoclast resorbing all the way through.

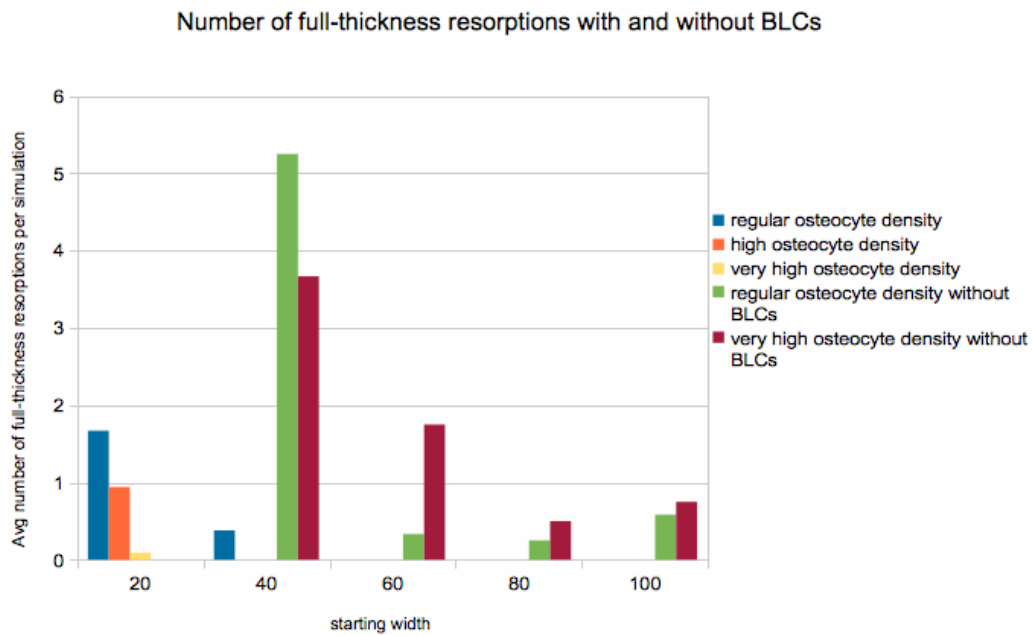


Figure 2.16. The simulations with BLCs and without BLCs show width dependant rates of breaking, but with bone-lining cells, that rate is zero past 40-60 microns wide.

Without bone-lining cells, it occurs so often at 40 microns that the 20 micron was not worth running.

2.4. Discussion

2.4.1 The effectiveness of osteocyte signaling

The simulations shown here show that just two or three cell types and one diffusible signal are able to preserve a trabecula's width above an optimized minimum based on load placed upon the bone. The ability of the simulation to dynamically tailor the trabecular thickness based only on the osteocytes' threshold level of force detection lends credence to the idea that one osteocyte-osteoclast signal could effectively safeguard the lower limit of trabecular thickness. This hypothesis provides a feasible mechanistic explanation for the disuse, or MES_y , threshold. There is clear evidence in the medical literature that a small amount of strain on bone per day is enough to prevent resorption, even if it is not enough to trigger deposition of mineralized matrix⁴¹. This model describes a mechanism that can mimic this effect while confined by the known ability and location of the cells. It is also observed that trabeculae thin over the lifetime of the patients, and that bone cells—including osteocytes—decrease in activity and sensitivity with age. The set of virtual experiments that changed the threshold signaling value of the osteocytes offers a mechanism for the correlation between decreased osteocyte sensitivity and thinning trabecular structures.

Looking at the standard deviations among the various osteocyte densities versus the other initial conditions, the model also shows that much of the randomness and variance in the simulation outcomes comes from the placement of the osteocytes within the trabecula, and not the randomly located activation of the osteoclasts. This is a somewhat unexpected result, for while the osteocytes are in different locations each simulation run, they qualitatively appear well and evenly distributed across and along the trabecular region, even in the cases of lower population densities.

It also appears from this model that bone can best use mechanical forces to greatly alter and optimize trabecular structure if there is a high density of osteocytes initially present, without needing the osteocytes to be any more sensitive to changes in strain. This could explain why woven bone, which is meant to be temporary and drastically remodeled, has a much higher osteocytes density than regular lamellar bone.

2.4.2. The kinetics of resorbing bone and its effects on Howship lacunae

The periodic resorptive and migratory behavior of the osteoclasts can be generated by the different activity rates of the cathepsin K and acid breaking down the organic and mineral components, respectively. Osteoclasts' preferred attachment to mineralized bone is well documented; they do not sufficiently seal onto collagenous surfaces^{18,98}. There have also been studies that show when cathepsin K activity is increased to match the rate of demineralization, e.g. under the influence of glucocorticoids, the resorption pits become unnaturally deep and the osteoclasts stop migrating normally^{98,105}. When the rule set for the osteoclast agents was first being developed, the rate of organic resorption and mineral resorption was the same, and the osteoclasts resorbed straight through the trabecula. The osteoclast rule set underwent a series of iterative revisions, making the cell shape, size, and enzymatic activity more precisely constrained and matched to literature values. The only literature-based adjustment of the osteoclast rule-set that produced morphologically accurate resorption pits was the calibration of the relative enzymatic rates of organic proteases and mineral breakdown, as well as the preferential resorptive binding to mineralized surfaces. This result supports the theory of Delaisse's group that the balance between the migratory and resorptive states of osteoclasts are regulated by the relative activity levels of the

different enzymes involved breaking down bone¹⁰⁴. When the ABM uses the more accurate and detailed enzymatic mechanism for resorption, the simulation unexpectedly created a resorption pit that mirrors the classic scalloped shaped edge typically observed in histological samples of resorptive pits.

2.4.3. The relationship between osteocyte density and trabecular perforations

The behavior of the trabecula without the bone lining cell agents shows a critical dependence on osteocyte density. In order to avoid the chance of perforations, the simulation requires more osteocytes than are typically found in adult human bone. Without the activity of bone lining cells, the simulation predicts that any space between osteocytes that exceeds the width of a resorption cavity would be vulnerable to perforating resorption.

In humans, as bones age the osteocytes within the lacunae occasionally apoptose with age. Consequently, even if a bone's lacunar density is high enough to initially protect the bone, after a few years there might not be as many osteocytes left alive to protect the trabeculae. While this could be used to explain how older bones are predispositioned for resorption, trabeculae cannot recover from being perforated and so apoptosis is too risky to be an optimal way to actively target older bone for resorption.

2.4.4. The effect of bone-lining cells as signaling intermediaries

There is a relationship between loss of cells in bone and a total loss of bone mass, for example, over-usage of cortical steroids that has been tied to the necrosis and collapse of bone as a result of osteocyte apoptosis. A large or complete loss of cells in an

area of bone leads to classic osteonecrosis and bone degeneration. Even this simple of an ABM simulation showed a tight dependence on the osteocyte density. Therefore, it is likely that there is a missing component that would otherwise be mitigating this risk, possibly by distributing the osteocytes' shielding signaling across the surface of the bone and/or throughout a larger area of the bone. The most likely source of this signal-distributing behavior would be the bone lining cells which cover the surface of all bone—including the trabeculae—and are known to interact with the osteoclasts when they are in the initiation stage of bone remodeling²⁵.

Indeed, when bone-lining cells are added as intermediary agents between the osteocytes and the osteoclasts, the strict dependence of trabecular perforations on the osteocyte density is sharply reduced. The bone lining cells were able to prevent full-width resorption under conditions where, without the bone lining cells, multiple breaks occurred in every run. It was also observed that with the bone lining cells, there was an increase in the average width once the width had reached a final, stable value. This is most likely due to the bone lining cells protecting surfaces from resorption sooner than the osteocytes alone would be able to.

Apart from BLC activity, another way this ABM model could lose its strict dependence on a high osteocyte population density would be to expand the communication network between neighboring osteocytes. In the simulation, the osteocyte agents only signaled if they sensed a force above the threshold within the radius of their canaliculi. In reality, all the osteocytes exist as a syncytium of cells connected via gap junctions, which are ideal for cell-cell communication. If the osteocyte agents produced a shielding signal when their neighboring osteocyte agents sensed a

large local strain, it could expand the region under protection from the osteocytes' signal, resulting in the more precisely optimized resorption seen with the BLCs' signaling.

There have been no studies comparing bone mass or trabecular width while restricting BLC or osteocyte signaling. Therefore, it is impossible to quantitatively match how accurate the simulation comes to stabilizing the width as compared to *in vivo*. However, the model still shows how, by adding the BLC agents following known behaviors, the simulation can better match the overall behavior of bone in cases of low osteocyte density.

2.4.5. Empirical comparison of the model with human trabecular parameters

The parameters for this model are close but not perfectly in alignment with the measurements from human trabecular bone. The osteocyte population densities used are higher than those found in human trabeculae, at least compared to the average density of lacunae in human vertebral cancellous bone¹¹³. The model's ability to best optimize the bone mass at higher osteocyte densities may be an indicator that this preliminary model underestimates the effective interconnectivity of the osteocytes or that the model underestimates the diffusion of the molecular signals protecting healthy, loaded bone from resorption. Either way, one of the future goals is to optimize the osteocyte density to more accurately represent adult trabecular bone.

This simulation also has focused on the first two steps of the remodeling cycle—activation and resorption. The long-term goals of this agent-based model will be to simulate current theories on the mechanics of the Reversal, Formation and Quiescence

steps as well, since these play an equally important role in the control of bone resorption.

Overall, this model shows the power of an agent-based model to take limited information from a wide variety of sources and apply it towards understanding a complex biological system. This is especially useful in bone biology where there is a lack of key information and an abundance of conflicting data about even the most basic aspects of its regulation. This early model supports the hypothesis that one signaling molecule diffused out from the osteocytes and received by the osteoclasts is sufficient to maintain a force-based disuse threshold that minimizes the required bone mass. The simulation also shows the minimum requirements for regulating the osteoclast resorption: accurate enzymatic descriptions of osteoclast activity, an even osteocyte density, and the unexpectedly important relaying of signal by the bone lining cells.

3. Second Model - Osteoclast/Osteoblast Coupling

3.1 Introduction

Apart from the brain, every human tissue must undergo natural turnover. In bone this turnover is called bone remodeling. However, whereas epidermal layers take only a month to form and be sloughed off, bones turnover exists on a much longer time scale. On average, bone is replaced every seven years. This is due both to the complex shapes that must be maintained as well as to the mineralized nature of the bone matrix itself. In bone, instead of apoptosis, a large, multinucleated cell called the osteoclast is required to remove old or damaged bone. Then, in order to maintain form and thereby function, a second cell—the osteoblast—fills the void with new bone.

Osteoclasts and osteoblasts are closely associated, both spatially and temporally, during bone remodeling. Osteoclasts and osteoblasts do not randomly activate on different sections of bone. Osteoclasts preferentially resorb damaged bone. Osteoblasts will localize to the resorption pits that the osteoclasts leave behind, altering their bone production to match the volume of bone removed. This close interaction between the osteoclasts and osteoblasts is called ‘coupling’. If osteoclasts and osteoblasts are not correctly coupled, the bone formation and bone resorption will not be even, leading to pathologies such as osteoporosis and osteopetrosis. In order to design effective treatments for these diseases, it is critical to understand the mechanisms behind coupling.

The most understood and canonical pathway for coupling osteoclasts and osteoblasts is the RANK/RANKL/OPG system. Osteoprotegerin (OPG) and Receptor Activator of Nuclear Factor kappa-B (RANK) are both receptors and receptor activator of

nuclear factor kappa-B ligand (RANKL) is a membrane-bound ligand. The RANK receptor is found on preosteoclasts and RANK/RANKL binding is capable of activating osteoclasts if there are also low levels of macrophage-colony stimulating factor around (M-CSF). RANKL is found on osteoblastic cells, allowing osteoblasts to upregulate osteoclast activity. OPG, on the other hand, is a soluble decoy receptor for RANKL; it will cover the ligand on the osteoblastic cells, preventing them from activating RANK and thereby osteoclastogenesis. It's produced by a number of cell types but it is particularly used by osteoblasts to regulate the production of osteoclasts⁵⁷. Multiple signals act through the osteoblastic cells to up or down regulate the production of bone or serum calcium, including PTH, vitamin D, estrogen, TGF- β , and glucocorticoids^{45,58,62,97,106}. However, as versatile as this OPG/RANK/RANKL system is, it cannot account for all osteoclast/osteoblast coupling.

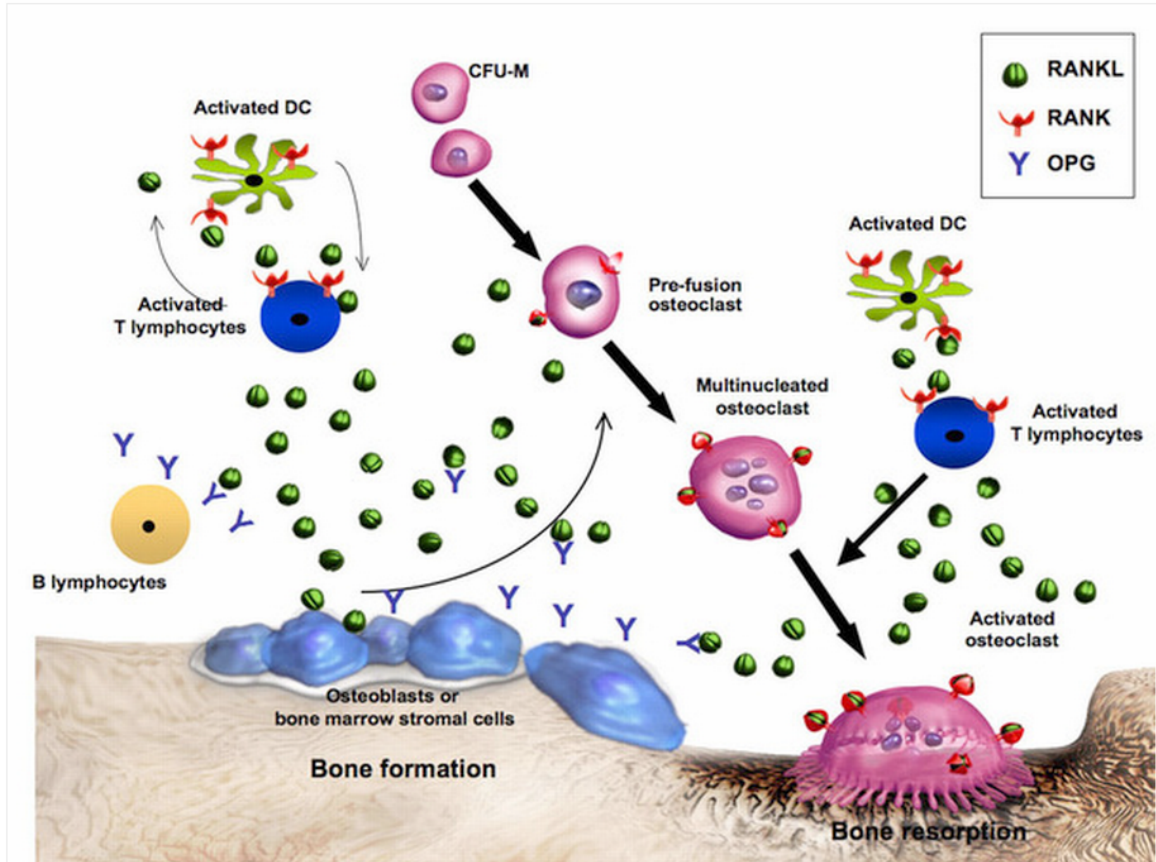


Figure 3.1. The RANKL protein stimulates osteoclast formation, function and thereby bone resorption. This ligand is produced by stromal cells, immune cells, osteoblastic and preosteoblast cells. Osteoblastic cells can additionally produce OPG which can competitively interfere with RANKL, thereby inhibiting osteoclastogenesis and bone resorption. Reproduced from Ferrari-Lacraz and Ferrari.³³

The problem with the RANKL/OPG system—excluding the debate about whether it is a more systemic versus local regulation—is the temporal nature of this pathway. The timing of the cell signals is backwards. In particular, with RANKL and OPG, osteoblasts are the cells affecting the activation of osteoclasts. However, in the bone remodeling unit, the osteoclasts are the first of these two cell types at the remodeling site; only after they finish resorbing can the osteoblasts do their job. The osteoblasts' RANKL does not cause the osteoclasts to activate on the bone surface and the mechanism for how osteoblasts are recruited to the remodeling site is still unaccounted for.

Coupling is term for the way in which osteoclasts and osteoblasts are spatially, temporally, and functionally tethered during bone remodeling. Active osteoblasts almost always deposit bone in the resorption pits that the osteoclasts had just left behind. There has to be some set of signals passing between these cell types to orchestrate this interaction. However, coupling is difficult to research; it cannot be replicated *in vitro* and is too dynamic to capture histologically. There is a long list of possible signals that osteoclasts and osteoblasts can produce to influence the other's activity levels, but the information gathered on each of these molecules is conflicting and no one signal has been proven to be important on the paracrine level. Different hypotheses for how coupling occurs exist, but none have been rigorously verified.

Computer simulations offer a chance to test the feasibility of these coupling hypotheses in a way a diagram or mental picture is unable to. A computer model can integrate large and disparate amounts of information across different scales and disciplines. This allows much of what is known about coupling and bone cells to be included to more accurately describe the mechanisms involved in this complex system. An agent-based computer model also allows for each of the objects, cells, signals and locations to be directly, one-to-one matched to the biology. This provides the advantage of constraining the model's independent variables and control variables to all be bounded by the physiological range seen in human bone. Similarly, the actions of the agents and the kinetics of all the signals are constrained to what is feasible and documented in literature. This grounding and constraining provides a way for the computer simulation to show when a hypothesized mechanism of action would be impossible for cells in the bone to carry out. At the minimum, the simulation can show that a hypothesis for coupling is feasible and a clear picture of where to look next to

better experimentally prove or disprove the proposed mechanisms.

The simulation described in this paper has osteoblast, osteoclast, osteocyte and bone lining cells, which are constrained with known parameters for size, location, and functionality. The agents' rule sets are based on the current hypothesis that osteoclasts can functionally and temporally couple osteoblasts by releasing and activating a diffusible "factor" from the resorbed bone. This hypothesis was constrained to simulate coupled remodeling, as defined by the localized replacement of bone and the maintenance of a stable trabecular width. Moreover, the simulation was challenged to replicate coupled remodeling through the empirical known range of values for osteoclast resorption rate, osteoblast resorption rate, osteoclast life span, and osteoblast life span.

3.2 Methods

3.2.1 Software

The ABM was built in NetLogo v5.0.1 freeware (from the Center for Connected Learning and Computer Based Modeling, Northwestern University). NetLogo allows for the creation of multiple agents that either may be free-moving through geographical space or fixed into grid locations.

A cluster of Linux computers was employed to run the NetLogo simulation over the multiple cases with multiple iterations, totaling more than 972 simulations for the virtual experiment. The data was collected and analyzed in Microsoft Excel and the R v2.15.1 statistical program.

3.2.2 Agent-based model

The agent-based model presented here is formed in NetLogo out of a 2D grid composed of 'extracellular' (ECM) agents and mobile 'cell' agents. It is based on an ABM of cancellous bone that focused on controlled resorption and osteocyte-osteoclast interactions. That simulation has been improved for this study by adjusting the cell sizes, bone lining cell shape, and population density to match adult human vertebral trabeculae. Most significantly, this model also now includes osteoblast agents.

In the simulation, the agents for each cell type--osteoclasts, osteoblasts, bone lining cells, or osteocytes--have their own class and rule set. The 'extracellular' agents represent the non-cellular components of mineralized bone, partially mineralized bone or marrow, as well as diffusible signals. Each agent runs through its rule set once per cycle, allowing the simulated trabecula to gradually change over iterations of each of the cells carrying out their known cellular activities (fig 3.2). One strut of trabecular bone is simulated in each run. Struts are roughly cylindrical and transversely isotropic, consequently, a simple 2D plane was considered sufficient to capture the basic spatial dynamics.

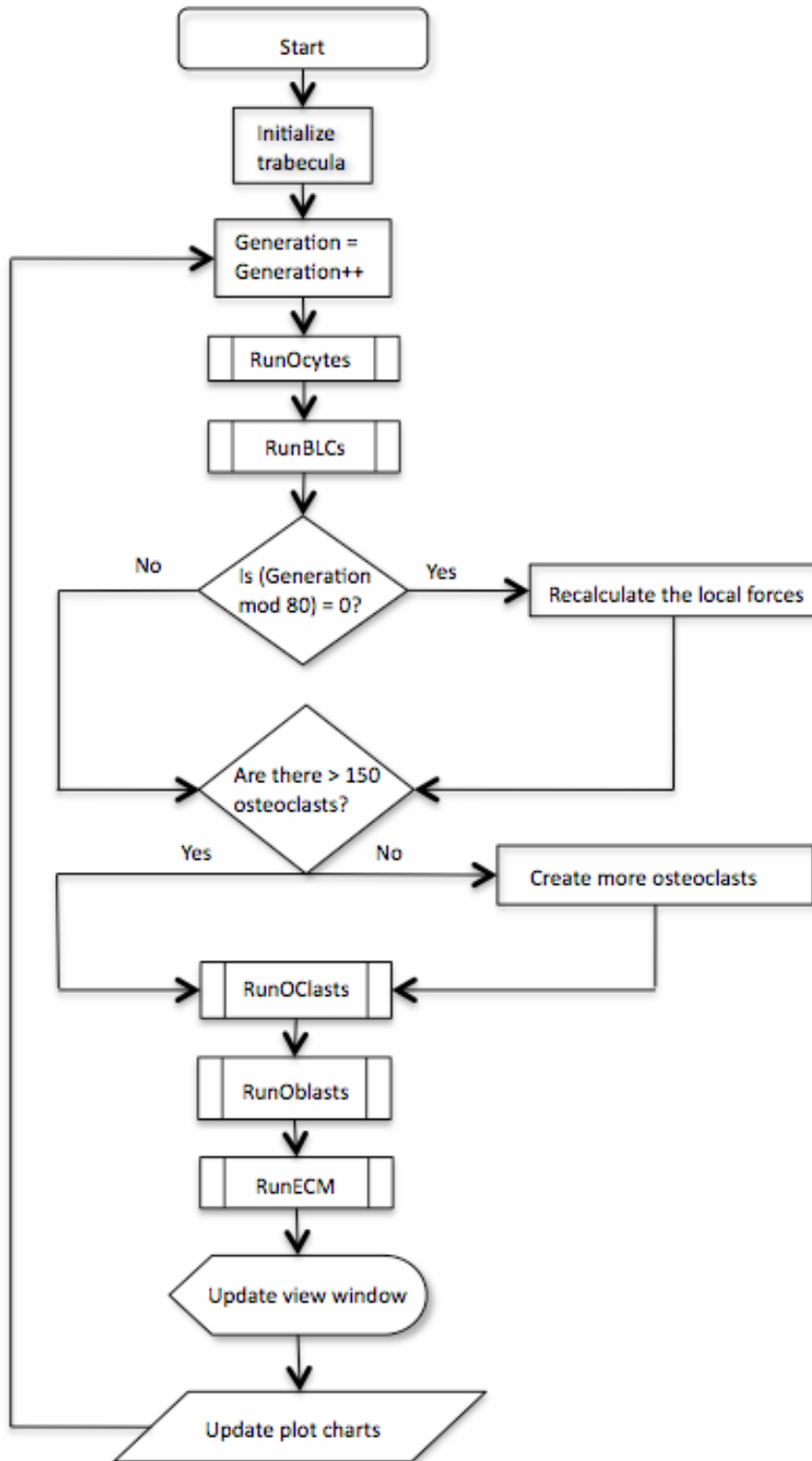


Figure 3.2 An flow diagram of the overall code run by the agent based model. The RunOClasts and RunOcytes subroutines are the same as in the previous model. (See Fig 2.5 and Fig 2.7)

Each ECM grid space has a *mineral* and an *organic component* (i.e., *variables*) that are set on a scale from 0 to 10. The bone marrow is defined by having zero for both of these variables. Fully mineralized bone has 10 for each variable. Each ECM agent has variables for the amount of *force* in that location and the amount of signaling molecules in that area. The ECM agents represent inanimate material and have a rule set for diffusing the signaling molecules and calculating the estimated *force* passing through that area of the trabecula (fig 3.3).

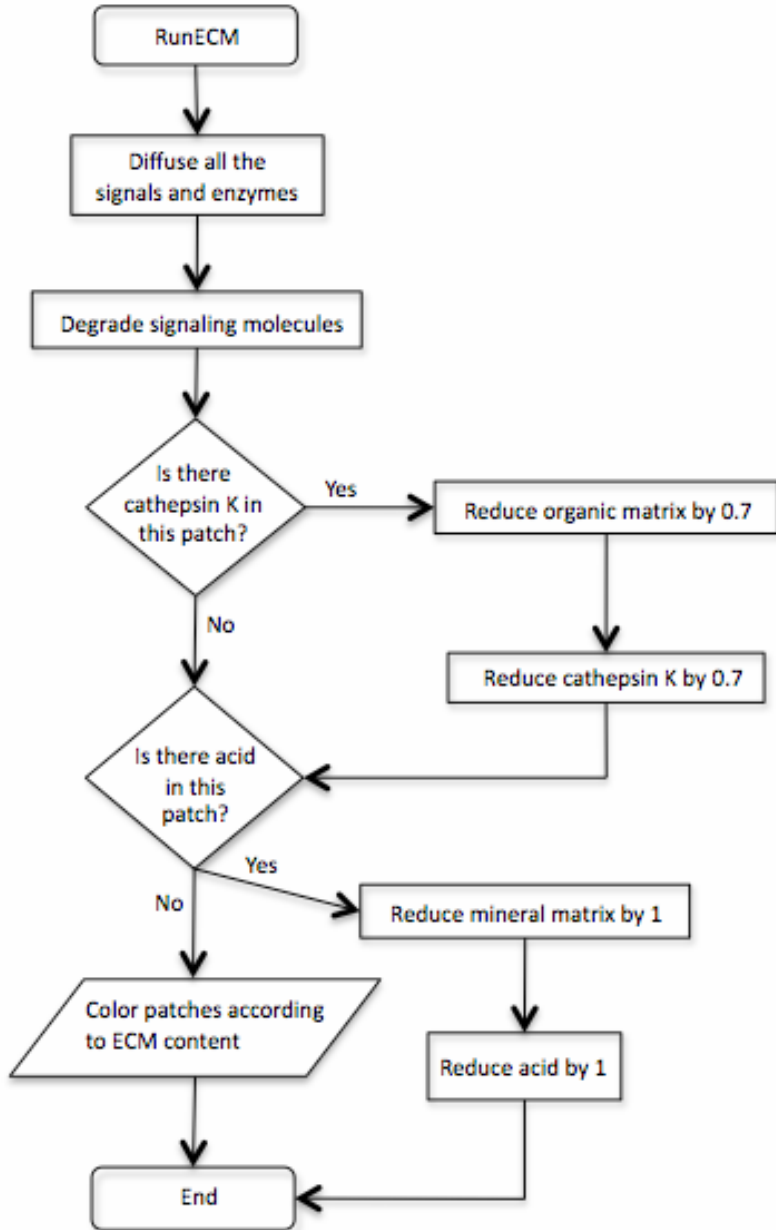


Figure 3.3 A flow diagram of the code run by all ECM patches.

The ECM agents start with an initial pattern of one column of ‘mineralized’ agents of uniform, user-specified width in the middle of a torus of empty ‘marrow’ agents (fig 3.4). The collection of ‘mineralized’ ECM grids is considered the trabecular region.

The average trabecular width is calculated as the number of mineralized ECM grids in each row divided by the total number of rows in the simulation. For the experiments in this paper, the ‘normal’ size of the trabecula was based off the width of healthy human vertebral trabeculae, which was measured by Chen et al, to be 115 ± 14 microns¹⁹.

While stationary agents represent the ECM, movable agents represent the cells. The code which creates the initial condition of the model—the setup of the trabecula’s ECM and initial cell positions—is available online at <https://sourceforge.net/projects/bone-abm-setup/>.

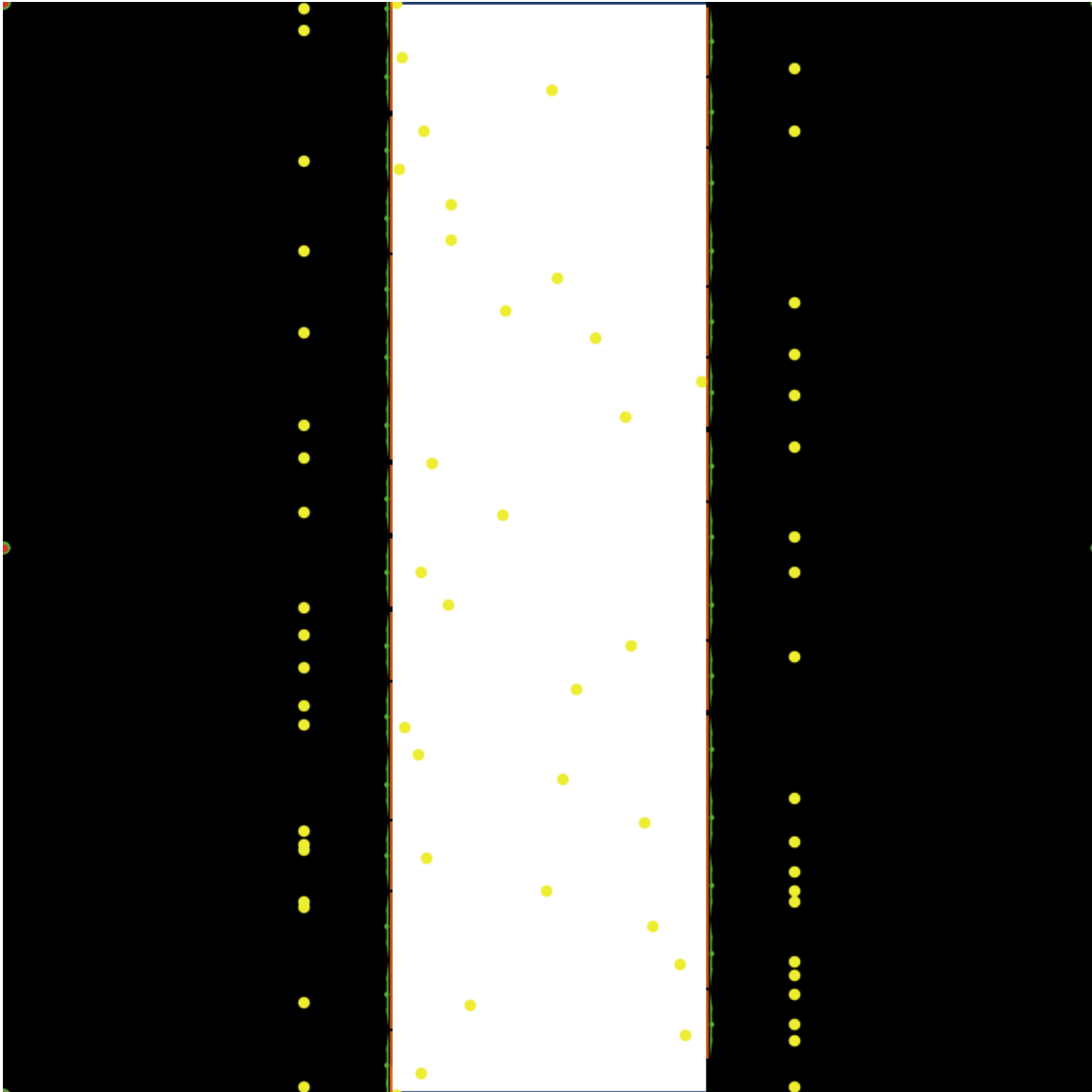


Figure 3.4. The initial condition of the ABM simulation is a smooth column of mineralized ECM agents (white), lined with bone lining cells (green) residing between the matrix ECM agents and the marrow ECM agents (black). The osteocytes are distributed evenly and randomly within the mineralized space (yellow dots within white area) and their initial placement is the greatest difference between the start conditions of each model. The preosteoblast agents are located above the surface of the mineralized trabecula (yellow dots within the black area) and the preosteoclast agents are initially located in the middle of the torus of marrow ECM agents (red/green spots).

The most abundant cell in bone is the osteocyte. These cells are the likely mechanosensors of the bone. They are the only cell within the bone matrix and so are uniquely positioned to monitor the local forces and microfractures that occur within the

mineralized matrix. While these cells are small and relatively quiescent, they have many long, thin—100 nm—dendritic processes that radiate out into the surrounding bone and connect via gap junctions to neighboring osteocytes¹⁰⁰.

The osteocyte agents are created when the model initializes. They are distributed evenly on top of random mineralized ECM agents at a population density within the physiological human range⁷⁹. It is also worth noting that since the osteocytes are placed using a pseudorandom algorithm, they are distributed as they would be in woven bone. In lamellar bone, the osteocyte lacunae are spaced more precisely and evenly. They are also never distributed in the exact same position from run to run since they are placed randomly. The osteocytes are set to be 5 microns in diameter to be consistent with literature⁶.

Osteocytes do not move through bone, so the osteocyte agents in the model have a *geographical location* and do not move. During the simulation, osteocyte agents ‘check’ the *force* variable of the ECM grids where they are located¹⁰⁹. If the force is above a certain threshold, the osteocyte agents will ‘send out’ a shielding signal by increasing the *shielding signal* in their ECM grid by 20 units⁶⁰. If the osteocyte is located on an ECM grid that changes states from mineralized to marrow, it will die; this mirrors how an osteocyte released from the bone during resorption will apoptose²⁸. This osteocyte rule set is adopted from the previous model simulating osteoclast/osteocyte interactions (fig 2.5).

The second most common bone cell—particularly on quiescent bone surfaces—is the bone lining cell (BLC), sometimes called a resting osteoblast or a surface

osteoblast^{4,42}. These extremely flat cells line the periosteum and endosteum, including the surfaces of the trabecular bone⁴⁷, spreading out to be roughly 20-30 μm across and thin enough to typically be invisible apart from the soma when using light microscopy^{31,66}. The BLCs have been observed connecting to the osteocytes through gap junctions at the tips of their dendritic processes, so it is possible that the BLCs are part of the osteocytes' syncytium³¹.

The BLC agents in this simulation lie along both surfaces of the strut of mineralized matrix; they are 25 microns across and one micron thick, approximating the average measured proportions³¹. The bone lining cell (BLC) agents are required to 'lift off' the bone surface before the osteoclast can pass through the BLC layer. Contact with an osteoclast will cause a BLC agent to lift unless that BLC agent is detecting (e.g., by a mechanotransduction) a protective signal from contiguous osteocytes^{16,17,77}. In the literature, there is debate over whether BLCs would normally apoptose, become active osteoblasts, or turn into canopy cells when no longer connected to the bone surface. To keep the model simple, the BLCs lift 10 μm off the surface without interfering with any processes until the osteoclasts and/or osteoblasts have left the bone surface and then reattach (fig 3.5).

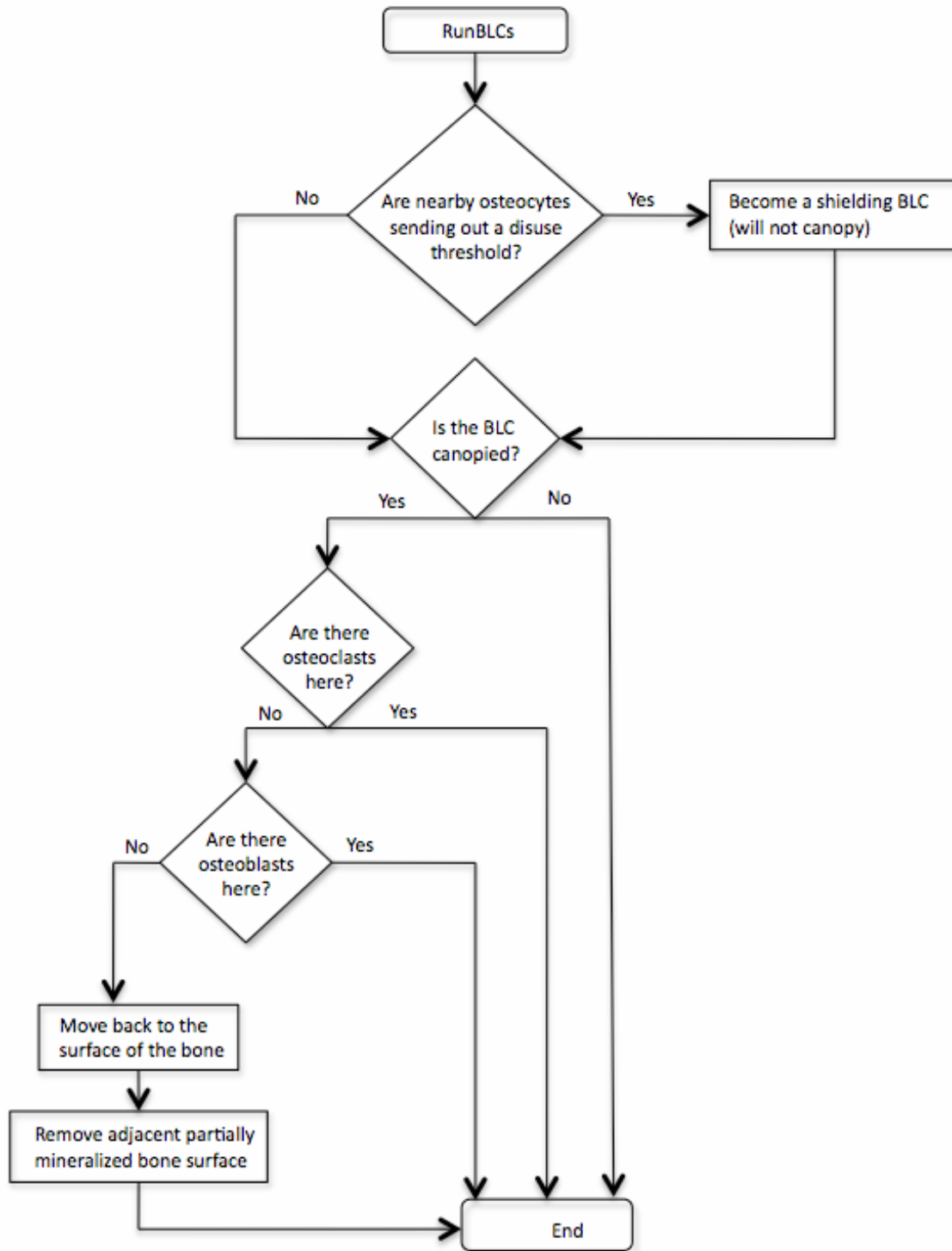


Figure 3.5 A flow diagram of the code run by all BLC patches.

The largest bone cell is the osteoclast, growing over 100 μm and having between 3 and 10 nuclei^{49,89}. It is descended from the monocyte cells of the hematopoietic lineage, allowing the cell to have the machinery needed to form into giant multinucleated cells that can seal onto bone surfaces and resorb the mineralized matrix.

The osteoclast agents in the model are initially located in the middle of the empty 'marrow' ECM area and are capable of randomly 'walking' one step per each cycle. They have two states: inactive or active. Once active, they are set to a width of 30 microns. The BLCs will lift off the surface of the bone when they come in contact with an osteoclast unless they are within 30 μm of an osteocyte sending out a shielding signal; this allows the osteoclasts to attach to a bare surface of mineralized matrix. There is *in vitro* evidence that osteoclasts transmigrate through osteoblastic cells⁹⁸. While the simulation is running, if the population of inactive osteoclasts falls below a certain number, a new osteoclast is added to the simulation to preserve the pool of osteoclast agents.

If active, the osteoclast agent first will check for the *shielding signal* in the ECM grid below it. If the *shielding signal* is above zero, the cell will die. If not, the osteoclast will either attach onto mineralized bone or migrate along the demineralized surface. The osteoclasts agents are unable to bind to bone to resorb if there is a layer of non-mineralized matrix under their bottom edges²². It has been reported that this migratory aspect of osteoclasts is important for replicating the scalloped shape of the resorption pits.

If the osteoclast attaches to the bone, it will release *cathepsin k* and *acid* (i.e., a

proton: H+) into three ECM agents spaced evenly on the surface of the bone between the agent and the surface of the attached bone below^{22,64}. The amounts of these two variables—*cathepsin k* and *acid*—are stored in the ECM agents in the same way as the *signaling molecule* and they will diffuse through any ECM square without an amount of *mineralized matrix* less than 1. The *cathepsin k* decreases the amount of *organic component* in each ECM agent and the *acid* decreases the amount of *mineral component* in each ECM agent. The *cathepsin k* works at a different rate than the *acid*. The parameters for this process were set to produce a resorption pit (define) that is an average of 25 microns wide and 8 microns deep. The resorption pit has histologically observed blurred edges formed from partially demineralized matrix^{30,66,104}, which are replicated in the model. Each ECM agent being resorbed releases an osteoblast chemoattractant signal that allows to diffuse through non-mineralized ECM agents^{11,12,96}. The osteoclast agents are given a ‘short lifespan’ once activated, correlating with osteoclasts’ average 16-day lifespan^{67,36}. As with the osteocyte agents, the osteoclast rule set is adopted from the previous model simulating osteoclast/osteocyte interactions (fig 2.7).

The last cell included in the model is the osteoblast. This cell type is responsible for creating new osteoid that will mineralize into bone matrix. In the simulation, the inactive osteoblast agents, which correspond to preosteoblasts in the stroma of the bone marrow, randomly walk $22.5 \pm 2.5 \mu\text{m}$ away from the bone surface⁹. If they detect the *signaling molecule* released by the osteoclasts at their location, they will partially activate, switching into a migratory mode (fig 3.6). While in the migratory mode, the osteoblasts migrate up the concentration gradient of released signaling molecule until they reach a mineralized surface where they complete their activation^{12,43}. Activated

osteoblast agents orient towards the bone surface; if there are osteoclasts at that location they wait on the bone surface, otherwise they will produce bone¹⁰¹. The osteoblast agents produce bone by, once a cycle, setting the *organic component* and *mineralized matrix* variables to 10 in the a set of ECM agents in front of them, taking a micron step backwards and setting their age plus one. If the osteoblast age is greater than their lifespan, the osteoblast agent dies.

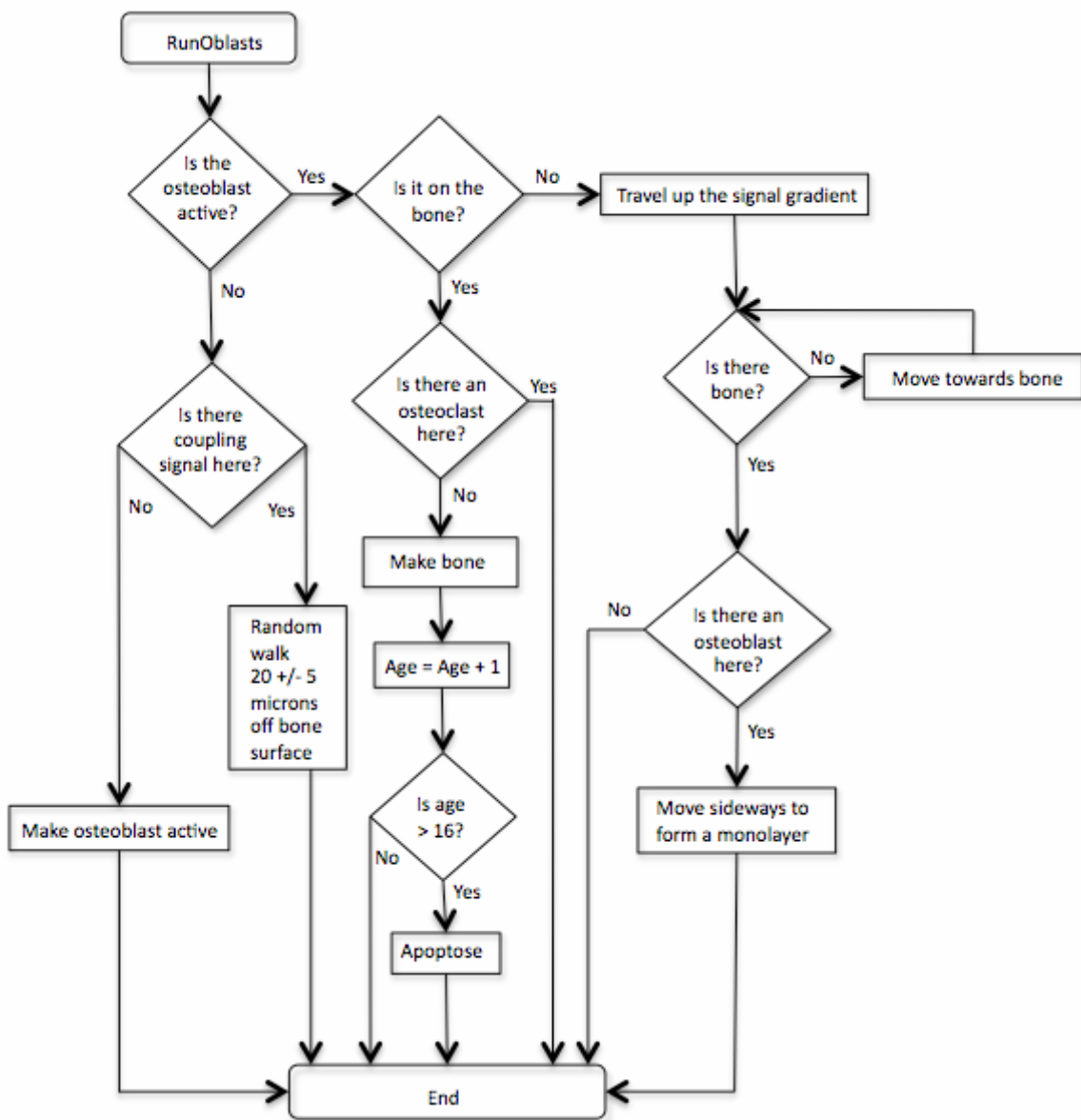


Figure 3.6 A flow diagram of the code run by all osteoblast agents.

3.2.3 Simulation setup and initial conditions

The simulation ran until the trabecula was fenestrated by osteoclasts, the trabecula expanded to the edge of the screen, or else when the simulation reached the 12,001st cycle. If the trabecula is fenestrated, the output is considered pathologic since the whole trabecula is then likely to be destroyed⁹⁴. When there is a fenestration in the trabecula, the osteoblasts lack the template for the new bone, no new bone is added, no force is transmitted through the bone, and osteoclasts do not receive inhibitory signals to prevent them from resorbing the rest of the unloaded strut. 12,000 cycles was found to be long enough for the simulation to develop a constant rate of bone formation or resorption, even in the most extreme cases.

The simulation was also run at least twelve times for each test case of input parameters. The standard number of replicates required to gauge the variance and reproducibility of an ABM is traditionally 25. However, recent work by Ju-Sung Lee has show that five is the minimum number of replicates required. This is similar to how $n = 3$ is the minimum number of replicates required in cell biology. Since this ABM simulation is particularly time consuming and the replicates did not have a high variance nor a bifurcation in the generated outcomes, twelve replicates was deemed sufficient to characterize the behavior of the simulation for each of the 81 cases.

The default parameters are set to mirror average values for human vertebral trabeculae, and constrained to within empirically measured values where possible (table 3.1). The three chosen values are the estimated average, low extreme, and high extreme for each independent variable.

A full-factorial analysis of the four independent variables at three different levels was simulated. The dependant variables are: average final width, trabecular smoothness, the number of trabecular perforations, rate of change in trabecular width, and the time it takes the width to stabilize. Each independent variable was collected from all 81 experimental conditions with twelve replicates each.

Table 3.1 Experimental Setup for the Osteoclast/Osteoblast Coupling Virtual Experiment, using values for variables based on literature^{9,19,76,77,79,105}.

Independent Variables	Number of Test Cases	Values Used
Osteoclast resorption rate	3	2, 4, 8 units of acid and cathepsin K released/cycle
Osteoblast apposition rate	3	0.1, 0.3, 0.5 microns/cycle
Osteoclast life span	3	120, 180, 240 cycles
Osteoblast life span	3	8, 11, 30 cycles
Control Variables	Number of Test Cases	Values Used
Osteoblast location	1	11-13 microns from surface (<i>Bianco, Mar 2011</i>)
Osteoclast location	1	Center of marrow (<i>Bianco, May 2011</i>)
Osteocyte location	1	Evenly distributed in trabecula (<i>Mullender, 1996</i>)
BLC location	1	On trabecular surface (<i>Miller, 1987</i>)
Preosteoclast population	1	50 agents
Osteocyte population density	1	30 per mm ² (<i>Mullender, 1996</i>) (<i>Metz, 2003</i>)
Osteocyte Threshold	1	Starts signaling at 143% initial strain
Osteoblast Threshold	1	0.1
Initial Width of Trabecula	1	100 microns +/- 0 microns (<i>Chen, 2008</i>)
Length of Trabecula	1	400 microns
Mineral / Organic Component of Trabecula	1	10 / 10
Resorption Pit Size	1	5 microns deep, 10 microns wide (<i>Delaisse, 2010</i>)
Dependent Variables	Number of Test Cases	Values Seen in Literature
Average Width + Std Dev	-	115 +/- 14 microns
Smoothness	-	2 – 30% variability in width
Time to Reach Equilibrium	-	0 days
Rate of change of trabecular width	-	0 microns/month (in young normal bone)
This is a 81 case experimental design		
The simulation will run 12 times for each test case, with a runtime of 12,000 cycles		

3.2.4. Methods of Analysis

The average trabecular width, plus or minus a standard deviation, is known for normal human vertebral trabeculae and can be compared to the ending widths of the simulations to estimate how much of the parameter space within the known ranges of

the input variables can successfully simulate normal remodeling. An estimated upper and lower bounds for the physiologically expected smoothness, rate of change of width, and number of trabecular perforations is also known and can be combined into a measure of the Z-score Euclidian distance to evaluate the ability of the model to correctly simulate multiple aspects of bone remodeling.

The specific effects of these independent variables on the size and health of the trabeculae is unknown (e.g. there is currently no literature on the effect of a 30% decrease in osteoclast life span and its impact on the trabecular width *in vivo*). However, the general effects of reducing or increasing the input parameters can be matched against a generally agreed upon expected direction of change in the trabecular width. For example, increasing osteoblast activity is known to increase bone production and mass, even if the amount bone increases has not been quantified. Additionally, the simulation's independent variables cover a broad range, allowing the simulation to address how extreme values for osteoclastic resorption or osteoblastic apposition could impact bone remodeling, within the assumption that this hypothesis for coupling is correct.

The simulations were evaluated in terms of their ability to recapitulate coupled remodeling as defined by average width, smoothness, trabecular perforations, time to reach equilibrium, and rate of change of the trabecular width. The simulation results were also assessed by the length of time required to reach a minimum width, which was the inflection point in the plot of the change of width over time. The rate of change in the trabecular width only reaches a constant rate after this inflection point. The simulations were also evaluated by the qualitative observations of the osteoblasts' ability to spatially and temporally fill the resorption pits left by the osteoclasts, as compared to

histological samples of mammalian bone remodeling.

The average width is calculated as the average number of patches along the x-axis with a *mineral* value ≥ 4 at the end of the simulation. The standard deviation of the average width is equal to the standard deviation of the average width for each of the 12 simulations per case. The expected value for the standard deviation is based off the experimentally measured values for human vertebra in adult premenopausal women—115 +/- 14 microns¹⁹.

The smoothness was calculated as the standard deviation of the width along the trabecula within each replicate. The higher the value for 'smoothness' is, the more its width varied along the length of the trabecula and the less smooth the ending trabecula actually was. Normal trabecular bone is very smooth, with only gradually varying by around 10-30% along the entire length²⁶. It is technically possible to calculate the standard deviation of the smoothness just as it was done for the average width, but as it would only be useable to gauge the stochasticity of the simulation, it was not analyzed. The number of trabecular perforations was calculated as the number of instances per row where there were no ECM patches with a *mineralization* value greater or equal to 4.

3.2.5 Validation of model and results

The ABM model described here underwent two different types of validation—first the validation of the code and, second, validation of the results. In validating the code, the goal was to ensure that the model's behavior was an accurate representation of the information given by the subject experts. This includes empirically constraining the initial conditions, quantifiable parameters, and the spatial aspects of the simulation, as

well as constraining the rules that govern the behavior of the agents to behaviors that are documented in the literature.

In ABM studies, this is often referred to as ‘empirically grounding’ the model, or ‘validation by inputs’. The validation of the code employed here can also qualify as validation by the subroutines. Each agent’s sub-routines are qualitatively checked to assure that they generate behavior matching their represented cells.

The ABM simulation was also validated by the generated results; the output parameters were compared to values known and reported in the literature. For example, the trabecular width and the ability to reach—or fail to reach—a stable width was compared against the data for healthy adult trabeculae in human vertebrae.

3.3 Results

Since the model initializes with only preosteoblasts and preosteoclasts, and the osteoblasts only activate upon the osteoclast activity, there is a delay in bone formation at the start of each simulation. This causes an initial condition of bone loss that stabilizes and then gives way to the stable, typically linear, rate of change in trabecular width (fig 3.7). Surprisingly, the time required for the simulation to reach the minimum width was not constant between cases (fig 3.9). Sometimes it took quite a while for the osteoblasts to functionally ‘catch-up’. Consequently, this value has been added to the panel of output variables used to analyze the model.

The rate of change of the width ranged from positive to negative given the different input conditions, showing that there exists a set of independent variables

within the range simulated in the virtual experiment that allow for the balanced (net zero) maintenance of trabecular width (fig 3.7-3.8). Since the independent variables were within literature values, the model suggests that this hypothesis for coupling osteoclasts and osteoblasts is feasible.

This hypothesis explains a normal pattern of bone remodeling, both in balanced formation and resorption, and in the correct pattern of cellular activity throughout the whole sequence of the remodeling process. However, this model is also more sensitive to perturbations in the independent variables than is observed in normal bone remodeling, particularly at the upper level of osteoblast activity, which caused the simulated trabeculae to dramatically increase in width (fig 3.12-3.13). This oversensitivity was expected since this ABM is still just a preliminary simulation—having only one signal to balance all of the cellular activities. There is evidence for dozens of signaling molecules necessary to orchestrate this balanced remodeling in mammalian bone. In terms of creating the spatial-temporal pattern of coupling while bounded by physiologically constrained parameters, the simulation was able to correctly simulate coupled remodeling using the ‘osteoclastic resorption released coupling signal’ hypothesis.

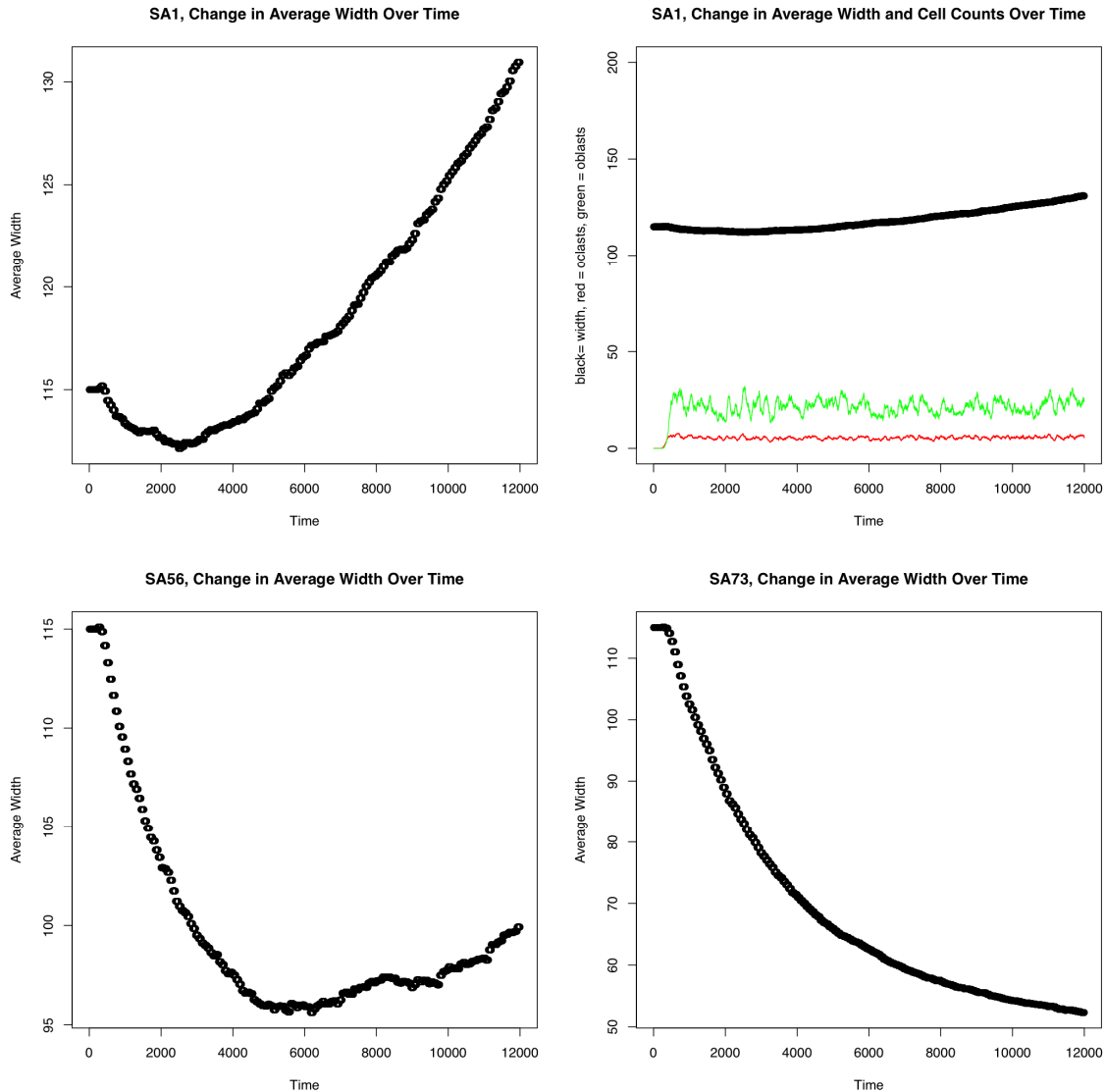


Figure 3.7. Four representative plots of the average width changing over time during the simulation. Top two graphs show an example of the width increasing, without or with the cell populations (red is the number of osteoclasts, green is the number of osteoblasts). The bottom left plot is an example of the rate change close to zero. The bottom right plot is an example of the average width's rate change being negative. If the plot had a time of minimum width less than 12000 cycles, the rate of change in width was calculated from the time between the minimum width and the end of the simulation. The complete set of plots can be found in the appendix.

Across the 81 cases, the simulation's time of minimum width is correlated with the rate of the width change (fig 3.8). The higher the rate, the faster the simulation stops reducing in width before expanding again. The few cases where the rate never becomes

positive, there are no specific times of 'minimum width', but the cases with the slowest increasing width have the highest time of minimum width (fig 3.9). However, plotting the rate as a function of the minimum time shows a non-linear relationship between the two outcome variables (A3.2).

Out of all the independent variables, the osteoclast lifespan has the smallest influence on any of the output variables. Osteoclast lifespan has no visual impact on the rate change (fig 3.10) and most of the slopes of its effect on the output parameters are close to zero, with a low R^2 (fig 3.15, 3.16). The largest impact the osteoclast lifespan has on anything is the time of minimum width (fig 3.14). It is to be expected that increasing the lifespan would increase the time of minimum width since the longer the osteoclasts persist, the more time passes before the osteoblasts can start depositing bone. Overall, the osteoclast's lifespan does the most to positively increase the time of minimum width while both of the osteoblast's independent parameters equally decrease the minimum width (fig 3.14, A3.6).

The osteoclastic rate of resorption has an impact on the ending width of the trabeculae, but it is a small influence that is overwhelmed by the osteoblast's two independent parameters (fig 3.11). The range of plot shapes for the different levels of each of the osteoclast's parameters is very diverse (fig 3.10, fig 3.11). The combination of the other three independent variables linear effects lead to a wide variety of outcome patterns for each osteoclast input. The osteoclast rate and the osteoblast lifespan have equal but opposite effects on the width rate change; longer-lived osteoblasts increase the rate of bone formation to the same extent that more active osteoclasts reduce rate of bone formation (fig 3.15). The greatest impact on the rate of width change is generated

by the different levels of osteoblast activity (fig 3.15).

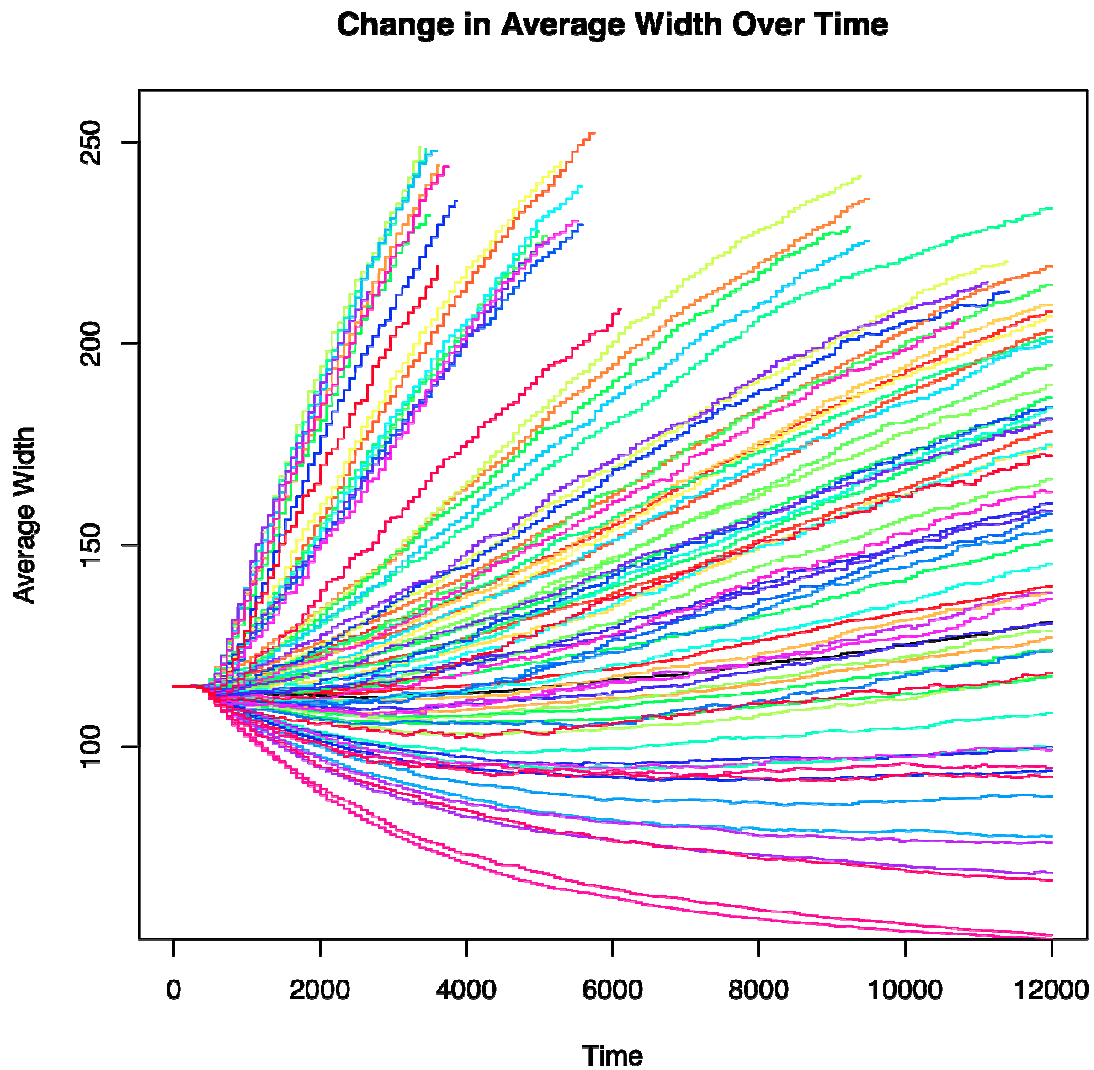


Figure 3.8. The plots of all 81 cases in the virtual experiment, showing the change of width over time. The width of the trabecula changes over time, either increasing, decreasing, or staying close to constant depending on levels of the four independent variables.

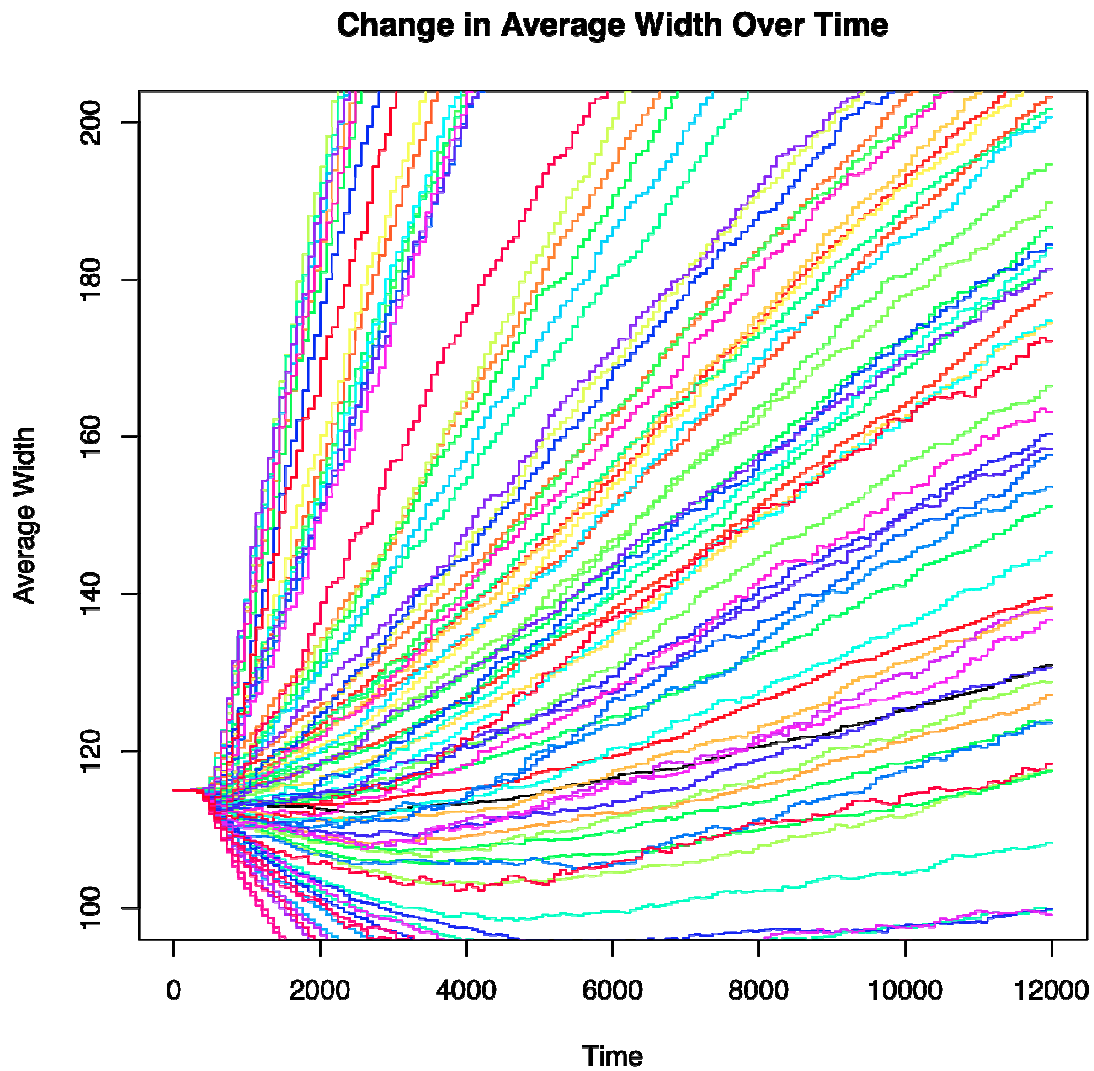


Figure 3.9. The 81 plots of the virtual experiment, focused on the range of 100 to 200 microns in width to show the details of the minimum width that occurs at the start of the simulation before the osteoblast activity can match or exceed the osteoclast activity.

Effect of Osteoclast Lifespan

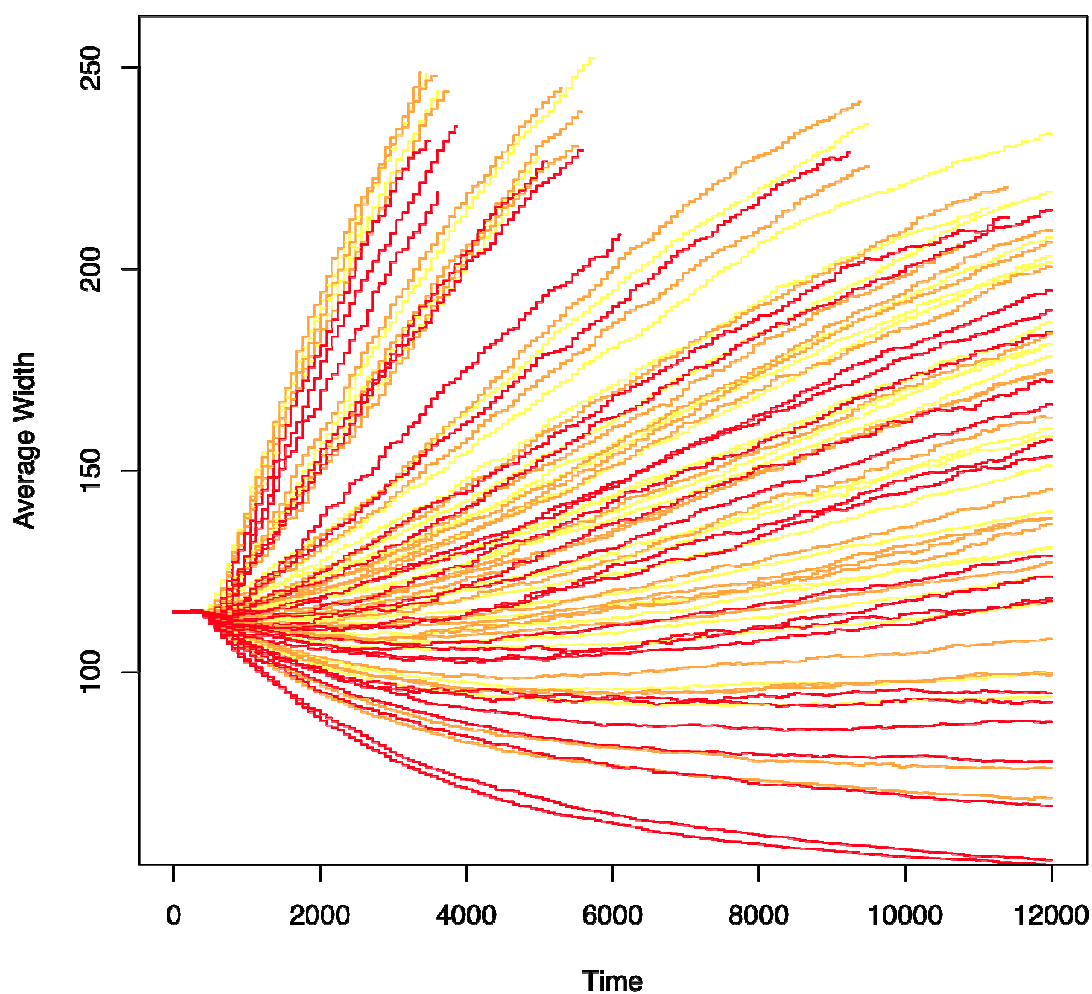


Figure 3.10. The effect of osteoclast's lifespan on the shape of 81 cases' plots is shown by coloring the simulations red, orange, and yellow based on whether they had a long, normal, or short osteoclast lifespan. The change in osteoclast lifespan does not have a large influence on the change in width over time.

Effect of Osteoclast Rate

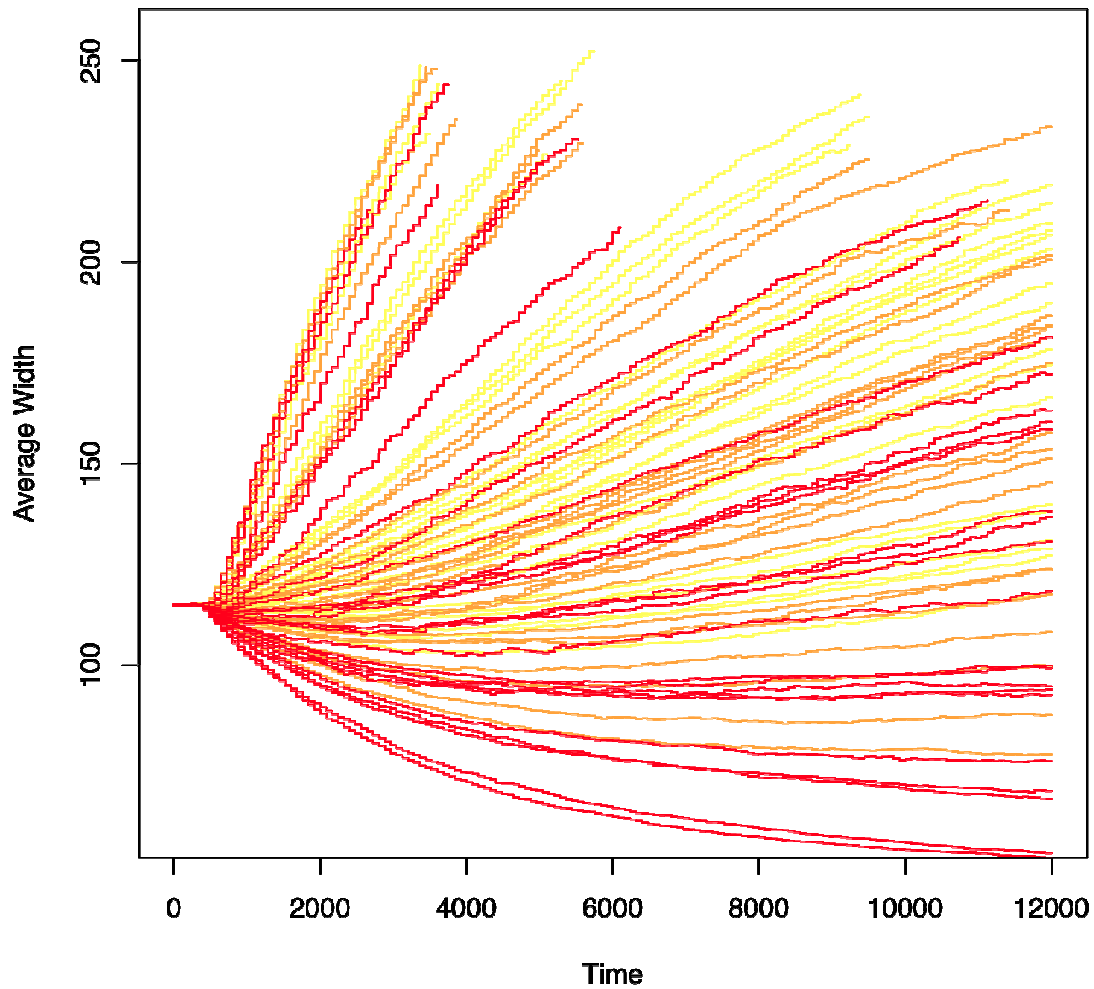


Figure 3.11. The effect of the Osteoclast Rate on the change of width over time with red coloring the plots with the most active osteoclasts and yellow coloring the plots with the least active osteoclasts. The change in osteoclast rate—like the osteoclast lifespan—does not have a large influence on the change in width over time.

The osteoblast rate and osteoblast lifespan have a significant impact on the change of width over time (fig 3.15), but the outcome is still a combination of all four independent variables together and so the outcomes are still very diverse (fig 3.12, 3.13). High osteoblast rates forced all 27 of their plots to increase the trabecular width over time (fig 3.12). Only one of the 27 high osteoblast lifespan plots had a large, positive rate of increase (fig 3.13).

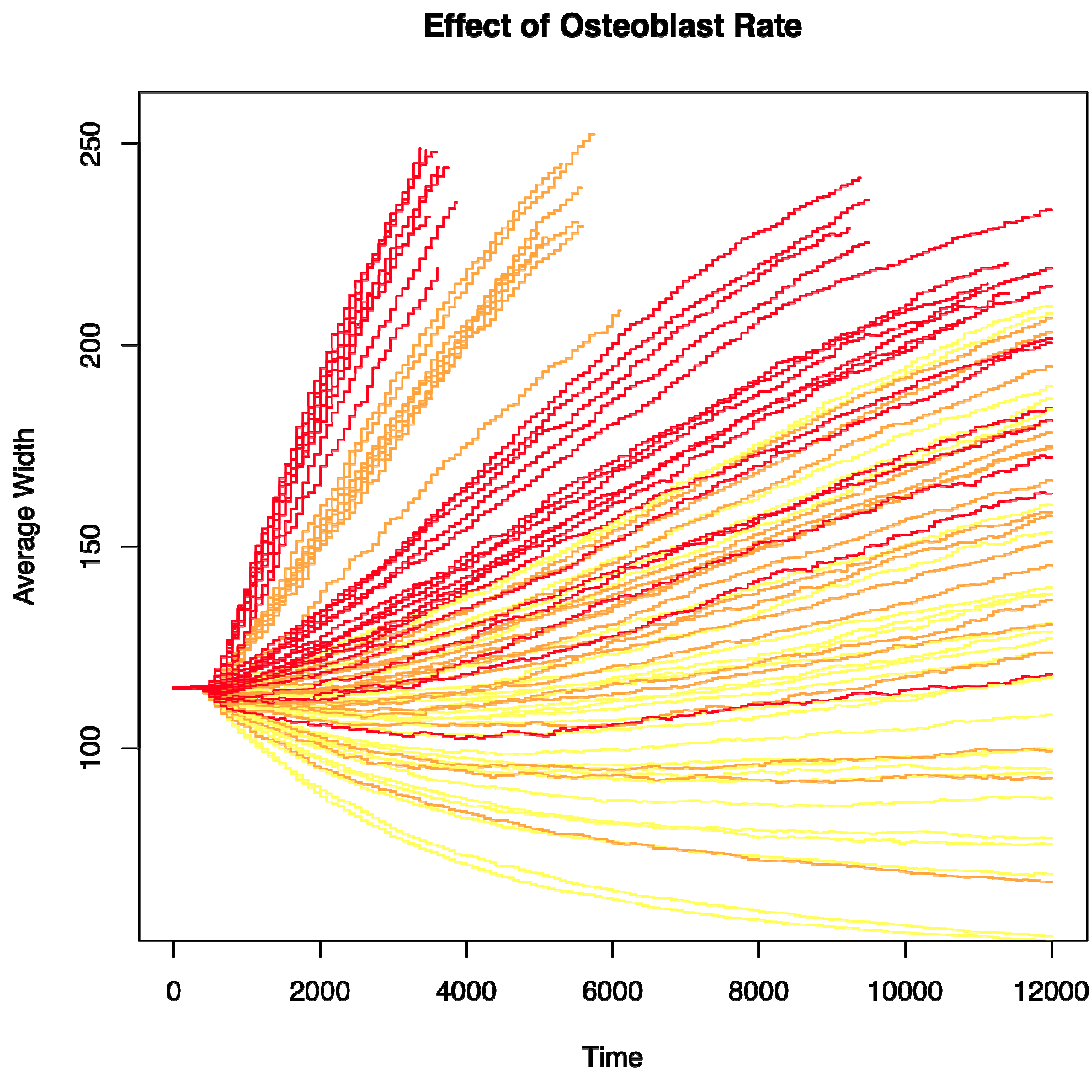


Figure 3.12. The effect of Osteoblast Rate on the change in the width of the simulated trabecula over time. Red marks the simulations with the most active osteoblast, orange the 'normal' amount of osteoblast activity, and yellow the simulations with the least active osteoblasts.

Effect of Osteoblast Lifespan

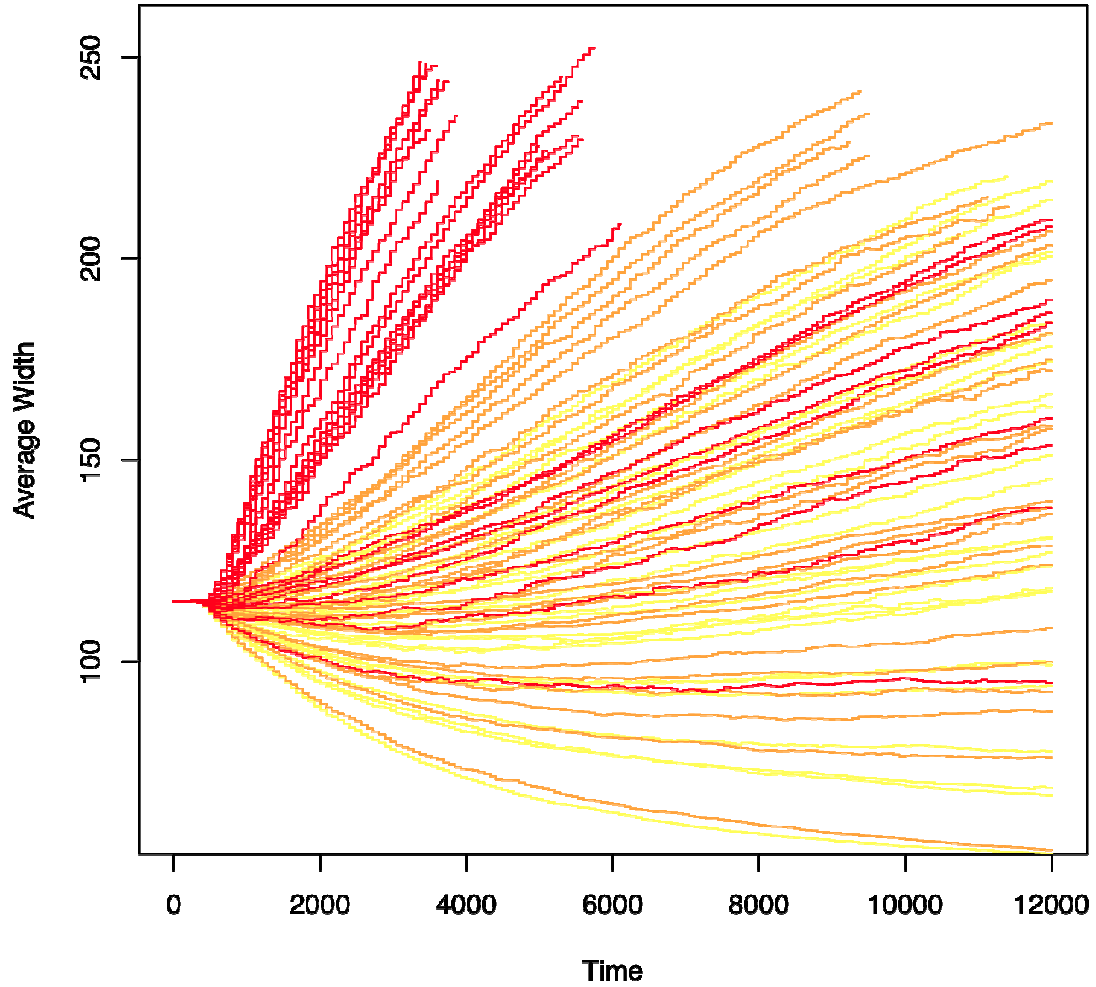


Figure 3.13. The effect of Osteoblast Lifespan on the change in the width of the trabecula over time. The longer-lived osteoblast simulations are red, the 'normal' osteoblast lifespan simulations are orange and the short-lived osteoblast simulations are colored yellow.

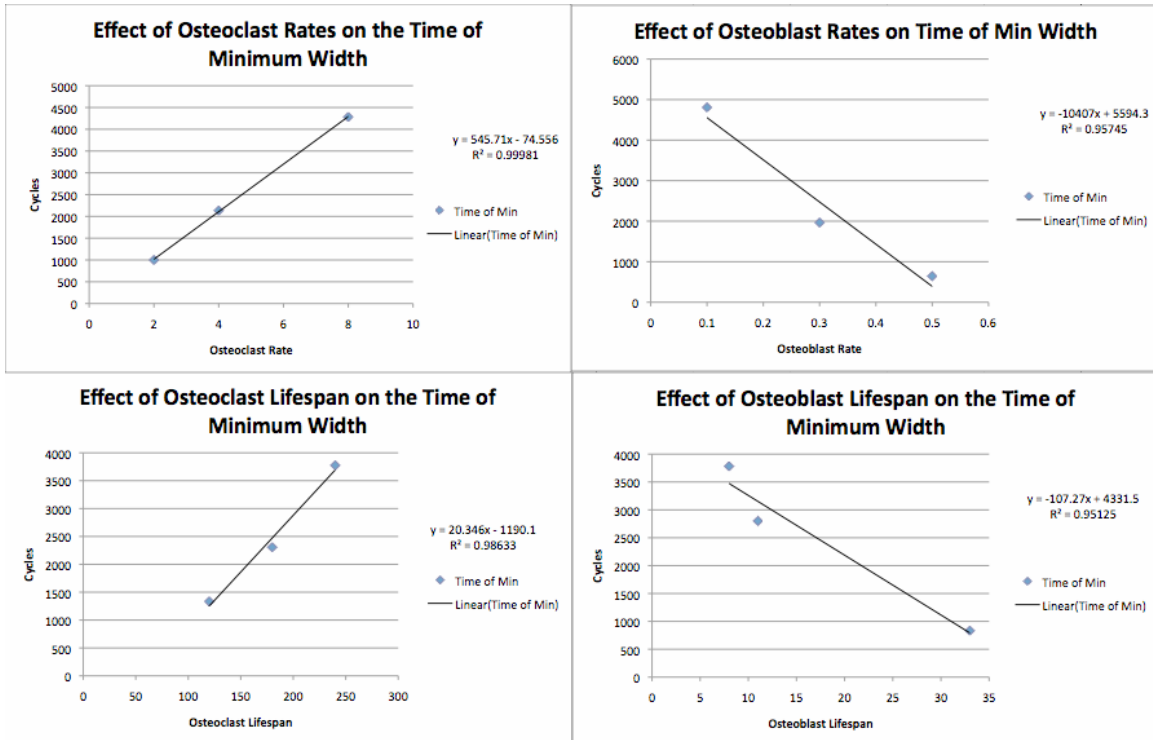


Figure 3.14. The effect of the independent variables on the time of minimum width.

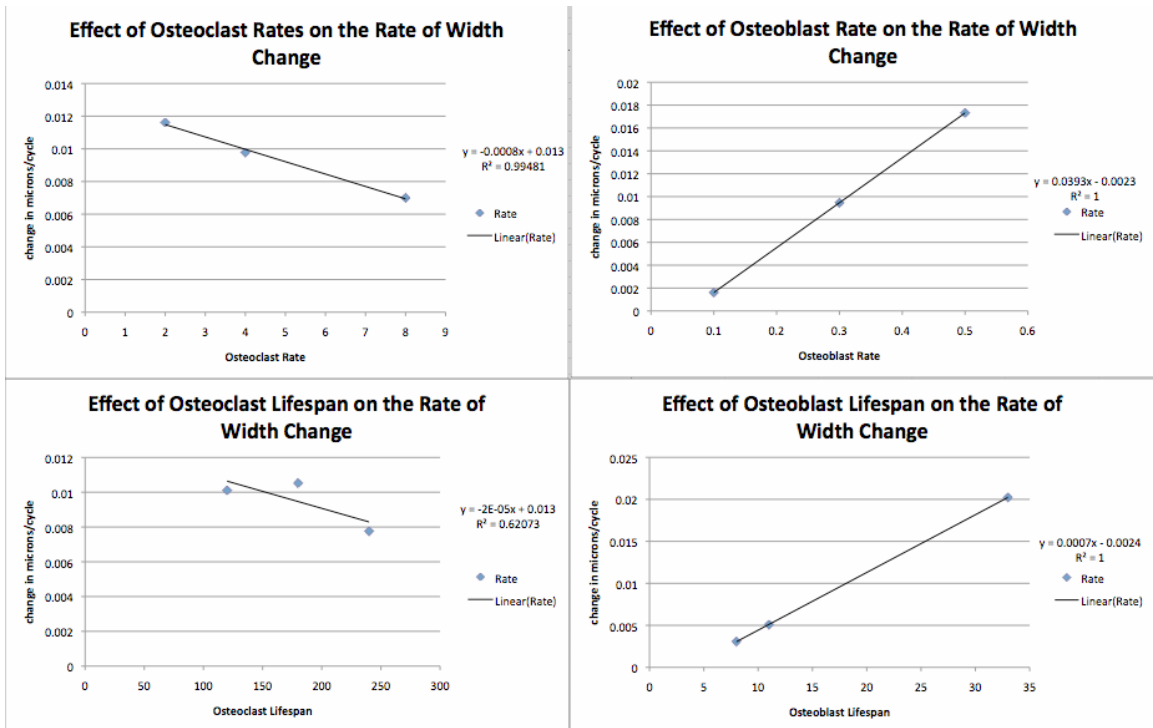


Figure 3.15. The effect of the independent variables on the rate of width change.

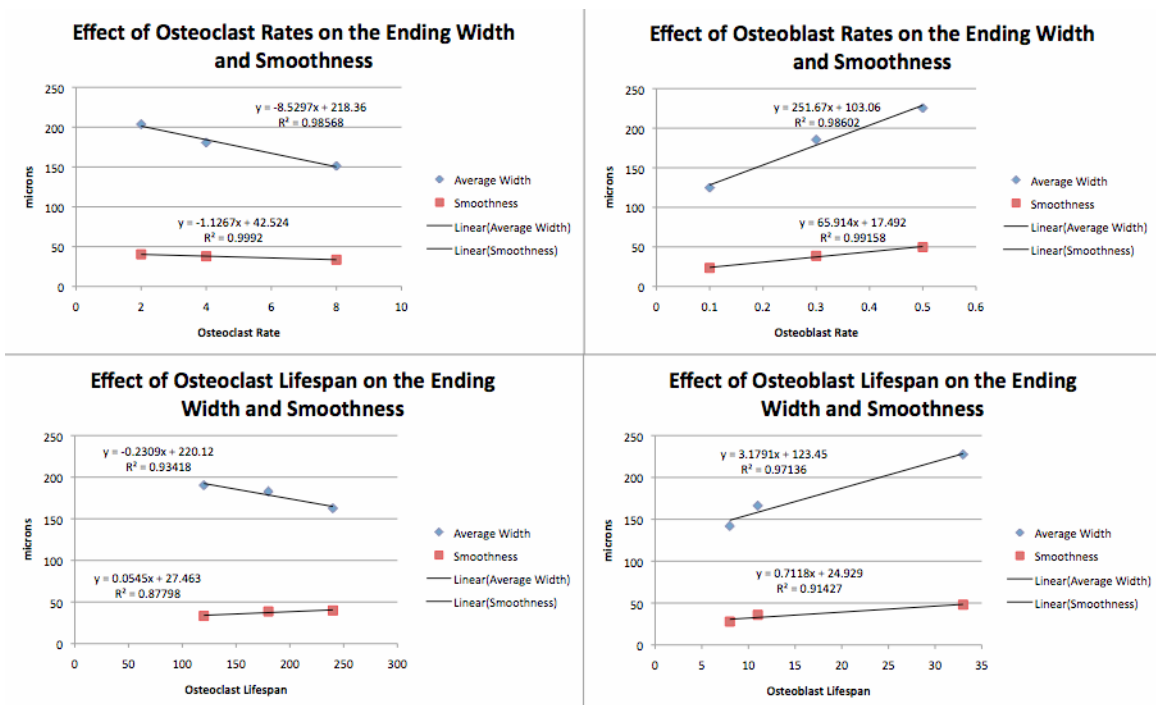


Figure 3.16. The effect of the four independent variables on the trabecular smoothness and the average ending width, both measured in microns. Smoothness is measured as the standard deviation of the width along each trabecula at the end of the simulations, so the higher the value, the less uniformly ‘smooth’ the trabeculae was at the end of the simulation.

The smoothness of the trabeculae is not strongly influenced by most of the independent variables, though the two osteoblast parameters increase the roughness of the trabecula’s ending widths (fig A3.5) and the osteoblasts’ rate of bone formation has a high R² correlation with the roughness of the trabecula (fig 3.16).

Normal bone should have a near zero change in trabecular width despite a constant level of bone turnover. Throughout all 81 cases of the virtual experiment, even though the width was not always kept constant (A3.10-A3.12), there was an observed constant bone turnover in the trabeculae across all simulations. Functionally, in terms of reducing the age of the bone, the simulation is mimicking bone remodeling.

3.4 Analysis of Results

The Z-score was calculated for each simulation, using the known expected values for average width, trabecular smoothness, and the range for the possible rates of change in bone mass. The width of healthy human female vertebral trabeculae is an average of 115 microns wide with a standard deviation of +/- 14 microns¹⁹. The value for trabecular smoothness is based on the expected range of 0-30 microns²⁶, and the standard deviation was approximated at 1/4th the range. The average rate for the change in width should be zero, but the standard deviation was more complicated to estimate. Using drugs like Alendronate can lead to an 8.8% increase in bone mineral density in the lumbar region over one year, and at perimenopause, the yearly decrease in bone mineral density for women's spines is 2.77%^{2,92}. Since the simulation is of an older pre-menopausal woman's lumbar spine, the rate of bone should be staying steady or slightly decreasing, not drastically reducing, so I used a 3% reduction as the lower bound for the rate of bone loss, and used a quarter of this range as the standard deviation (0.0025%).

The Z-score is a measure of how far the results of the simulation from the measured biology in units of standard deviation. The Z-score can also combine multiple outcome measures into one score by treating them as orthogonal and taking the square root of the sum of each of the outcomes' squared Z-scores. This hypotenuse describes how far the set of outcome variables are from the empirically measured biology.

The Z-score for each of the 81 cases was calculated twice—once for average width, rate of width change, and smoothness, and once for just the rate and smoothness, since the edge effect that generates the time of minimum width also artificially reduces the

width, skewing the Z-scores, for the simulations with the stable near-zero rates of change (table 3.2).

Table 3.2. The Z-score for each simulation, calculated from the comparison of the simulations' results and corresponding measured parameters in the literature.

Cell in the Design	Z-score	Z-score (w/o ending width)	osteoclast rate	osteoclast lifespan	osteoblast rate	osteoblast lifespan
SA76	3.816	0.022	8	240	0.3	8
SA55	1.522	0.092	8	120	0.1	8
SA65	3.069	0.105	8	180	0.1	11
SA74	4.872	0.123	8	240	0.1	11
SA64	3.674	0.193	8	180	0.1	8
SA28	0.621	0.232	4	120	0.1	8
SA46	2.938	0.234	4	240	0.1	8
SA56	1.142	0.282	8	120	0.1	11
SA73	4.972	0.379	8	240	0.1	8
SA1	1.440	0.400	2	120	0.1	8
SA47	2.222	0.416	4	240	0.1	11
SA67	1.249	0.454	8	180	0.3	8
SA2	2.114	0.482	2	120	0.1	11
SA29	1.114	0.512	4	120	0.1	11
SA38	0.884	0.531	4	180	0.1	11
SA77	1.834	0.585	8	240	0.3	11
SA75	1.723	0.602	8	240	0.1	33
SA37	1.282	0.623	4	180	0.1	8
SA10	1.346	0.629	2	180	0.1	8
SA11	2.152	0.683	2	180	0.1	11
SA19	1.153	0.852	2	240	0.1	8
SA31	3.095	0.926	4	120	0.3	8
SA4	5.141	1.033	2	120	0.3	8
SA58	1.814	1.083	8	120	0.3	8
SA20	1.877	1.242	2	240	0.1	11
SA49	1.835	1.286	4	240	0.3	8
SA68	2.479	1.509	8	180	0.3	11
SA59	3.820	1.512	8	120	0.3	11
SA5	7.190	1.561	2	120	0.3	11
SA13	5.027	1.582	2	180	0.3	8
SA40	3.043	1.591	4	180	0.3	8
SA57	4.033	1.636	8	120	0.1	33
SA66	2.696	1.680	8	180	0.1	33
SA79	1.939	1.755	8	240	0.5	8
SA32	5.605	1.774	4	120	0.3	11
SA3	7.691	2.071	2	120	0.1	33
SA30	6.137	2.148	4	120	0.1	33
SA50	4.249	2.305	4	240	0.3	11
SA41	5.422	2.469	4	180	0.3	11

SA22	4.838	2.470	2	240	0.3	8
SA61	5.865	2.553	8	120	0.5	8
SA7	8.614	2.568	2	120	0.5	8
SA34	7.388	2.580	4	120	0.5	8
SA48	4.191	2.627	4	240	0.1	33
SA39	6.148	2.641	4	180	0.1	33
SA70	4.900	2.818	8	180	0.5	8
SA12	8.173	3.089	2	180	0.1	33
SA14	8.012	3.235	2	180	0.3	11
SA36	17.881	3.648	4	120	0.5	33
SA21	7.043	3.673	2	240	0.1	33
SA23	7.406	3.718	2	240	0.3	11
SA63	18.062	3.852	8	120	0.5	33
SA9	17.095	3.874	2	120	0.5	33
SA80	6.064	3.918	8	240	0.5	11
SA33	13.300	4.030	4	120	0.3	33
SA52	6.971	4.063	4	240	0.5	8
SA43	7.990	4.078	4	180	0.5	8
SA16	9.696	4.174	2	180	0.5	8
SA35	10.411	4.393	4	120	0.5	11
SA6	14.480	4.475	2	120	0.3	33
SA62	9.507	4.494	8	120	0.5	11
SA18	20.180	4.561	2	180	0.5	33
SA45	19.200	4.783	4	180	0.5	33
SA72	18.939	4.820	8	180	0.5	33
SA8	11.683	4.892	2	120	0.5	11
SA25	9.474	5.150	2	240	0.5	8
SA60	13.683	5.162	8	120	0.3	33
SA27	18.023	5.293	2	240	0.5	33
SA71	9.489	5.362	8	180	0.5	11
SA54	17.345	5.611	4	240	0.5	33
SA42	14.411	5.788	4	180	0.3	33
SA15	15.767	5.849	2	180	0.3	33
SA81	16.157	6.244	8	240	0.5	33
SA69	14.007	6.297	8	180	0.3	33
SA17	12.784	6.335	2	180	0.5	11
SA44	11.533	6.339	4	180	0.5	11
SA53	10.321	6.363	4	240	0.5	11
SA24	14.720	6.776	2	240	0.3	33
SA51	14.209	6.877	4	240	0.3	33
SA26	12.237	6.973	2	240	0.5	11
SA78	12.518	7.240	8	240	0.3	33

The first Z-score had only two simulations that fell within one standard deviation, SA28 and SA38 (table 3.2). Those simulations had a normal osteoclast rate, low or medium osteoclast lifespan, a low osteoblast rate, and either a low or medium

osteoblast lifespan. However, while these two cases did particularly well in both Z-score calculations, they likely rose to the top of the first Z-score calculation because they had the combination of matching low or matching medium levels of osteoclast lifespan and osteoblast activity along with low osteoclast activity and medium osteoclast activity. These two values would allow for the shortest time of minimum width without forcing the trabecula to grow wider or thinner than normal.

Using the second Z-score calculation, there are 22 simulations that fall within one standard deviation of the documented literature values (table 3.2), roughly 27% of the simulations. The closest to zero is SA76, which had a high osteoclast rate and lifespan with a medium osteoblast rate and low osteoblast lifespan. All three values of the osteoclast rate and osteoclast lifespan were represented by multiple simulation cases. All three values for osteoblast lifespan were present, but in that case, the osteoblast rate had to be at its lowest value and the two osteoclast variables at their highest level. Almost all of the 22 simulations are at the lowest value for the osteoblast rate, though there are four cases—including the one with the lowest Z-score—with the medium level of osteoblast activity.

There were thirteen cases that fell within one standard deviation of both the expected rate of change and the smoothness, five of which also fell within one standard deviation of the expected ending width, despite the initial edge effect that depressed all the ending widths (table 3.3). All thirteen cases are in the lower range of osteoblast rate, and all but one have a normal or short osteoblast lifespan. However, the whole range of osteoclast rate and osteoclast lifespan is represented in the cases that correctly fall within expected outcomes. In order to correctly simulate bone remodeling, it is much more

important to stay at the low end of the osteoblast range; this is explained more in the discussion.

Table 3.3. The Z-scores for the 22 cases with an average Z-score below one σ , in order of the summed individual Z-scores. The first five cells are within one standard deviation in each of the three output measures. The first thirteen cells (not in italics) are within one standard deviation of the literature values for Smoothness and Rate change.

Cell in the Design	Average Ending Width	Z-score for Average	Smoothness	Z-score for Smoothness	Rate change	Z-score for Rate change
SA28	117.404	0.172	17.739	0.232	0.00138	0.550
SA38	108.296	-0.479	19.981	0.531	0.00130	0.520
SA19	117.582	0.184	22.392	0.852	0.00189	0.754
SA29	124.147	0.653	19.839	0.512	0.00186	0.742
SA10	127.165	0.869	20.717	0.629	0.00203	0.813
SA56	100.061	-1.067	18.114	0.282	0.00074	0.295
SA55	93.923	-1.505	16.692	0.092	0.00051	0.205
SA67	99.294	-1.122	19.401	0.454	0.00078	0.310
SA37	99.970	-1.074	20.675	0.623	0.00080	0.319
SA1	130.899	1.136	18.998	0.400	0.00198	0.790
SA75	94.522	-1.463	20.513	0.602	-0.00171	-0.683
SA77	92.954	-1.575	20.388	0.585	-0.00184	-0.735
SA47	87.313	-1.978	19.123	0.416	-0.00231	-0.923
SA79	118.417	0.244	29.159	1.755	0.00197	0.789
SA49	123.725	0.623	25.648	1.286	0.00288	1.151
SA58	130.808	1.129	24.121	1.083	0.00230	0.919
SA20	128.464	0.962	25.311	1.242	0.00257	1.027
SA2	139.781	1.770	19.614	0.482	0.00263	1.051
SA11	138.582	1.684	21.123	0.683	0.00288	1.152
SA46	77.849	-2.654	17.756	0.234	-0.00310	-1.238
SA65	76.088	-2.779	15.216	-0.105	-0.00324	-1.297
SA31	151.221	2.587	22.942	0.926	0.00356	1.424

Table 3.4. The initial conditions of the four independent variables for the thirteen cases that fell within one standard deviation of expected values.

Cell in the Design	osteoclast rate	osteoclast lifespan	osteoblast rate	osteoblast lifespan
SA28	4	120	0.1	8
SA38	4	180	0.1	11
SA19	2	240	0.1	8
SA29	4	120	0.1	11
SA10	2	180	0.1	8
SA56	8	120	0.1	11
SA55	8	120	0.1	8
SA67	8	180	0.3	8
SA37	4	180	0.1	8

SA1	2	120	0.1	8
SA75	8	240	0.1	33
SA77	8	240	0.3	11
SA47	4	240	0.1	11

A MANOVA and a set of ANOVA analyses were run on the simulation to determine how significant the independent values were on the dependent variables (table A3.2-A.3.8). The MANOVA found that all four independent variables had a significant effect on the output measures (table A3.2). The rest of the ANOVA analysis between each combination of independent and dependent variables found a statistically significant p value (table A3.3), including the osteoclasts' two parameters. The osteoclast lifespan's effect on the rate of width change had the lowest p value at 0.00757 (table A3.8). The majority of the p-values were equivalent to zero.

A linear regression analysis was run on the data just an exploratory measure. The results are still preliminary, but they show the independent variables to have a mostly linear effect on the output measures (table 3.5). The regression analyses also shows that the model has significant interaction effects, particularly in respect to the osteoblast and osteoclast lifespans. With just the main effects, the R² value was 0.8174, explaining 82% of the variance. When the interaction effects are added into the linear regression, the R² jumps up to 0.9649, explaining all but 4% of the outcome variance.

Table 3.5. Multiple linear regression analysis of the main effects of the independent variables on the rate of trabecular width change.

	Coefficient	Standard Error	t value	P > t
(Intercept)	- 7.470E-03	7.843E-04	- 9.525	< 2E-16
Osteoblast Rate	4.008E-02	9.846E-04	40.705	< 2E-16
Osteoblast Lifespan	7.217E-04	1.443E-05	50.027	< 2E-16
Osteoclast Rate	- 7.352E-04	6.446E-05	- 11.406	< 2E-16

Osteoclast Lifespan	- 2.020E-05	3.282E-06	- 6.154	1.1E-09
------------------------	-------------	-----------	---------	---------

Table 3.6. Multiple linear regression analysis of the main and interaction effects of the independent variables on the rate of trabecular width change.

	Coefficient	Standard Error	t value	P > t
(Intercept)	1.122E-03	9.427E-04	1.190	0.234335
Osteoblast Rate (OBR)	- 6.550E-03	1.957E-03	- 3.347	0.000847
Osteoblast Lifespan (OBL)	- 4.597E-05	2.933E-05	- 1.567	0.117433
Osteoclast Rate (OCR)	1.991E-04	1.277E-04	1.559	0.119288
Osteoclast Lifespan (OCL)	1.175E-05	4.631E-06	2.537	0.011346
OBR x OBL	2.408E-03	3.885E-05	61.969	< 2E-16
OCR x OBL	1.169E-05	2.544E-06	4.594	4.92E-06
OCR x OBR	6.261E-04	1.736E-04	3.606	0.000327
OCL x OBL	- 5.126E-08	1.295E-07	- 0.396	0.692354
OCL x OBR	1.096E-05	8.840E-06	1.239	0.215514
OCL x OCR	- 7.359E-06	5.787E-07	- 12.717	< 2E-16

When the interaction effects are included, the main effects of the osteoblast and osteoclast lifespan are negligible; the lifespan only is significant in combination with their respective cell's rate of activity (table 3.6). The only independent variable that maintains a main effect is the osteoblast rate, whose coefficient switches from positive to negative, amending the effects of the combined osteoblast rate and lifespan (fig 3.17). The two most significant coefficients in the regression analysis looking at interaction effects were the osteoblasts' lifespan and rate combined and the osteoclasts' combined lifespan and rate. Each of these inputs has an opposite effect to respectively increase or decrease the rate of width change (fig 3.18).

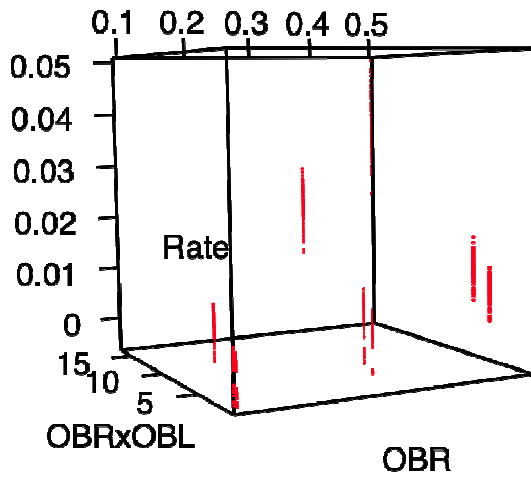


Figure 3.17. The combined effects of the osteoblast rate and the (osteoblast rate * osteoblast lifespan) on the rate of the change in trabecular width.

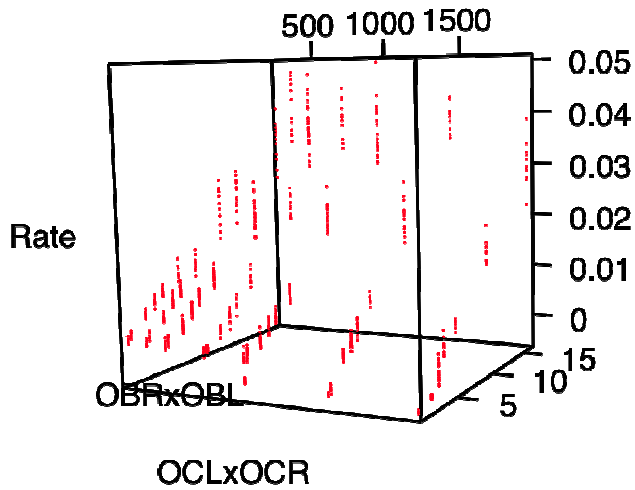


Figure 3.18. The combined effects of the osteoblasts' lifespan and rate with the osteoblasts' lifespan and rate on the rate of change in trabecular width.

3.5. Discussion

Overall, the independent variables simulated the expected impact on the output variables (table 3.7). The average ending width increased with increased osteoblast rate and lifespan and decreased with increased osteoclast rate and lifespan. The rate of change was increased by an increased osteoblast lifespan and rate, decreased by osteoclast rate, and relatively unaffected by osteoclast lifespan. The trabecula became smoother—measured as a decrease in the standard deviation of ending widths—when osteoclast activity increased, and became rougher when the osteoblast lifespan and bone production increased (table 3.7). The time of minimum width takes longer with a larger osteoclast rate and lifespan and takes less time with a larger osteoblast rate and lifespan.

The effect of osteoclast lifespan was very minimal compared to expected trends (table 3.7). In the simulation, the longer the osteoclasts lived and resorbed, the more bone they resorbed, the more signal they released, and therefore the greater number of osteoblast agents they activated. The number of activated osteoblasts was limited to the number that could form a monolayer on the resorption pit, but the osteoclast agents were still able to couple the osteoblast activity functionally, as well as spatially and temporally. The coupling signal was not encoded with the intent to increase the number of osteoblasts whenever the osteoclasts lived longer or resorbed more bone—it was merely a way to signal to osteoblasts as to when and where they should activate. While it is interesting that the osteoclast lifespan had this effect, canceling out any large difference that would have resulted from an extra wide resorption cavity, there are likely other pathways used by bone to regulate the relative activity level of the osteoblasts and osteoclasts. The osteoclast's lifespan and activity levels having minimal effect on the

relative bone formation/resorption balance may show a way in which the paracrine coupling of these two cells to the same location can be done in a neutral manner that will not off-balance the signaling networks that adjust the relatively activity of bone formation and resorption.

Most of the independent variables have a linear effect on the outcomes. The exceptions to this include: the osteoclast lifespan's effect on the rate of change, smoothness and ending width (fig 3.15, fig 3.16); the osteoblast lifespan's effect on time of minimum width and smoothness (fig 3.14, 3.16). In most cases, the non-linearity is likely due to there being no strong effect on the dependent variables by the independent variables—especially in the case of osteoclast lifespan.

Table 3.7. The positive or negative correlation between the independent variables and the outcome variables, both in the simulation and the expected correlation in bone. In cases with a green arrow, the simulation followed the expected biological outcome. In cases with a red ‘x’, there was a discrepancy in the simulation and the expected biological response. The effect of osteoblast or osteoclast activity on the smoothness of the trabeculae is largely unknown, and so cannot be as well correlated to the behavior of the simulation.

	Avg Width	Rate change of Width	Smoothness
Osteoblast Lifespan	↗ in simulation ↗ in bone ✓	↗ in simulation ↗ in bone ✓	↘ in simulation unkown in bone ?
Osteoclast Lifespan	→ in simulation ↘ in bone ✗	→ in simulation ↘ in bone ✗	→ in simulation unkown in bone ?
Osteoblast Activity	↗ in simulation ↗ in bone ✓	↗ in simulation ↗ in bone ✓	↘ in simulation unkown in bone ?
Osteoclast Activity	→ in simulation ↘ in bone ✗	↘ in simulation ↘ in bone ✓	↗ in simulation ↘ in bone (Paget’s disease) ✗

Paget’s disease is a case where the smoothness of the trabeculae—or lack there of—is correlated to cellular activity³². There is not much data on what else effects the smoothness. In Paget’s disease, the increased osteoclast rates lead to the mosaic, disordered bone structure, which was not captured when the osteoclasts increased their activity in the model. There are two main reasons why there was a discrepancy in this expected roughness and the osteoclast activity level (table 3.7). First, in Paget’s disease, the osteoclast activity is increased far beyond a normal range and in the simulation; the range for the osteoclast activity only went up to a ‘high normal’ level of activity—a fraction of what is seen in Paget’s. Secondly, Paget’s disease is characterized by woven bone formation—a malformation in the organization and amount of bone produced by the osteoblasts. It is very likely that the lack of smooth bone formation can be equally caused by the osteoblasts’ dysfunction, rather than the osteoclasts. The simulation,

lacking dysfunctional osteoblasts, would not be able to respond to the odd osteoclast behavior with the roughly formed bone and so the simulation would not be capable of matching the pathology of Paget's disease even if the osteoclast agents were perfectly matched to their cellular counterparts.

Overall the osteoblast parameters have a much larger influence than the osteoclast parameters. It is important for the simulation to stay within the lower ranges in order to have the model simulate correct remodeling. The osteoblast activity was most likely overestimated when translating from bone production per day to bone production per cycle. There is an order of magnitude difference between the speed of osteoblast bone production and osteoclast bone resorption, and the osteoblast parameters had a much larger percent change in range than the osteoclasts. Essentially, the two agent types are on two different relative timeframes, which could explain why the faster osteoblasts have a much larger effect than the osteoclasts.

In addition, the osteoblast agents create new bone immediately after the osteoclasts finish resorbing; this could negate any lasting effects of independent variables like the osteoclast lifespan. Therefore, the next step towards improving this ABM is to empirically ground the resorption and deposition rates—setting all rates of activity to be in units of days or weeks rather than arbitrary time units. This will better constrain the model, allow it to be more precisely validated by a wider range of clinical data, and will allow a better estimation of the relative impact of the osteoclast and kinetics on the overall remodeling process.

It is interesting that the osteoblast lifespan also needed to stay in the lower range

of what was estimated from literature. In more recent literature the lifespan has been calculated at an average of ~12 days, but it is largely based on mouse biology which may or may not correlate to human osteoblasts^{54,91}. The older literature, which is still commonly cited, estimated that osteoblasts lived more on the order of three months⁸⁴. This research was done in humans, but were not done with as invasive and accurate a technique. The range of the osteoblast lifespan was relatively large in order to simulate both high and low estimates. From this preliminary model, it appears that the lower range of the osteoblast lifespan is more reasonable. The simulation will be better equipped to more definitively provide support for the lower osteoblast lifespan in the future version of the model when the rates and lifespans are in units of days and can be more accurately constrained and verified.

The smoothness and solidity of the remodeled trabecula also shows room for improvement. None of the simulations' trabeculae were as smooth as actual bone, which only gradually changes its width. The osteoblast agents tended to create very rough-edged patches of new bone that did not smoothly follow the original surface of the bone or resorption pit. This is due to the code for osteoblastic bone formation being overly simplistic. The subroutine for bone formation did not use any of the necessary pieces of information that real osteoblasts use to deposit organized sheets of organic matrix. As a result, the edges of the trabecula are very choppy and holes were left behind in the middle of the new bone (fig A3.8, A3.10). Therefore, along with setting all the cellular kinetics to be in units of days, a second future aim is to encode more precise descriptions of osteoblast matrix production in order to improve the morphology of the new bone.

The results of the model show that a single, osteoclastic resorption released

signal can activate and attract osteoblasts to the remodeling site. Normal coupling, defined as coupling that generates trabecular morphology within a standard deviation of expected values, was generated while using only documented cell behaviors within the estimated ranges of cell activity.

There were four general outcome patterns generated by this model: increasing width, decreasing width, nearly stable increasing width and nearly stable decreasing width (table A3.1). None of the widths have a completely zero rate of width change, but the 'nearly stable' patterns are within one standard deviation of the estimated bone mass changes seen in healthy human adults. The expected change of width is zero, with a range of +/- 3% mass change per year, as estimated from the literature. From this we calculated one standard deviation of the expected rate of width change to be 0.0025 microns/cycle.

There were only six cases (7%) that generated decreasing width patterns. This would represent a pathologic condition, e.g. osteoporosis. The highest osteoclast variables were expected to cause at least a third of the cases to fall into the decreasing width category, being at the extremes of their estimated ranges. Instead, the osteoblast agents' bone production completely overwhelmed the osteoclasts' effects. When the osteoclast agents scaled up the amount of bone they resorbed, it scaled up the amount of released signal, leading to more osteoblast agents present.

The vast majority of the cases—60 cases—generated the pattern of increasing width. This is due to an overestimation of the osteoblasts' independent variables, and potentially due to the lack of information on the exact timing of the activation and

migration of osteoblast cells. The model correctly simulates the activation and homing of the osteoblast agents, but it has not been grounded to measurements for how far, how fast, and how many osteoblast cells will migrate to a resorption pit. The model may be overestimating the number of osteoblast agents that would activate at a resorption pit, causing the osteoblasts to create too much bone even with a short lifespan or a sluggish bone production. Many of these properties can only be vaguely estimated based on *in vitro* work and there are multiple theories for the origin and state of the preosteoblasts at the time of activation; possible future work may involve simulating multiple hypothesis for the timing of osteoblastogenesis and how that maybe impact bone remodeling and bone healing.

There were only three cases that had the pattern of just slightly decreasing in width, but twelve cases that slightly increased in width. Together they make up for 15 cases. The Z-score only had thirteen 'successful simulations of remodeling' since two of these fifteen fell outside of the expected range of smoothness. Overall, though, 18.5% of the simulations generated by this model showed a relatively stable simulated width throughout the remodeling simulations. This is due to the model having multiple independent variables that can increase or decrease to compensate for the effects of a low or high value in the other independent variables.

Along with oversimplifying the osteoblast activation, the initial shape of the trabecula was a simple, straight column of mineralized ECM agents. However, starting with a more realistically variable width or starting with a wishbone shaped trabecula would likely only add noise to the simulation. The osteoclasts activate randomly on the surface of the bone, activating at the first bone surface they random walk to, and so

would not specifically target thicker or thinner sections of the trabecula.

The osteocytes are distributed at a set osteocyte density, and would not cluster in a thicker or thinner section. They would, however, be sparser along the length of a thinner region of trabecula, potentially leaving that length more vulnerable to fenestrations due to a lack of osteocyte shielding. If the osteocytes were sufficiently dense enough to protect an overly thin region of trabecula, that region would have no osteoclast resorption and therefore no osteoblast deposition, effectively just reducing the length of trabecula being simulated in each case. In reality, bone that is too thin will microfracture and cause osteocytes to signal for osteoclast resorption followed by a large amount of osteoblast bone deposition. This will lead to a new and stronger section of bone in place of the cracking, thin bone. However, this osteoclast chemotactic signal is beyond the scope of this simulation.

4. Conclusions and Future Directions

4.1. Motivations

There are multiple areas of science and medicine that can be directly impacted by an agent-based model (ABM) of bone remodeling, including our knowledge of basic bone biology, drug development, and patient-specific care. Medicine and basic biology are both making steady progress towards improving our understanding of the human body and its mechanisms of healing, but the process is too slow, current treatments fail, and the process of drug development grows longer and ever more expensive. Even with the advent of bioinformatics and systems biology, the integration and utilization of the sheer amount of multi-level data being collected has reached a bottleneck. Only limited progress can be made if these puzzle pieces of information are not fitted together into a clear, accessible whole. This ABM of bone remodeling is still in the beginning stages and has not incorporated enough of these pieces to currently predict outcomes based on patient-specific care, but it has already shown progress in organizing and utilizing data from decades of literature.

ABMs represent a computational method to intelligently represent, integrate, and simulate the human body from the molecular and cellular level up to the tissue and patient level. Because ABMs are fundamentally structured differently from traditional mathematical, systems dynamics, and statistical models, they have the special ability to represent heterogeneous, spatio-temporal systems. This is critical for representing the behavior of cellular processes that are entirely based on the local microenvironment as it evolves through time. An ABM will also solve the stalemates that exist between models of different scales by its ability to integrate information from any size and time scale. Cell level information is entered one-to-one into the agents and the tissue-level behavior

is the direct emergent behavior of the simulation. Patient and clinical databases of medical data empirically ground, calibrate, and validate the model while sub-cellular and molecular models can be inserted into, or interfaced with, the simulation's subroutines.

This ability to absorb and naturally combine this wide disparity of information—across fields, across time and size scales, and within each discipline's own complex behaviors—can free biology from the confines of the reductionist approach. As information is pooled into the model the ABM will literally become a replicate of tissue within the computer. All the components will be alterable and any property of the system can be monitored. Scientists will be able to run virtual experiments on the computer and test hypothesized biological mechanisms against what is known about bone in corresponding disciplines. Researchers will also gain a clearer picture of what is yet unknown, where there are variables missing, and which assumptions do not prove true in the light of the more current research.

Having this functional, interactive representation of human tissue will not just benefit the academic labs, but will radically empower drug developers and bioengineers working on new therapeutics. It can provide a way to rapidly and cost-effectively prototype, test and modify designs for efficacy and safety. Also, since the ABM is based on systems biology and generates emergent behavior, unexpected side effects—even those that would take years to develop—can be generated when the simulation is left to run through longer time periods.

While medicine will be improved any time basic science and the biotech industry are integrated together, there is one particular quirk of ABMs that can have profound

implications on patient treatment. ABMs are dynamically initiated. Each time a simulation starts, the first step is to populate the model with the location and starting statuses of the cells; the simulation can start with any configuration of cells and ECM.

An academic researcher might only study the model initiated with the parameters for an average male bone, the model will function correctly according to whatever the simulation is initiated to. All a physician needs to do to create a patient-specific model is to change the average starting parameters to reflect that patient. Defects, diseases, drug interactions, genetic predispositions, age and gender differences, current blood tests, and more can all be inputted from any available source to create a predictive model for that patient in their current state. This will quickly allow the physician to tailor the treatment plan accordingly and have warning against otherwise unexpected complications. The ABM can even be run multiple times to produce the percent likelihood of complications, give comparisons among multiple treatment options, and generate a list of any early warning signs to monitor for in each patient's case using the most up to date research from multiple disciplines.

In order to use the results of the ABM on a repeated basis, e.g. if a physician wanted to use it to predict the effectiveness of a drug he would like to prescribe, a regression analysis can be performed on the outputs of the simulation that had previously been validated to correctly simulate that drug mechanisms of action. The regression analysis will fit an equation that will map a set of inputs to the predicted outputs. The equation can be run at a fraction of the time and generate predictions that are still be tailored to specific characteristics of that patient. The regression analysis would not be mechanistically based, so any new factors, e.g. any new drug or disease,

would have to be added to the ABM and a new regression model created before any new emergent behaviors could be predicted.

4.2 Contributions to the Field

4.2.1 Techniques

Previous computational models of bone have focused largely on describing the mechanical environment of bone—mapping the stresses, strains, fluid sheers, and microfractures that occur under different loading conditions. The few simulations that have modeling cellular behaviors have approximated their behaviors based on general equations. This simulation models the cells and tissue in a much more biomimetic way—using if/then responses to the local microenvironment, thresholds, and recapitulating the spatiotemporal signaling patterns. While the ABM is still in the early stages, it has been able to incorporate the whole remodeling process with only those behaviors documented in literature. There was a risk that not enough would be known about the behaviors of bone cells to generate a working remodeling cycle constrained to observed cellular reactions.

In addition, previous simulations of remodeling focused on cortical bone remodeling¹⁴. These models have many more spatial constraints, which can lead the simulation to predict the shape of the cutting cone or osteon without any of the cellular mechanisms. If the same rules were applied to a trabecular remodeling site, the model would not be able to predict the shape or order of trabecular remodeling. The generation of an organized bone remodeling complex is more difficult for trabecular remodeling since the spatial constraints that might be used to explain the shape of the cutting cone do not exist. It is unlikely that the processes controlling remodeling in cortical and

trabecular bone are significantly different since both processes require the same cells carrying out the same actions in the same order. For this reason, simulating the trabecular bone remodeling was considered a better way challenge our hypotheses of bone remodeling.

4.2.2 Validation of Hypotheses

The simulations show that both hypotheses are feasible, and were also able to sketch out the general effect the major independent variables will have on the overall system within those hypotheses.

The hypothesis that osteocytes shield the healthy bone from osteoclastic resorption with a diffusible signal is not the only explanation for how a disuse threshold could be generated. The classic examples of osteocyte signaling are generated above the microfracture threshold and can be anything from proteins to apoptotic bodies. There are two well documented mechanical thresholds on either side of a range of applied force that calls for no net changes in bone mass during remodeling. Above the upper threshold there are the amounts of stress that will lead to increased bone mass. Below the lower threshold are the amounts of stress which will decrease the bone mass.

However, the lower stress threshold might not need to be mediated by a released signal. Potentially the mere presence of a healthy osteocyte cell could reduce osteoclastic activity in that area. There is evidence that osteocytes will apoptose if they are not mechanically stimulated, so apoptosis could lead to osteoclastic activity above and below both thresholds. The disadvantage of this system would be the lack of guidance from osteocytes; for example, if a woman were on bed rest and the majority of all her

osteocytes apoptosed, there would be no cells left to guide the remodeling of bone once she was mobile again and started accruing microfractures. To better theorize about the osteocytes' mechanism of mediating the lower threshold, the change in osteocyte morphology and activity on both sides of the disuse threshold should be experimentally observed.

The hypothesis that osteoclasts and osteoblasts can couple with a single released signal from resorbed bone matrix preformed well in the second ABM. The hypothesis did create a mechanistic simulation generating a balanced and coupled remodeling process. The hypothesis is far from being proven true, but a continued refinement of the ABM will be able to either challenge or affirm the likelihood that this released signal drives the chemotaxis of the osteoblasts. Overall, the simulation was more robust in generating the spatial patterns seen in remodeling than in orchestrating the timing seen in the remodeling cycle. This is at least partially due to the absence of detailed information on the timing of osteoblast differentiation. The exact source of osteoblasts and the level of differentiation of the preosteoblasts are at when they detect the chemotactic signal is still under debate. This information might constrain the simulation enough that correct coupling would not be feasible with this one signal, or a more accurate delay in osteoblast activation, representing differentiation and migration, could improve the simulation's overall timing.

4.3 Future Directions

A future aim for the ABM of bone is to make the temporal pace of osteoblast and osteoclasts quantifiably accurate, rather than based on relative numbers of cycles. This would significantly ground many of the control variables to their documented values,

would further constrain the model, and would allow the outputs to be compared to a wider range of experiments—including literature on pathologies such as osteoporosis.

The ability of the ABM to simulate remodeling when the kinetics are adjusted to match literature will likely guide the necessary future additions to the model that will be needed to make the simulation better match the biology. If the simulation is capable of simulating bone remodeling on an accurate time scale, the next step would be to challenge the simulation to predict the pathology of bone diseases using just the hypothesized mechanism of action for the disease. When the model is able to predict those morphologic changes and clinical manifestations, then the input and control variables can be altered to match particular patient populations to begin predicting patient-specific outcomes.

Much more likely, the simulation will slip out of alignment with the expected outcomes as more detailed information is added. This will highlight and characterize deficiencies in our understanding of the mechanisms taking place in bone and will point to the next simplest hypothesis able to explain the behaviors of bone. Proving that a hypothesis is insufficient or incapable to explain an observed biological behavior is way to justify adding extra complexity, e.g. variables and reactions, to the model. Unless the simulation disproves the simpler explanation, the ABM should only improve the accuracy and precision of its representation of the cells, signals, and processes. Real bone remodeling is known to be extremely complex; in order to incorporate its structure, many iterations of constraining and adjusting, all based on well documented behaviors, will be required to incorporate all the information needed to create a predictive system.

4.4 Concluding Remarks

Overall, the work presented in this thesis is an examination of the feasibility of a mechanistic agent-based model to incorporate a biological system on the cellular scale and represent the data in a meaningful way. The creation of such a simulation is largely a test of one's breadth and depth of knowledge of the system, and therefore should be undertaken with the input of as many subject experts as are interested in participating.

An ABM is also not the optimal model for all biological questions. Finite-element models (FEM) are better suited to quantify the distribution of stress, strain, and fluid shear. Regression analysis of clinical data can more quickly find and predict correlations between key factors and patient outcomes. Bayesian networks are better suited to reconstruct complex signaling pathways and the genetic systems level information, since those models can organize massive amounts of information even with minimal knowledge of the underlying structure or mechanisms.

If detailed mapping of the mechanical forces or a complete network of the bone-related genes is required to mechanistically simulate a biological system, it may be more effective to use an FEM or graphical model to manage that information, and feed their outputs into the ABM. However, the ABM is arguably the best way to simulate the emergent effects of autonomous cells as they propagate the spatiotemporal patterns that orchestrate complex tissue dynamics.

References

1. Abdallah, B. M., and M. Kassem. New factors controlling the balance between osteoblastogenesis and adipogenesis. *Bone* 50:540–5, 2012.
2. Alekel, D. L., a S. Germain, C. T. Peterson, K. B. Hanson, J. W. Stewart, and T. Toda. Isoflavone-rich soy protein isolate attenuates bone loss in the lumbar spine of perimenopausal women. *The American journal of clinical nutrition* 72:844–52, 2000.
3. Andersen, T. L., T. E. Sondergaard, K. E. Skorzynska, F. Dagnaes-Hansen, T. L. Plesner, E. M. Hauge, T. Plesner, and J.-M. Delaisse. A physical mechanism for coupling bone resorption and formation in adult human bone. *The American journal of pathology* 174:239–47, 2009.
4. Andersen, T. L., T. E. Sondergaard, K. E. Skorzynska, F. Dagnaes-Hansen, T. L. Plesner, E. M. Hauge, T. Plesner, and J.-M. Delaisse. A physical mechanism for coupling bone resorption and formation in adult human bone. *The American journal of pathology* 174:239–47, 2009.
5. Anderson, E. J., and M. L. Knothe Tate. Idealization of pericellular fluid space geometry and dimension results in a profound underprediction of nano-microscale stresses imparted by fluid drag on osteocytes. *Journal of biomechanics* 41:1736–46, 2008.
6. Ardizzoni, A. Osteocyte Lacunar Size – Lamellar Thickness Relationships in Human Secondary Osteons. 28:215–219, 2001.
7. Ausk, B. J., T. S. Gross, and S. Srinivasan. An agent based model for real-time signaling induced in osteocytic networks by mechanical stimuli. *Journal of biomechanics* 39:2638–46, 2006.
8. Bezooijen, R. L. V., B. A. J. Roelen, A. Visser, L. V. D. Wee-pals, E. D. Wilt, M. Karperien, H. Hamersma, S. E. Papapoulos, P. Dijke, and C. W. G. M. Löwik. Sclerostin Is an Osteocyte-expressed Negative Regulator of Bone Formation, But Not a Classical BMP Antagonist. *The Journal of Experimental Medicine* 199:, 2004.
9. Bianco, P., B. Sacchetti, and M. Riminucci. Osteoprogenitors and the hematopoietic microenvironment. *Best practice & research. Clinical haematology* 24:37–47, 2011.
10. Bonabeau, E. Agent-based modeling: methods and techniques for simulating human systems. *Proceedings of the National Academy of Sciences of the United States of America* 99 Suppl 3:7280–7, 2002.
11. Bonewald, L., and S. Dallas. Role of active and latent transforming growth factor beta in bone formation. *Journal of cellular biochemistry* 55:350–357, 1994.
12. Bonewald, L. F., and S. Dallas. Role of active and latent transforming growth factor in bone formation. *Journal of cellular biochemistry* 55:350–357, 2004.
13. Bonivtch, A. R., L. F. Bonewald, and D. P. Nicoletta. Tissue strain amplification at the osteocyte lacuna: a microstructural finite element analysis. *Journal of biomechanics* 40:2199–206, 2007.
14. Buenzli, P. R., J. Jeon, P. Pivonka, D. W. Smith, and P. T. Cummings. Investigation of bone resorption within a cortical basic multicellular unit using a lattice-based computational model. *Bone* 50:378–89, 2012.
15. Burghardt, A. J., T. M. Link, and S. Majumdar. High-resolution computed tomography for clinical imaging of bone microarchitecture. *Clinical orthopaedics and related research* 469:2179–93, 2011.
16. Chambers, T. J., J. a Darby, and K. Fuller. Mammalian collagenase predisposes bone surfaces to osteoclastic resorption. *Cell and tissue research* 241:671–5, 1985.
17. Chambers, T. J., and K. Fuller. Bone cells predispose bone surfaces to resorption by exposure of mineral to osteoclastic contact. *Journal of cell science* 76:155–65, 1985.
18. Chambers, T. J., B. M. Thomson, and K. Fuller. Effect of substrate composition on bone resorption by rabbit osteoclasts. *Journal of cell science* 70:61–71, 1984.
19. Chen, H., S. Shoumura, S. Emura, and Y. Bunai. Regional variations of vertebral trabecular bone microstructure with age and gender. *Osteoporosis International* 19:1473–1483, 2008.
20. Chilibeck, P., D. Sale, and C. Webber. Exercise and bone mineral density. *Sports Medicine* 19:103–122, 1995.
21. Daoussis, D., A. P. Andonopoulos, and S.-N. C. Lioussis. Wnt pathway and IL-17: novel regulators of joint remodeling in rheumatic diseases. Looking beyond the RANK-RANKL-OPG axis. *Seminars in arthritis and rheumatism* 39:369–83, 2010.
22. Delaisse, J.-M., T. L. Andersen, and et al. Matrix metalloproteinases (MMP) and cathepsin K contribute differently to osteoclastic activities. *Microscopy research and technique* 61:504–513, 2003.

23. Diaz-Flores, L., R. Gutierrez, A. Lopez-Alonso, R. Gonzalez, and H. Varela. Pericytes as a supplementary source of osteoblasts in periosteal osteogenesis. *Clinical Orthopaedics & Related Research* 275:280–286, 1992.
24. Doblaré, M., J. M. García, and M. J. Gómez. Modelling bone tissue fracture and healing: a review. *Engineering Fracture Mechanics* 71:1809–1840, 2004.
25. Dobnig, H., and R. Turner. Evidence that intermittent treatment with parathyroid hormone increases bone formation in adult rats by activation of bone lining cells. *Endocrinology* 136:3632–3638, 1995.
26. Doube, M., M. M. Klosowski, A. M. Wiktorowicz-Conroy, J. R. Hutchinson, and S. J. Shefelbine. Trabecular bone scales allometrically in mammals and birds. *Proceedings. Biological sciences / The Royal Society* 278:3067–73, 2011.
27. Edwards, C. M., and G. R. Mundy. Eph receptors and ephrin signaling pathways: a role in bone homeostasis. *International journal of medical sciences* 5:263–72, 2008.
28. Elmaridi, A., M. Katchburian, and E. Katchburian. Electron microscopy of developing calvaria reveals images that suggest that osteoclasts engulf and destroy osteocytes during bone resorption. *Calcified Tissue International* 46:239–45, 1990.
29. Eriksen, E. F., G. Z. Eghbali-fatourehchi, and S. Khosla. Remodeling and Vascular Spaces in Bone. 22:1–6, 2007.
30. Everts, V., J. Delaisse, W. Korper, D. Jansen, W. Tigchelaar-Gutter, P. Saftig, and W. Beertsen. The Bone Lining Cell: Its Role in Cleaning Howship's Lacunae and Initiating Bone Formation. *Journal of Bone and Mineral Research* 17:77–90, 2002.
31. Eyden, B. R. A study of intercellular relationships between trabecular bone and marrow stromal cells in the murine femoral metaphysis. 9–20, 1995.
32. Favus, M. J., and T. J. Vokes. CHAPTER 29: PAGET'S DISEASE AND OTHER DYSPLASIAS OF BONE. In: *Harrison's Endocrinology*, edited by J. Jameson. McGraw Hill, 2010, pp. 462–474.
33. Ferrari-Lacraz, S., and S. Ferrari. Effects of RANKL inhibition on inflammation and immunity. *IBMS BoneKEy* 6:116–126, 2009.
34. Fornells, P., J. M. García-Aznar, and M. Doblaré. A finite element dual porosity approach to model deformation-induced fluid flow in cortical bone. *Annals of biomedical engineering* 35:1687–98, 2007.
35. Frost, H. From Wolff's Law to the Utah Paradigm: Insights About Bone Physiology and Its Clinical Applications. *The Anatomical Record* 22:398–419, 2001.
36. Frost, H. M. Dynamics of Bone Remodeling. In: *Bone biodynamics*. Boston, MA: Brown and Company, 1964, pp. 315–333.
37. Frost, H. M. The Utah paradigm of skeletal physiology: an overview of its insights for bone, cartilage and collagenous tissue organs. *Journal of bone and mineral metabolism* 18:305–16, 2000.
38. Frost, H. M. Why should many skeletal scientists and clinicians learn the Utah paradigm of skeletal physiology? *Journal of musculoskeletal & neuronal interactions* 2:121–130, 2001.
39. Gilbert, N., and P. Terna. How to build and use agent-based models in social science. *Mind & Society* 1:57–72, 1999.
40. Guo, X., and X.-F. Wang. Signaling cross-talk between TGF-beta/BMP and other pathways. *Cell research* 19:71–88, 2009.
41. Hall, B. Bone Volume 3: Bone Matrix and Bone Specific Products. Boca Raton, Florida: CRC Press, 1992.
42. Hauge, E. M., D. Qvesel, E. F. Eriksen, L. Mosekilde, and F. Melsen. Cancellous bone remodeling occurs in specialized compartments lined by cells expressing osteoblastic markers. *Journal of bone and mineral research •: the official journal of the American Society for Bone and Mineral Research* 16:1575–82, 2001.
43. Hauschka, P. V. Growth factors effects. In: *Bone*, Vol. 1., edited by B. K. Hall. Boca Raton, FL: CRC Press, 1989, p. 512.
44. Hernandez, C. J., R. J. Majeska, and M. B. Schaffler. Osteocyte density in woven bone. 35:1095–1099, 2004.
45. Hofbauer, L., F. Gori, B. Riggs, D. Lacey, C. Dunstan, T. Spelsberg, and S. Khosla. Stimulation of osteoprotegerin ligand and inhibition of osteo- protegerin production by glucocorticoids in human osteoblastic lineage cells: potential paracrine mechanisms of glucocorticoid-induced osteoporosis. *Endocrinology* 140:4382– 4389, 1999.
46. Imai, Y., S. Kondoh, A. P. Kouzmenko, and S. Kato. Minireview •: Osteoprotective Action of

- Estrogens Is Mediated by Osteoclastic Estrogen Receptor- α . *Molecular Endocrinology* 24:877–885, 2010.
47. Islam, A., C. Glomski, and E. Henderson. Bone lining (endosteal) cells and hematopoiesis: a light microscopic study of normal and pathologic human bone marrow in plastic-embedded sections. *Anatomical record* 227:300–306, 1990.
 48. Janssen, M. A., and E. Ostrom. Empirically Based , Agent-based models. 11:, 2006.
 49. Jaworski, Z. F., B. Duck, and G. Sekaly. Kinetics of osteoclasts and their nuclei in evolving secondary Haversian systems. *Journal of anatomy* 133:397–405, 1981.
 50. Jaworski, Z., and E. Lok. The rate of osteoclastic bone erosion in Haversian remodeling sites of adult dog's rib. *Calcified Tissue Research* 10:103–112, 1972.
 51. Jee, W. Histology: cell and tissue biology. 1983.
 52. Jee, W. The past, present, and future of bone morphometry: its contribution to an improved understanding of bone biology. *Journal of Bone Mineral Metabolism* 23:1–10, 2005.
 53. Jiang, Y., J. Zhao, B. Mitlak, O. Wang, H. Genant, and E. Eriksen. Recombinant Human Parathyroid Hormone (1-34) [Teriparatide] Improves Both Cortical and Cancellous Bone Structure. *Journal of bone and mineral research* 18:1932–1941, 2003.
 54. Jilka, R. L., R. S. Weinstein, and E. A. Osteoblast programmed cell death (apoptosis): modulation by growth factors and cytokines. *Journal of bone and mineral research* 13:793–802, 1998.
 55. Karsenty, G. Transcriptional control of skeletogenesis. *Annual review of genomics and human genetics* 9:183–96, 2008.
 56. Karsenty, G. Minireview•: Transcriptional Control of Osteoblast. 142:2731–2733, 2009.
 57. Khosla, S. Minireview: the OPG/RANKL/RANK system. *Endocrinology* 142:5050–5, 2001.
 58. Kitazawa, R., S. Kitazawa, and S. Maeda. Promotor structure of mouse RANKL/ TRANCE/OPGL/ODF gene. *Biochimica et Biophysica Acta* 1445:134 –141, 1999.
 59. Kogianni, G., V. Mann, and B. S. Noble. Apoptotic Bodies Convey Activity Capable of Initiating Osteoclastogenesis and Localized Bone Destruction. 23:, 2008.
 60. Lanyon, L. E. Osteocytes, Strain Detection, Bone Modeling and Remodeling. 53:102–107, 1993.
 61. Lecka-Czernik, B., and L. J. Suva. Resolving the Two “Bony” Faces of PPAR- γ . *PPAR research* 2006:27489, 2006.
 62. Lee, S.-K., and J. Lorenzo. Parathyroid hormone stimulates TRANCE and inhibits osteoprotegerin messenger ribonucleic acid expression in murine bone marrow cultures: correlation with osteoclast-like cell formation. *Endocrinology* 140:3552–3561, 1999.
 63. Leucht, P., S. Minear, D. Ten Berge, R. Nusse, and J. a Helms. Translating insights from development into regenerative medicine: the function of Wnts in bone biology. *Seminars in cell & developmental biology* 19:434–43, 2008.
 64. Li, Z., K. Kong, and W. Qi. Osteoclast and its roles in calcium metabolism and bone development and remodeling. *Biochemical and biophysical research communications* 343:345–50, 2006.
 65. Lian, J. B., G. S. Stein, A. Javed, A. J. van Wijnen, J. L. Stein, M. Montecino, M. Q. Hassan, T. Gaur, C. J. Lengner, and D. W. Young. Networks and hubs for the transcriptional control of osteoblastogenesis. *Reviews in endocrine & metabolic disorders* 7:1–16, 2006.
 66. Luk, S. C., C. Nopajaroonsri, and G. T. Simon. The U Itrastructure of Endosteum•: A Topographic Study in Young Adult Rabbits I. 183:165–183, 1974.
 67. Manolagas, S. C. Birth and Death of Bone Cells: Basic Regulatory Mechanisms and Implications for the Pathogenesis and Treatment of Osteoporosis. *Endocrine Reviews* 21:115–137, 2000.
 68. Marotti, G., a Favia, and a Z. Zallone. Quantitative analysis on the rate of secondary bone mineralization. *Calcified tissue research* 10:67–81, 1972.
 69. Martin, R. B. Targeted bone remodeling involves BMU steering as well as activation. *Bone* 40:1574–80, 2007.
 70. Martin, T. J., and K. W. Ng. Mechanisms by which cells of the osteoblast lineage control osteoclast formation and activity. *Journal of cellular biochemistry* 56:357–66, 1994.
 71. Martin, T. J., and E. Seeman. Bone remodelling: its local regulation and the emergence of bone fragility. *Best practice & research. Clinical endocrinology & metabolism* 22:701–22, 2008.
 72. Martin, T. J., and N. a Sims. Osteoclast-derived activity in the coupling of bone formation to resorption. *Trends in molecular medicine* 11:76–81, 2005.
 73. Martin, T. J., and N. Udagawa. Hormonal regulation of osteoclast function. *Trends in endocrinology and metabolism: TEM* 9:6–12, 1998.
 74. McGarry, J. G., J. Klein-Nulend, M. G. Mullender, and P. J. Prendergast. A comparison of strain

- and fluid shear stress in stimulating bone cell responses--a computational and experimental study. *FASEB journal* •: official publication of the Federation of American Societies for Experimental Biology 19:482–4, 2005.
75. McNamara, L. M., and P. J. Prendergast. Perforation of cancellous bone trabeculae by damage-stimulated remodelling at resorption pits •: A computational analysis. 42:99–109, 2005.
 76. Metz, L. N., R. B. Martin, and A. S. Turner. Histomorphometric analysis of the effects of osteocyte density on osteonal morphology and remodeling. 33:753–759, 2003.
 77. Miller, S., and W. Jee. The Bone Lining Cell: A Distinct Phenotype? *Calcified Tissue International* 41:1–5, 1987.
 78. Mullender, M. G., and R. Huiskes. Osteocytes and bone lining cells: which are the best candidates for mechano-sensors in cancellous bone? *Bone* 20:527–532, 1997.
 79. Mullender, M. G., R. Huiskes, and H. Versleyen. Osteocyte Density and Histomorphometric Parameters in Cancellous Bone of the Proximal Femur in Five Mammalian Species. , 1996.
 80. Muller, R. Modeling and Simulation Techniques in Assessing Microstructural Bone
 81. Mödder, U. I., and S. Khosla. Skeletal stem/osteoprogenitor cells: current concepts, alternate hypotheses, and relationship to the bone remodeling compartment. *Journal of cellular biochemistry* 103:393–400, 2008.
 82. Nie, H., and R. B. Richardson. Radiation dose to trabecular bone marrow stem cells from (3)H, (14)C and selected alpha-emitters incorporated in a bone remodeling compartment. *Physics in medicine and biology* 54:963–79, 2009.
 83. van Oers, R. F. M., R. Ruimerman, E. Tanck, P. a J. Hilbers, and R. Huiskes. A unified theory for osteonal and hemi-osteonal remodeling. *Bone* 42:250–9, 2008.
 84. Parfitt, a M. Osteonal and hemi-osteonal remodeling: the spatial and temporal framework for signal traffic in adult human bone. *Journal of cellular biochemistry* 55:273–86, 1994.
 85. Parfitt, A. M. Bone Histomorphometry: Proposed System for Standardization of Nomenclature, Symbols, and Units. *Calcified Tissue International* 42:284–286, 1988.
 86. Parfitt, A. M., J. Podenphant, A. Villanueva, and B. Frame. Metabolic Bone Disease With and Without Osteomalacia After Intestinal Bypass Surgery: A Bone Histomorphometric Study. *Bone* 6:211–220, 1985.
 87. Parfitt, A., C. Mathews, A. Villanueva, M. Kleerekoper, B. Frame, and D. S. Rao. Relationships between surface, volume, and thickness of iliac trabecular bone in aging and in osteoporosis: implications for the microanatomic and cellular mechanisms of bone loss. *Journal of Clinical Investigation* 72:1396–1409, 1983.
 88. Piper, K., A. Boyde, and S. J. Jones. Anatomy and Embryology The relationship between the number of nuclei of an osteoclast and its resorptive capability in vitro. 291–299, 1992.
 89. Piper, K., A. Boyde, and S. J. Jones. The relationship between the number of nuclei of an osteoclast and its resorptive capability in vitro. *Anatomy and embryology* 186:291–299, 1992.
 90. Plotkin, L. I., I. Mathov, J. I. Aguirre, A. M. Parfitt, S. C. Manolagas, and T. Bellido. Mechanical stimulation prevents osteocyte apoptosis •: requirement of integrins , Src kinases , and ERKs. *American Journal of Physiology and Cell Physiology* 289:633–643, 2005.
 91. Plotkin, L. I., R. S. Weinstein, A. M. Parfitt, P. K. Roberson, S. C. Manolagas, and T. Bellido. Prevention of osteocyte and osteoblast apoptosis by bisphosphonates and calcitonin. 104:1363–1374, 1999.
 92. Pols, H. A. P., D. Felsenberg, D. A. Hanley, J. Stepan, M. Munoz-Torres, T. J. Wilkin, G. Qinsheng, A. M. Galich, K. Vandormael, A. J. Yates, and B. Stych. Alendronate on Bone Density and Fracture Risk in Postmenopausal Women with Low Bone Mass •: Results of the FOSIT Study. *Osteoporosis International* 9:461–468, 1999.
 93. Prendergast, P. J., and R. Huiskes. Microdamage and osteocyte-lacuna strain in bone: a microstructural finite element analysis. *Journal of biomechanical engineering* 118:240–6, 1996.
 94. Reeve, J. A stochastic analysis of iliac trabecular bone dynamics. *Clinical Orthopaedics & Related Research* 213:264–78, 1986.
 95. Roberts, W. E., J. a. Roberts, B. N. Epker, D. B. Burr, and J. K. Hartsfield. Remodeling of Mineralized Tissues, Part I: The Frost Legacy. *Seminars in Orthodontics* 12:216–237, 2006.
 96. Roodman, G. Cell biology of the osteoclast. *Experimental Hematology* 27:1229–1241, 1999.
 97. Saika, M., D. Inoue, S. Kido, and T. Matsumoto. 17B-Estradiol stimulates ex- pression of osteoprotegerin by a mouse stromal cell line, ST-2, via estrogen receptor-a. *Endocrinology* 142:2205–2212, 2001.

98. Saltel, F., A. Chabadel, and et al. Transmigration: a new property of mature multinucleated osteoclasts. *Journal of bone and mineral research* 21:1913–1923, 2006.
99. Schmitt, J. M., K. Hwang, S. R. Winn, and J. O. Hollinger. Bone morphogenetic proteins: an update on basic biology and clinical relevance. *Journal of orthopaedic research* •: official publication of the Orthopaedic Research Society 17:269–78, 1999.
100. Schneider, P., M. Meier, R. Wepf, and R. Müller. Towards quantitative 3D imaging of the osteocyte lacuno-canalicular network. *Bone* 47:848–858, 2010.
101. Shih, Y., K. Tseng, C. Lin, and O. Lee. Matrix stiffness regulation of integrin-mediated mechanotransduction during osteogenic differentiation of human mesenchymal stem cells. *Journal of bone and mineral research* 26:730–738, 2011.
102. Slomianka, L. Blue Histology - Skeletal Tissues - Bone. , 2009.at <<http://www.lab.anhb.uwa.edu.au/mb140/CorePages/Bone/Bone.htm#Bone>>
103. Steck, R., P. Niederer, and M. L. Knothe Tate. A Finite Element Analysis for the Prediction of Load-induced Fluid Flow and Mechanochemical Transduction in Bone. *Journal of Theoretical Biology* 220:249–259, 2003.
104. Søre, K., and J.-M. Delaissé. Glucocorticoids maintain human osteoclasts in the active mode of their resorption cycle. *Journal of bone and mineral research* •: the official journal of the American Society for Bone and Mineral Research 25:2184–92, 2010.
105. Søre, K., and J.-M. Delaissé. Glucocorticoids maintain human osteoclasts in the active mode of their resorption cycle. *Journal of bone and mineral research* •: the official journal of the American Society for Bone and Mineral Research 25:2184–92, 2010.
106. Takai, H., M. Kanematsu, K. Yano, E. Tsuda, K. Higashio, K. Ikeda, K. Watanabe, and Y. Yamada. Transforming growth factor- stimulates the production of osteoprotegerin/osteoclastogenesis inhibitory factor by bone marrow stromal cells. *J Biol Chem* 273:27091–27096, 1998.
107. Tan, S. D., a D. Bakker, C. M. Semeins, a M. Kuijpers-Jagtman, and J. Klein-Nulend. Inhibition of osteocyte apoptosis by fluid flow is mediated by nitric oxide. *Biochemical and biophysical research communications* 369:1150–4, 2008.
108. Udagawa, N. Mechanisms involved in bone resorption. *Biogerontology* 3:79–83, 2002.
109. Ulrich, D., B. Rietbergen, a Laib, and P. Rügsegger. Mechanical analysis of bone and its microarchitecture based on in vivo voxel images. *Technology and health care* •: official journal of the European Society for Engineering and Medicine 6:421–7, 1998.
110. Urist, M., A. Mikulski, and A. Lietze. Solubilized and insolubilized bone morphogenetic protein. *Proceedings of the National Academy of Sciences of the United States of America*. 76:1828–1832, 1979.
111. Vander Wiel, C., S. Grubb, and E. Al. The presence of lining cells on surfaces of human trabecular bone. *Clinical Orthopedic Related Research* 134:350–355, 1978.
112. Varanasi, S. S., O. K. Olstad, D. C. Swan, P. Sanderson, V. T. Gautvik, S. Reppe, R. M. Francis, K. M. Gautvik, and H. K. Datta. Skeletal site-related variation in human trabecular bone transcriptome and signaling. *PloS one* 5:e10692, 2010.
113. Vashishth, D., G. J. Gibson, and D. P. Fyhrie. Sexual dimorphism and age dependence of osteocyte lacunar density for human vertebral cancellous bone. *The anatomical record. Part A, Discoveries in molecular, cellular, and evolutionary biology* 282:157–62, 2005.
114. Villanueva, A., E. Sedlin, and H. M. Frost. Variations in Osteoblastic Activity with Age by the Osteoid Seam Index. *The Anatomical record* 146:209–213, 1963.
115. Wilensky, U. NetLogo. , 1999.at <<http://ccl.northwestern.edu/netlogo/>>
116. Wolff, J., P. Maquet (Translator), and R. Furlong (Translator). The Law of Bone Remodeling. Springer, .